THE ROLE OF MICRORNA-150 IN TYPE 2 DIABETIC RETINOPATHY

A Dissertation

by

FEI YU

Submitted to the Graduate and Professional School of
Texas A&M University
in partial fulfillment of the requirements for the degree of

DOCTOR OF PHILOSOPHY

Chair of Committee,	Gladys Y. Ko
Committee Members,	Robert Burghardt
	Gregory Johnson
	Chaodong Wu
Head of Department,	Todd O'Hara

December 2021

Major Subject: Biomedical Sciences

ABSTRACT

Diabetic retinopathy (DR) is a chronic complication associated with diabetes and the number one cause of blindness in working adults in the US. More than 90% of diabetic patients have obesity-associated type 2 diabetes (T2D), and 60% of T2D patients will develop DR. Degeneration of retinal neurons and vasculature manifests in the diabetic retina and early stage of DR. Photoreceptors undergo apoptosis shortly after the onset of diabetes, which contributes to the retinal dysfunction and microvascular complications leading to vision impairment. Chronic inflammation is a hallmark of obesity and T2D and a contributor to apoptosis; and retinal photoreceptors are a major source of intraocular inflammation which contributes to vascular abnormalities in diabetes. However, how diabetic insults cause inflammation and apoptosis in photoreceptors remains unclear. MicroRNA-150 (miR-150) is downregulated in diabetic patients and is a regulator that suppresses inflammation, apoptosis, and pathological angiogenesis. Several confirmed target genes of miR-150, including the ETS-domain transcription factor (*Elk1*), regulate both inflammation and apoptosis. In this study, I used a high-fat diet (HFD)-induced T2D mouse model and cultured photoreceptors treated with palmitic acid (PA) to decipher the functions of miR-150 and its target genes in mediating the high-fat-induced retinal degeneration, apoptosis, and inflammation. I found that deletion of miR-150 exacerbated HFD-induced dysfunction and inflammation in the neural retina. The miR-150 knockout (miR-$150^{-/-}$) mice also had increased numbers of degenerated retinal capillaries and apoptotic photoreceptors compared to WT

mice. Knocking down miR-150 also exacerbates the PA-elicited apoptosis and inflammation in cultured photoreceptors. The functional screen showed that *Elk1* is the target gene of miR-150 that responses to the PA treatment in photoreceptors. The phosphorylated ELK1 at threonine 417 ($pELK1_{T417}$) and phosphorylated ELK1 at serine 383 ($pELK1_{S383}$) are the active forms of ELK1 that can regulate apoptosis and inflammation, respectively. I found that miR-150 knockout/ knockdown upregulates the expressions of ELK1, $pELK1_{T417}$, and $pELK1_{S383}$ in photoreceptors. Knocking down *Elk1* alleviated the PA-induced inflammation and decreased the nuclear-to-cytoplasmic (N/C) ratio of $pELK1_{S383}$ in cultured photoreceptors. However, *Elk1* knockdown did not rescue the apoptosis or decrease the N/C ratio of $pELK1_{T417}$ in PA-treated photoreceptors.

ACKNOWLEDGEMENTS

I would like to thank my committee chair, Dr. Ko, and my committee members, Dr. Burghardt, Dr. Johnson, and Dr. Wu, for their guidance and support throughout the course of this research.

Thanks also go to my friends and colleagues and the department faculty and staff for making my time at Texas A&M University a great experience.

CONTRIBUTORS AND FUNDING SOURCES

Contributors

This work was supervised by a dissertation committee consisting of Professors Gladys Ko, Robert Burghardt, and Gregory Johnson of the Department of Veterinary Integrative Biosciences and Professor Chaodong Wu of the Department of Nutrition.

The data in Figure 2-1 was provided by Dr. Lisheng Shi and Dr. Janet Ya-an Chang in Ko's lab of the Department of Veterinary Integrative Biosciences. The analyses depicted in Figure 2-3 were conducted in part by Ms. Samantha Chapman of the Department of Veterinary Integrative Biosciences and were published in 2020.

All other work conducted for the dissertation was completed by the student independently.

Funding Sources

Graduate study was supported by the grants from the College of Veterinary Medicine and Biomedical Sciences (CVMBS), Texas A&M University: 2018 Graduate Research-Core Facility Grant and 2020 Graduate Student Trainee Research Grant.

This work was also made possible in part by the National Eye Institute of the National Institutes of Health under Grant Number NIHR21EY031813-01A1. Its contents are solely the responsibility of the authors and do not necessarily represent the official views of the National Eye Institute of the National Institutes of Health.

TABLE OF CONTENTS

Page

LIST OF FIGURES

Page

1. INTRODUCTION

1.1. Retina and Diabetic Retinopathy

1.1.1. Structure of Retina

The vertebrate retina in the eye detects the light/darkness and relays the information into the brain, so it is the first neural tissue in the visual system that we depend on to see the world. The retina is a layered structure. Under the light microscope, the retina comprises 10 layers from the innermost to the outermost side of the retina: the inner limiting membrane (ILM), the nerve fiber layer (NFL), the ganglion cell layer (GCL), the inner plexiform layer (IPL), the inner nuclear layer (INL), the outer plexiform layer (OPL), the outer nuclear layer (ONL), the outer limiting membrane (OLM), the inner and outer segments of photoreceptors (IS+OS), and the retinal pigmented epithelium (RPE) [1]. There are three major categories of cells in the retina: neurons, glial cells, and vascular cells. The retinal neurons include photoreceptors, bipolar cells, retinal ganglion cells, horizontal cells, and amacrine cells. The glial cells include Müller glia, astrocytes, and microglia. The endothelial cells and pericytes compose the microvasculature of the retina [2]. The locations of retinal cells in different layers are illustrated in Figure 1-1.

1.1.2. Detection and Transmission of Visual Signals by Retinal Neurons

1.1.2.1. Phototransduction

Phototransduction is the detection of photons and the transmission of light stimuli to changes of membrane potentials in photoreceptors. There are two types of photoreceptors: rods and cones. The principal mechanism of phototransduction is

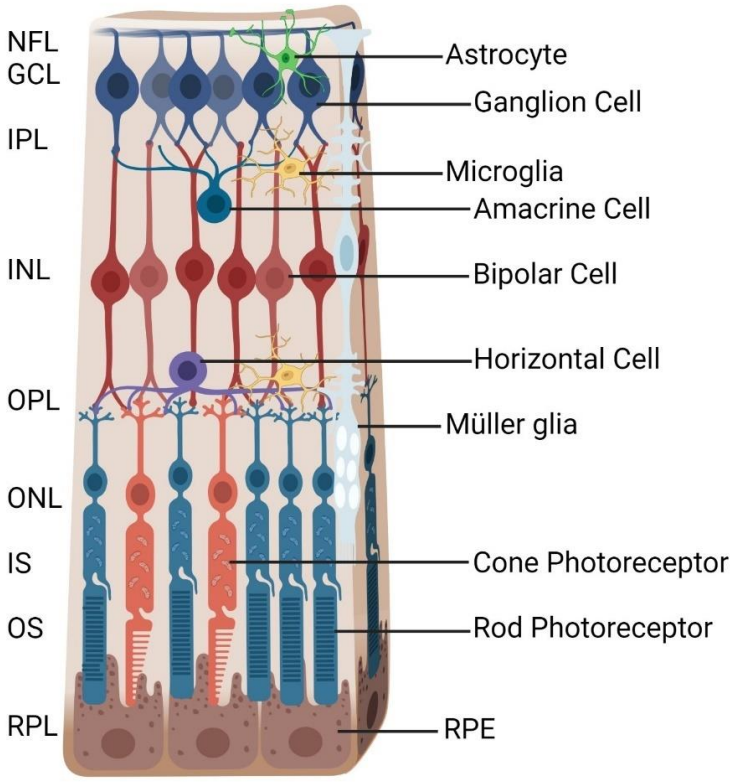

Figure 1-1 Structure of retina and locations of retinal cells.
NFL, nerve fiber layer; GCL, ganglion cell layer; IPL, inner plexiform layer; INL, inner nuclear layer; OPL, outer plexiform layer; ONL, outer nuclear layer; IS, inner segment of photoreceptor; OS, outer segment of photoreceptor; RPE, retinal pigmented epithelium. Created with BioRender.com.

similar between rods and cones. The rod rhodopsin (or cone opsins) is a G protein-coupled receptor consisting of opsin and 11-cis-retinal and resides on the membrane disks in the outer segments of photoreceptors. After rhodopsin absorbs a photon, the 11-cis-retinal changes to all-trans-retinal, which triggers the conformational change of rhodopsin and generates the metarhodopsin II (R*) [3]. The R* stimulates the heterotrimeric G protein transducin and activates the α subunit of transducin (Tα*). The Tα* binds to guanosine-5'-triphosphate (GTP) and dissociates from the β and γ subunits

(Tβγ). The Tα* then activates the phosphodiesterase (PDE) which hydrolyzes the cyclic guanosine monophosphate (cGMP) to GMP [4]. Decreased cGMP in the cytoplasm of photoreceptors leads to the closure of cGMP-gated cation channels which reduces the influx of sodium (into rods and cones) and calcium (mostly into cones only). Therefore, the photoreceptors become hyperpolarized under light stimulus which reduces the presynaptic release of the excitatory neurotransmitter glutamate [5]. There are three types of cone photoreceptors based on their sensitivities to different wavelengths of light. The short (S), medium (M), and long (L) opsins in cones are best activated by the blue, green, and red light, respectively. The activated cone-opsins induce the phototransduction cascade in cones, which is similar to that in rods [6].

The phototransduction cascade is modulated by at least three proteins that regulate the deactivation of rhodopsin. The R* can be phosphorylated by rhodopsin kinase and lose the ability to activate transducin. Recoverin is a calcium-binding protein that inhibits the function of rhodopsin kinase and suppresses the phosphorylation of R*. Arrestin binds and deactivates R* [7]. Proper deactivation of rhodopsin is important to maintain the function of photoreceptors.

1.1.2.2. Visual Circuit in the Retina

Photoreceptors synapse with bipolar cells and horizontal cells in the OPL. The bipolar cells are functionally divided into ON and OFF bipolar cells. The ON-bipolar cells express a metabotropic glutamate receptor mGluR6 that binds to glutamate and leads to the closing of the cation channel. Therefore, the reduced release of glutamate by photoreceptors under light suppresses the activity of mGluR6 and depolarizes the ON-

bipolar cells. The OFF bipolar cells express ionotropic glutamate receptors (e.g., AMPA receptor) and depolarize in the dark due to the release of glutamate by photoreceptors [8]. The horizontal cells also express ionotropic glutamate receptors and provide inhibitory feedback to photoreceptors and bipolar cells by releasing the inhibitory neurotransmitter γ-aminobutyric acid (GABA) [9, 10]. The neighboring horizontal cells are inhibitory neurons that control the intensity of the output signal from the photoreceptors. Therefore, the signals received by the inner retina can be maintained within an operating range [11].

The bipolar cells synapse with the retinal ganglion cells (RGCs) and amacrine cells in the IPL. In the primate retina, the major types of bipolar cells are the inner (ON) and outer (OFF) midget cells and parasol cells. The dendrites of the ON/OFF ganglion cells are located in the inner/outer sublamina of the IPL, respectively. The midget ganglion cells receive inputs from relatively small regions of the outer retina (receptive fields) and therefore function in the high-acuity vision. In the fovea, each of the midget bipolar cells (ON/OFF) connect to one midget ganglion cell (ON/OFF) to ensure high acuity [12]. The parasol ganglion cells receive input from the ON/OFF diffuse bipolar (DB) cells, which connect more cones than the midget bipolar cells. The parasol ganglion cells contribute to the sense of contrast and motion detection [13]. Around 30 types of amacrine cells have been identified based on their morphologies and specific functions. In general, the amacrine cells provide inputs to the ganglion cells and bipolar cells by releasing inhibitory neurotransmitters GABA and glycine. This helps the motion

detection in ganglion cells and improves the fidelity of signal transmission in the bipolar cells [14].

1.1.3. Retinal Glia

Müller glia and astrocytes are the two types of macroglia in retina. The Müller glia are the most abundant glial cells in the retina [15]. Their cell bodies localize in the INL and the processes span between the inner and outer limiting membranes (ILM, OLM). The endfoot of Müller glia forms the ILM with the basal lamina while the adherens junctions between photoreceptors and Müller glia form the OLM. The Müller glia also contact synapses and neurons through lateral processes [16]. The major functions of Müller glia include nutritional support to the neurons, maintaining potassium homeostasis, as well as the uptake and recycling of neurotransmitters (glutamate and GABA). Activated Müller glia under pathological stimuli display insufficient support to neurons and decreased uptake of glutamate. Sustained activation of glutamate receptors on neurons will induce glutamate excitotoxicity which leads to the apoptosis of neurons [17]. Müller glia activation also induces the secretion of vascular endothelial growth factor (VEGF) and TNF-α, which promote pathological angiogenesis and inflammation in the diabetic retina [18].

Astrocytes mainly reside in the GCL and NFL and contact the superficial vascular plexus and RGCs. Astrocytes maintain the hemostasis of the extracellular environment by taking up the excess ions and metabolites for RGCs [16]. Activated astrocytes may mediate oxidative stress in the retina after injury [19] and contribute to the dysfunction of RGCs [20] and compromised vascular integrity under diabetes [21].

Microglia are monocytes that enter the retina during development. Microglia locate in the OPL, IPL, and GCL where they function as the resident immune cells. The high motility of microglia enables the surveillance of the retinal microenvironment [16]. The process motility of microglia is increased by glutamate and decreased by GABA, suggesting the interactions between microglia and retinal neurons [22]. Microglia can be activated by various stimuli including lipopolysaccharide and inflammatory cytokines and chemokines. The activated microglia have enhanced proliferation and migration and promote inflammation in the retina by secreting proinflammatory factors, such as tumor necrosis factor (TNF) and interleukins (IL). The activated microglia also contribute to the apoptosis of neurons, suggesting the functions of microglia in neurodegeneration [23]. Other studies indicate that microglia also have neuroprotective and anti-inflammatory functions based on their secretions of brain-derived neurotrophic factor (BDNF) and IL-10. Therefore, microglia may switch phenotypes that exhibit paradoxical functions in neurodegeneration [24].

1.1.4. Retinal Blood Supply and Blood-Retinal Barrier

There are two sets of vascular supplies in the retina: the central retinal artery and its branches supplying the inner retina and the choroidal circulation supplying the photoreceptors and fovea. The central retinal artery enters the optic disc and branches into smaller arterioles to supply the different quadrants of the retina. Two plexuses of continuous capillaries are formed after the terminal arterioles. The superficial plexus locates in the NFL and GCL and the deep plexus locates in the INL and OPL. The capillaries are composed of endothelial cells and pericytes that share the basement

membrane. Post-capillary venules converge and form the central retinal venule that leaves the optic disc. The arteries of choroidal circulation originate from ciliary arteries and branch into smaller arterioles. The choriocapillaris is fenestrated with fewer pericytes. The venules in the choroid merge and join the vortex veins and leave the eye [25].

The Blood-retinal barrier (BRB) regulates the exchange of molecules between the neural retina and the vasculature [1]. In addition, the BRB protects the neural retina from the immune attack of the systemic circulation [26]. The inner BRB is composed of the tight junctions between endothelial cells, the basement membrane, and pericytes. The astrocytes and Müller glia also contribute to the inner BRB by ensheathing the vascular plexuses [25]. The outer BRB mainly refers to the tight junctions between RPE cells [27]. Pathological conditions can disrupt the BRB and disrupt the homeostasis in the retina. For example, the elevated level of VEGF in the diabetic retina can downregulate the expression of tight junction protein Occludin and break down the BRB [28]. Systemic immune cells that are released from the compromised BRB exacerbate the inflammation in the retina [26].

1.1.5. Diabetic Retinopathy

1.1.5.1. Prevalence of Diabetic Retinopathy

Diabetic retinopathy (DR) is a chronic complication caused by type 1 and type 2 diabetes (T1D, T2D). DR impacts 4.2 million people in the US and 93 million people worldwide [29] and is a leading cause of blindness among the working population in the US [30]. The incidence of diabetes is projected to increase to 33% of the US population

by 2050 [31]. Overall, DR is diagnosed in 30% of diabetic patients. About 90% of T1D patients and 60% of T2D patients develop DR in their lifetime [32]. The risk factors for developing DR include the duration of diabetes (≥ 20 years), poor control over blood glucose levels, hypertension, and obesity [33].

1.1.5.2. Manifestations and Therapies of DR

DR affects both the retinal vasculature and neural retina [34]. Diabetes impairs the integrity of retinal vasculature and induces pathological angiogenesis [35]. Depending on the severity of the vascular pathologies, DR is be divided into the non-proliferative and proliferative phases clinically. The non-proliferative DR (NPDR) manifests mild-to-moderate vascular abnormalities including microaneurysms, intraretinal hemorrhages, and venous beading. The proliferative DR (PDR) displays neovascularization and preretinal hemorrhages [32]. Neural dysfunction can be detected in the diabetic retina by electroretinography (ERG) before any vascular pathologies are found. ERG measures the amplitudes and implicit times of the retinal light response. Diabetic patients usually have lower amplitudes and longer implicit times than healthy subjects [36]. In addition, the decreased ERG amplitudes correlate with more severe vascular pathologies in NPDR patients [37], suggesting the communication between retinal neurons and vascular cells.

Laser photocoagulation is a standard therapy for PDR, but it is invasive and induces blind spots in the retina [32]. The most used therapy for DR is intraocular injections of anti-Vascular Endothelial Growth Factor (VEGF) reagents [38]. However, less than 50% of patients have improved vision after 1-2 years of anti-VEGF therapies

[39]. Repeated anti-VEGF treatments are needed to conquer the recurrent pathological angiogenesis, but often cause unwanted side-effects including retinal detachment [39]. In addition, current therapies for DR mainly target neovascularization at the late stage of DR and rarely restore the normal visual function [32]. Therefore, investigating the pathogenic mechanisms at the early stage of DR is in great need.

1.1.5.3. Neural and Vascular Degenerations in Diabetic Retina

Neurodegeneration occurs early in the diabetic retina. In T1D patients without retinopathy, the thickness of NFL decreases compared to the healthy subjects, suggesting the loss of axons from RGCs [40]. In type 2 diabetic patients with mild NPR (microaneurysms), the thicknesses of NFL, GCL, and IPL decrease, indicating neurodegeneration in the initial stage of DR [41]. Moreover, the decreased thickness of NFL correlates with the presence of DR in T2D patients, suggesting that neurodegeneration in the diabetic retina contributes to the development of DR [42]. Loss of pericytes and the formation of acellular capillaries are the major signs of vascular degeneration. Degenerated vessels can be detected in mild NPR and may contribute to the formation of microaneurysms [43].

The neural and vascular degenerations could result from the upregulated apoptosis in the diabetic retina. In diabetic patients without retinopathy, the apoptotic cells increase in the neural retina compared to the healthy subjects. Most apoptotic cells are found in the GCL but the ONL also displays apoptosis [44]. In patients with 6 years of diabetes duration, the apoptotic cells increase in the retina from ONL to GCL [45]. In the retinal vasculature of diabetic patients, increased apoptotic pericytes and endothelial

cells are detected compared to the healthy subjects [46]. Since apoptosis may contribute to the neural and vascular degeneration which leads to the development of DR, it is necessary to investigate the consequences and mechanisms of diabetes-induced apoptosis in the retina.

1.2. Apoptosis in the Diabetic Retina and its Mechanisms

1.2.1. Apoptosis

Apoptosis is the programmed cell death that requires energy and activities of the caspases. The apoptotic cells undergo the concentration of chromosomes, fragmentation of DNA, shrinkage, and blebbing of the cytoplasm [47]. The apoptotic bodies containing organelles and nuclear fragments within the complete membrane are generated from the apoptotic cells [48]. Macrophages engulf and digest the apoptotic bodies which prevent the triggering of the inflammatory reactions in the surrounding tissue [49]. The apoptotic cell death may transition to necrotic cell death depending on the cell death signal and cell type [50]. Necrosis is passive and energy independent. The necrotic cells often suffer from swelling and the disruption of the cell membrane, which releases the cell content into the extracellular matrix and triggers inflammatory responses [51]. Two major pathways mediate the apoptotic reactions: intrinsic and extrinsic [52]. The intrinsic pathway is activated in cells under stress such as hypoxia [47]. Stress induces mitochondrial dysfunctions such as the opening of mitochondrial permeability transition pore (mPTP) and the depolarization of the inner membrane [53]. Cytochrome c is released from mitochondria and induces the activation of caspase-9 and caspase-3 [54]. In addition, the endonucleases released from the mitochondria translocate to the nuclei

and induce the fragmentation of chromosomal DNA [55]. The extrinsic pathway starts with the binding of ligands with the tumor necrosis factor (TNF) receptor family, including the binding of fatty acid synthetase ligand (FasL) with Fas receptor (FasR), and TNF-α with TNF receptor 1 (TNFR1) [56]. The receptors will recruit adaptors to their intracellular domain and form the death-inducing signaling complex (DISC) which activates the caspase-8 and caspase-3 [57]. Activated caspase-3 cleaves the inhibitor of caspase-activated DNAse (ICAD) and releases CAD to induce the fragmentation of DNA and chromatin condensation [58]. Caspase-3 also induces the degradation of the cytoskeleton [59], which leads to the formation of apoptotic bodies and noninflammatory phagocytosis.

1.2.2. Apoptosis in Diabetic Retina

In section 1.1.5.3, I briefly introduced the neural and vascular degeneration and upregulated apoptosis in the retina of diabetic patients. In this section, I will discuss in detail the diabetes-induced apoptosis of neurons and vascular cells in patients and animal models. Apoptosis of retinal neurons contributes to neural dysfunction [60, 61] while apoptosis of vascular cells leads to local hypoxia and subsequent angiogenesis [62, 63].

1.2.2.1. Apoptosis of Neurons in the Diabetic Retina

Apoptotic non-vascular cells can be found in the retina of diabetic patients before the onset of DR [64]. The expressions of apoptotic markers are detected in the retina of diabetic patients, including caspase-3 in the ganglion cell layer (GCL) and FasL in various locations from the nerve fiber layer (NFL) to the outer nuclear layer (ONL) [65]. In T2D patients with NPDR, the thickness of GCL measured with optical coherence

tomography (OCT) decreases compared to non-diabetic subjects [66]. In T2D patients without retinopathy, the thicknesses of retinal layers from GCL to the outer plexiform layer (OPL) decrease after one year of follow-up [67]. In a mouse model of T2D (KKAY), the terminal UTP nick-end label (TUNEL) staining shows an increased number of apoptotic neurons in the GCL [68]. Decreased thicknesses of the inner nuclear layer (INL) and inner plexiform layer (IPL) also occur in the retina of T1D mice (Ins2Atita) with increased expression of caspase-3 [69]. The number of cells decreases while the expression of caspase-3 increases in GCL after 10 weeks of diabetes in streptozotocin (STZ)-induced T1D mice [70]. These findings have discovered the degeneration of the inner retina, which may explain the dampened light response reflected by the decreased amplitude and increased implicit time of b-wave on the electroretinography (ERG) [71, 72]. However, the a-wave on ERG from diabetic patients [73] and animals [74] also display similar abnormalities compared to the healthy counterparts, which indicate the diabetes-induced impairment to the photoreceptors. In T2D patients, decreased thicknesses of ONL and the inner and outer segments of photoreceptors associate with the development of retinopathy [67]. In patients with metabolic syndrome, the thickness of the photoreceptor layer decreases compared to healthy subjects [75]. The TUNEL staining shows an increased number of apoptotic photoreceptors in STZ-induced T1D rats [76] while the thickness of ONL decreases in STZ mice after 10 weeks of diabetes [70]. Electron microscopy shows disorganization and degeneration of the outer segments in STZ rats, suggesting diabetes-induced apoptosis of photoreceptors [77]. In addition, 28-week-old T2D mice (db/db) have

decreased thickness of ONL, accompanied by dampened light responses on ERG [78]. Therefore, diabetes-induced apoptosis also occurs in photoreceptors, which may contribute to the dampened light response reflected in the a-wave of ERG.

Overall, apoptosis of neurons in the diabetic retina contributes to neural dysfunction. In T1D patients, the thickness of multiple retinal layers decreases while the visual function is impaired. Specifically, the decreased thickness of the ganglion cell layer correlates with dampened visual function [60]. In T2D adolescents with an average of two years of diabetes, the thickness of the retina measured by OCT decreases while the visual function measured by ERG is dampened [61]. On the contrary, the administration of neuroprotective drugs can alleviate the loss of neurons and impairment of neural function induced by diabetes [79]. In STZ mice with diabetes for 5 months, the thickness of the retina and number of ganglion cells decreases while the amplitude on ERG is reduced. Intravitreal injection of neuropeptide Y ameliorates the loss of neurons and the impairment of neural function [80].

1.2.2.2. Apoptosis of Vascular Cells in the Diabetic Retina

The microvasculature in the retina comprises endothelial cells and pericytes. Microvascular degeneration occurs at an early stage of DR [34]. Acellular capillaries are typical pathological changes that can be found in the trypsin-digested diabetic retina [17]. This kind of capillaries only contains the basement membrane and cytoplasm of the endothelial cells while the cell nuclei are lost. Another sign of microvascular degeneration is the loss of pericytes or the existence of “ghost” pericytes which appear as light-stained pockets around the basement membrane [81]. TUNEL staining of the

trypsin-digested retina from diabetic patients shows apoptotic endothelial cells and pericytes [82]. In alloxan-induced T1D rats, the numbers of apoptotic vascular cells and the acellular capillaries increase in the trypsin-digested retina [83]. Apoptotic endothelial cells also increase in the retina of STZ rats while inhibiting FasL rescued apoptosis [84]. Apoptotic pericytes expressing the pro-apoptotic BCL2 associated X protein (BAX) can be detected in the retina of diabetic patients [85]. TUNEL positive pericytes are detected in the retina of STZ rats [86] and loss of pericytes is found in T2D mice (db/db) [87]. The numbers of acellular capillaries and pericyte ghosts increase in the retina of T1D (STZ) and T2D (Zucker) rats with elevated activity of caspase-3, and inhibiting TNF-α alleviates those pathological changes [88]. Microvascular degeneration may contribute to the breakdown of the blood-retina barrier (BRB) [89] and exacerbate the decrease of blood flow and hypoxia in the diabetic retina [62]. Retinal hypoxia stimulates the secretion of angiogenic factors such as VEGF from various cell types in the retina including astrocytes and Müller glia cells [63]. The upregulated VEGF eventually leads to pathological angiogenesis in DR.

1.2.3. Mechanisms for Diabetes-Induced Apoptosis

The commonly recognized mechanisms for diabetes-induced apoptosis in the retinal neurons and microvasculature include oxidative stress and inflammation. Glutamate excitotoxicity may also contribute to the apoptosis of retinal neurons in the diabetic retina.

1.2.3.1. Oxidative Stress

1.2.3.1.1. Generation of Reactive Oxygen Species

Oxidative stress is the accumulation of reactive oxygen species (ROS) due to overproduction or decreased removal of ROS. Mitochondria are major organelles producing ROS during oxidative phosphorylation [90]. Under normal conditions, the electrons donated by reduced nicotinamide adenine dinucleotide (NADH) and flavin adenine dinucleotide (FADH2) are transferred from complex I to complex IV on the inner mitochondrial membrane by coenzyme Q and cytochrome C. Meanwhile, protons are transferred to the intermembrane space to generate a gradient of protons between the mitochondrial matrix and the intermembrane space. The influx of protons drives the synthesis of ATP while the electrons are consumed to produce H2O [91]. The high-glucose environment in diabetes promotes the generation of electron donors NADH and FADH2, which pushes the gradient of protons to the threshold and hinders the transfer of electrons. Alternatively, electrons are provided to O2 by coenzyme Q and to generate superoxide and ROS [92]. Nicotinamide adenine dinucleotide phosphate (NADPH) can also donate electrons to O2 through the membrane proteins NADPH oxidases (Nox) [93]. Under diabetic conditions, protein kinase C (PKC) is activated and in turn increases the activity of Nox [94]. The Nox proteins are highly expressed in the vasculature, and ROS generated from Nox are believed to impair vascular function [95]. The increased ROS in mitochondria promotes the opening of mPTP and increases the release of cytochrome C [96], which eventually induces apoptosis.

1.2.3.1.2. Oxidative Stress in Diabetic Retina

The 8-hydroxydeoxyguanosine (8-OHdG) is a marker for oxidative stress-induced DNA damage. In T2D patients, 8-OHdG increases in the vitreous indicating upregulated oxidative stress in the retina [97]. Glutathione (GSH) is a major antioxidant that helps remove ROS and suppress oxidative stress. In STZ mice, GSH decreases in the mitochondria of the retina while the acellular retinal capillaries increase [98]. Antioxidant reagents have been used to alleviate the apoptosis of retinal neurons and endothelial cells under diabetes [90]. Antioxidant α-Lipoic acid decreases the TUNEL positive cells in the trypsin-digested retina after 11 months of diabetes while it decreases 8-OHdG and increases GSH [99]. In STZ mice, the antioxidant Lutein alleviates the neural dysfunction and apoptosis of neurons, while the activity of caspase-3 is reduced [100]. Peroxisome proliferator-activated receptor-alpha (PPARα) is an antioxidant transcription factor that is expressed in the neurons, glia, and microvasculature of the retina. In a mouse model of pathological angiogenesis, the activation of PPARα suppresses hypoxia-induced apoptosis in the outer nuclear layer (ONL) and inner nuclear layer (INL), and decreases the expression of Nox4, suggesting the PPARα alleviates the neuronal apoptosis under hypoxia by reducing the production of ROS and oxidative stress [101].

1.2.3.2. Inflammation

1.2.3.2.1. Activation of Microglia in Diabetic Retina

Inflammation is a hallmark of diabetes that manifests in the diabetic retina [102]. The functional BRB in the diabetic retina protects the neural retina from invasion of

immune cells in the circulation [26]. Therefore, the retinal glial cells, neurons, and endothelial cells are the major sources and regulators of the diabetes-induced inflammation until the breakdown of BRB in the advanced stages of DR [103]. The innate immune system in the retina responds to the diabetic insults by activating microglia and secreting pro-inflammatory molecules. Microglia are the resident immune cells in the retina from the monocyte lineage. Microglia can be differentiated from macrophages in the circulation by the low expression of CD45. Resting microglia reside in the inner and outer plexiform layers with ramified shapes while the activated microglia change to an amoeboid shape and migrate to various retinal layers [26]. The toll-like receptors (TLRs) and receptors for advanced glycation end-products (AGE) on microglia detect the noxious molecules in the environment, including ROS and AGEs [104]. The AGEs are produced by the reaction of glucose and amino groups in proteins. In the diabetic retina, AGEs are found to be accumulated in the capillaries, nuclear layers, and plexiform layers [105, 106]. In the retina of STZ rats, the accumulated AGEs colocalize with the activated microglia. Intraocular injections of AGEs increased the expression of Iba-1, which is a marker for microglia activation. The retinal level of TNF-α is also upregulated by injecting AGEs. Neutralizing AGEs by the anti-AGE antibody reduces TNF-α and Iba-1, suggesting that activated microglia by AGEs upregulates the secretion of TNF-α [107].

In mouse retina under oxidative stress, the apoptosis of photoreceptors increases concurrently with the activation of microglia in the photoreceptor layers. Knocking out TLR2 diminishes the increased activation of microglia and mitigates the apoptosis of

photoreceptors [108]. The results suggest that the activation of microglia is mediated by the detection of oxidative stress through TLR2, which is essential to induce neuronal apoptosis in the retina. In high-fat diet (HFD)-induced T2D mice, the expression of Nox and the level of 8-OHdG increases in the retina, indicating increased production of ROS and apoptosis. The HFD also increases the level of interleukin-6 (IL-6) in the retina which correlates with the upregulated TLR4 and microglia activation. Knocking out TLR4 decreases the activation of microglia and reduces the level of IL-6 [109]. These results suggest that the T2D-induced increase of ROS activates microglia through TLR4, which increases the secretion of IL-6.

1.2.3.2.2. Inflammatory Responses in the Vascular and Neural Retina

Activated microglia secrete pro-inflammatory factors, including TNF-α and interleukins, which activate inflammatory reactions and promote apoptosis in vascular cells and neurons [110]. In cultured human retinal endothelial cells (REC), treatments of IL-1β and TNF-α increase the activities of caspase-3 and caspase-8 under normal and high glucose concentrations [111]. The proinflammatory nuclear factor kappa B (NFκB) in HRECs is activated while the expressions of intracellular adhesion molecule (ICAM)-1 and vascular cell adhesion molecule (VCAM)-1 are upregulated by IL-1β and TNF-α treatments [112]. The ICAM-1 and VCAM-1 induce leukostasis (adherence of leukocytes) in the retinal vessels and promote further inflammatory reactions by mediating the migration of leukocytes [104]. In STZ mice with diabetes for 7 months, acellular capillaries and activities of caspase-3 and -8 increase compared to the non-diabetic mice. Knocking out the type 1 interleukin-1 receptor (IL1R1) in STZ mice

largely decreases the number of acellular capillaries and the activities of the caspases [113]. Treatment of IL-1β exacerbates the increases of NFκB expression and caspase-3 activity in the retinal endothelial cells under high glucose while neutralizing IL-1β with antibodies blocks the expression of NFκB and reduces caspase-3 activity [114]. Inhibiting TNF-α decreases the apoptosis of retinal endothelial cells and the activities of caspase-3 and -8 in STZ rats. Hyperglycemic mice with deficient TNF receptors (TNF-R1 and TNF-R2) have decreased acellular capillaries and increased pericytes compared to wildtype (WT) mice [115].

The increased IL-1β and TNF-α also stimulate retinal neurons and induce apoptosis. Exposure to hypoxia increases the expression of IL-1β and TNF-α in retinal microglia and upregulates the corresponding receptors IL-1R1 and TNF-R1 in ganglion cells. Hypoxia induces apoptosis in ganglion cells, while neutralizing IL-1β and TNF-α with antibodies suppresses apoptosis [116]. In the retinal degeneration 1 (rd1) mouse model, blocking the downstream signaling of interleukin-1 receptors (IL-1R) alleviates the degeneration of photoreceptors and improves the light responses of the retina [117]. Therefore, the pro-inflammatory molecules secreted by microglia under diabetes can trigger the extrinsic apoptotic pathway in retinal neurons and vascular cells.

1.2.3.2.3. Inflammation Mediated by Astrocytes and Müller Glia

The astrocytes and Müller glia cells also contribute to the inflammatory environment in the diabetic retina. Under high glucose treatment, the astrocytes have increased activation of NFκB and production of ROS, as well as elevated levels of pro-inflammatory factors including IL-1β, TNF-α, and monocyte chemoattractant protein-1

(MCP-1) [118]. The MCP-1 may recruit and activate microglia, which accelerate the local inflammatory response [119]. The Müller glia cells from STZ rats express increased pro-inflammatory factors, such as ICAM-1 [120]. Increased IL-1β in the diabetic retina can stimulate the expression of IL-6 and activate NFκB in Müller cells, suggesting that the Müller cells mediate the exacerbation of inflammation in the diabetic retina [121]. In addition, the production and secretion of the anti-inflammatory pigment epithelium-derived factor (PEDF) [122] are decreased in Müller cells under high glucose [123] or hypoxia [124], while the expression of pro-inflammatory VEGF in Müller cells increase [125, 126]. Therefore, the suppression of inflammation by Müller cells is dampened in the diabetic retina.

1.2.3.3. Glutamate Excitotoxicity

One mechanism of apoptosis that may apply to the retinal neurons under diabetes is glutamate excitotoxicity. Glutamate is an excitatory neurotransmitter that mediates the signal transduction in the retina [127]. Uptake of glutamate in the synaptic cleft by neurons and glial cells is necessary to maintain the concentration of extracellular glutamate and cease the activation of the postsynaptic receptors [128]. Studies have found increased glutamate [129] and upregulated expression of the glutamate receptors [130] in the diabetic retina. In addition, the activity of glutamate transporter is reduced in Müller glia cells under diabetes [131, 132]. Therefore, diabetic insults induce extended activation of the glutamate receptors, which allows the influx of calcium [133]. The elevated intracellular calcium is transported into the mitochondrial matrix and activates

the PTP which facilitates the release of cytochrome C and leads to the apoptosis of neurons [134].

1.3. MicroRNAs and Diabetic Retinopathy

Apoptosis of retinal neurons and vascular cells contributes to the development of DR. Therefore, it is important to investigate how apoptosis and the mechanisms contributing to apoptosis are regulated in the diabetic retina. MicroRNAs (miRNAs) are small non-coding RNAs that normally suppress the expression of targeted messenger RNAs (mRNAs) and lead to the degradation of mRNAs [135]. The levels of many miRNAs are changed in the blood circulation and retina of diabetic patients [136]. Some of these miRNAs regulate apoptosis, oxidative stress, and inflammation [137], so diabetes-elicited changes in these miRNAs might further contribute to the development of DR.

1.3.1. Biogenesis of MicroRNAs

The genes encoding microRNAs (miRNAs) are transcribed by RNA polymerase II (Pol II) to generate the primary miRNAs (pri-miRNAs) in the nucleus. The pri-miRNA contains a 7-methylguansine triphosphate (m7G) cap at the 5’ end and a polyadenylated (poly(A)) tail at the 3’ end and folds into a double-stranded hairpin [138]. The RNase III enzyme Drosha and the DiGeorge critical region 8 (DGCR8) recognize the stem and the single-stranded/double-stranded RNA junction of the pri-miRNA respectively and cleave the pri-miRNA into a ~70-nucleotide (nt) hairpin precursor miRNA (pre-miRNA) [139]. The 3’ overhang of the pre-miRNA is recognized by Exportin 5 and transported to the cytoplasm through the nuclear pore complex [140].

The pre-miRNA is then recognized by another RNase III enzyme Dicer and the associated transactivation response element RNA-binding protein (TRBP) and cleaved near the terminal loop [141]. This generates a ~21-nt miRNA: miRNA* duplex. The miRNA guide strand is incorporated into the miRNA-induced silencing complex (miRISC) which contains Dicer, TRBP, and argonaut proteins (AGOs). The passenger strand miRNA* is degraded [142]. Previous studies indicate that the miRNA guide strand is derived from one arm of the duplex where the 5' end is paired with less stability [143]. Recent studies have found that the miRNA guide strand can be generated from both arms of the duplex, which yields the -5p and -3p miRNAs with different expression levels [144].

1.3.2. Functions of microRNAs

1.3.2.1. MicroRNAs Inhibit the Translation of Target mRNAs

The seed sequence of miRNA (nucleotides 2-8) pairs with the complementary 3' untranslated region (UTR) of the target mRNAs and guide the miRISC to inhibit the translation or induce the degradation of the mRNAs, which reduce the synthesis of the target proteins [142]. Studies have found that the RNAs interfere with the initiation of translation and block the elongation of the polypeptide [138].

1.3.2.1.1. MicroRNAs Inhibit the Initiation of Translation

The initiation of translation for eukaryotic mRNAs requires the binding of the cap-binding complex with the m7G cap and the poly(A) tail of mRNAs, which is recognized by the pre-initiation complex (PIC) that scan the start codon AUG. Another mechanism of initiation requires the association between the PIC and the internal

ribosome entry site (IRES) at the 5' end [145]. The cap-binding complex is composed of the eukaryotic initiation factors (eIFs) and poly(A)-binding protein (PABP) while the 43S pre-initiation complex comprises eIFs and the 40S ribosomal subunit. The 80S initiation complex (IC) forms after the joining of the 60S ribosomal subunit [146]. Modifying the m7G cap structure, removing the poly(A) tail, or replacing the IRES significantly decreases the repression of mRNA expression by miRNA [147]. Treatment of eIF4F abolishes the translational inhibition of miRNA let-7 [148], and knocking down eif-6 disrupts the translational repression mediated by miRNA lin-4 [149], indicating that microRNAs target the initiation of translation.

1.3.2.1.2. MicroRNAs Inhibit the Elongation of Translation

The elongation phase of translation starts as the aminoacyl-transfer RNA (tRNA) enters the A site of the ribosome with elongation factor 1 (EF-1) and GTP, which is directed by the codon on mRNA. The ribosome shifts conformation when GTP is hydrolyzed, moving the aminoacyl-tRNA at the A site and the polypeptide-bearing tRNA at the P site into proximity. The polypeptide is then transferred to the aminoacyl-tRNA and the new peptide bond forms when the aminoacyl-tRNA moves to the P site. Then EF-2 enters to reset the conformation of the ribosome to receive another aminoacyl-tRNA at A site [150]. In HeLa cells, the level of the reporter transcript that coimmunoprecipitate with polypeptides is decreased by miRNA let-7a, indicating that let-7a represses the expression of the reporter gene by blocking the elongation of polypeptide [151]. In the breast cancer cell line, miR-663 and miR-744 decrease the

expression of EF-1A2, which belongs to the EF-1 family and performs polypeptide elongation in the neural, muscular, and cardiac tissues [152].

1.3.2.2. MicroRNAs Induce the Degradation of Target mRNAs

MiRNAs also induce the degradation of target mRNAs by promoting the shortening of the 3' poly(A) tail (deadenylation) and the removal of the 5' m7G cap (decapping). The deadenylated and decapped mRNAs are degraded by the 5'-to-3' exoribonuclease 1 (XRN1) [153]. MiR-125b and let-7 accelerate the deadenylation and decay of target mRNAs in HeLa and 293T cells, while the mRNAs that lack the binding sites of the miRNAs show delayed deadenylation and minimum decay [154]. Knocking down mRNA-decapping enzymes 1 and 2 (DCP1, DCP2), or depleting human enhancer of decapping large subunit (Ge-1) suppresses the miRNA-mediated degradation of target mRNAs [155]. Some studies indicate that the perfect or near-perfect complementary pairing between the miRNA and mRNA leads to the degradation of mRNA, while imperfect pairing leads to translational repression [156]. However, other studies show that mRNAs without perfect complementary binding sites in 3'-UTR can also be targeted by miRNAs and undergo degradation [157, 158]. This suggests that the initiation of miRNA-mediated degradation depends on multiple factors besides the sequence pairing with 3'-UTR.

1.3.2.3. Critical Proteins in microRNAs-Mediated Silencing of mRNAs

The argonaut (AGO) proteins are essential for translational inhibition and mRNA degradation mediated by miRISC. In HeLa cells, the AGO2 tethered to the 3'-UTR of the reporter transcript represses the translation probably by binding to the m7G cap and

inhibiting the initiation of translation [159]. Knocking down Ago2 releases the inhibition of reporter genes mediated by let-7 and restores the mRNA levels of reporter transcripts [160]. The interaction between AGO proteins and their partner trinucleotide repeat-containing 6 (TNRC6/ GW182) proteins is indispensable for translational inhibition and mRNA degradation. GW182 binds to AGO2 with multiple binding sites within the N-terminal that contains the glycine-tryptophan (GW) repeats [161]. In Drosophila Schneider 2 (S2) cells, depleting AGO1 or GW182, or interrupting the binding of AGO1 and GW182 abrogates the repression and degradation of reporter genes mediated by miRNAs [162]. AGO2 also interacts with the deadenylases CAF1 and CCR4 and promotes the deadenylation of reporter transcripts mediated by let-7. Decreased association between AGO2 and GW182 relieved the deadenylation [163]. The miRNA-mediated degradation of mRNAs depends on the functions of the deadenylase (CAF1+CCR4) and the decapping (DCP1+DCP2) complexes [135]. Knocking down the complexes abolishes the degradation of reporter transcripts mediated by GW182 and miRNAs [164].

1.3.3. MicroRNAs in Diabetic Retinopathy

1.3.3.1. Altered Levels of microRNAs in Diabetic Patients and Animals

The change of miRNA levels can be detected in the blood circulation and retina of diabetic patients and animals, and changes in miRNA levels have been suggested as biomarkers for the development of DR [136]. For example, in the blood circulation of T1D patients, miR-29a, miR-148a, miR-181a, and miR-200a are upregulated while miR-21a, miR-93, miR-126, and miR-146a are downregulated [165]. The level of miR-126

negatively correlates with the risk of developing PDR [166]. In the extracellular vesicles derived from the plasma of T1D patients, decreased miR-150 and increased miR-30b are associated with the development of DR [167]. In the plasma of T2D patients and mice (ob/ob), the levels of miR-15a, miR-20b, miR-21, miR-24, miR-126, miR-191, miR-197, miR-320, miR-486, and miR-150 decrease [168]. The downregulation of miR-20b in the serum of T2D patients correlates with the development of DR and may be used to predict the severity of DR [169].

1.3.3.2. Examples of MicroRNAs Involved in the Processes of Apoptosis, Oxidative Stress, and Inflammation in Diabetic Retinopathy

The upregulated or downregulated miRNAs modulate the pathogenic processes of DR including apoptosis, oxidative stress, and inflammation [137]. MiR-495 increases in the retinal ganglion cells (RGCs) treated with high glucose (HG). Overexpressing miR-495 exacerbates the HG-induced apoptosis in RGCs while inhibiting miR-495 protects RGCs against apoptosis [170]. MiR-93-5p decreases in the retina of high-fat diet-induced T2D rats. Overexpressing miR-93-5p in the diabetic retina alleviates the microvascular degeneration, downregulates the pro-inflammatory factors (IL-1β, IL-6, and TNF-α), and elevates the levels of antioxidants including GSH and superoxide dismutase (SOD) [171]. MiR-21 decreases in the retina of T2D mice (db/db), and in the RECs treated with palmitic acid (PA) which generates a high-fat extracellular environment. Knocking out miR-21 in T2D mice alleviates the degeneration and leukostasis of retinal vasculature, decreases the levels of pro-inflammatory factors (TNF-α and VCAM-1), and upregulates the antioxidant PPARα in the retina [172].

Overexpression of miR-145 alleviates the HG-induced apoptosis in RECs while inhibiting the production of ROS and pro-inflammatory factors (IL-1β and TNF-α). The production of SOD is upregulated by miR-145 in HG-treated RECs [173]. The activation of toll-like receptor 4 (TLR4) mediates inflammatory responses and promotes the activation of NFκB [174]. TLR4 is a downstream target of miR-145. Overexpressing miR-145 suppresses the expression of TLR4 and inhibits the activation of NFκB in HG-treated RECs [173].

MiR-195 increases in GCL, INL, ONL, and endothelial cells in the retina of STZ rats compared with the non-diabetic rats. The upregulation of miR-195 also occurs in the HG-treated retinal endothelial cells (RECs). The STZ and HG treatments decrease the expression of antioxidant manganese superoxide dismutase (MnSOD) in the retina and RECs, which may promote oxidative stress and apoptosis [175]. Inhibition of miR-195 mitigates the STZ/HG-induced suppression of MnSOD [176]. MiR-29b-3p increases in the blood of DR patients. Increased apoptosis and caspase-3 activity are observed in the RECs cultured under HG and hypoxia, which mimics the environment of the diabetic retina. The ratio between the pro-apoptotic BCL2 associated X protein (BAX) and the anti-apoptotic B-cell lymphoma protein 2 (BCL2) is also increased. Inhibition of miR-29b alleviates the apoptosis-associated changes probably by increasing the expression of the antioxidant silent information regulator 1 (SIRT1) [177], which is a downstream target of miR-29b [178].

MiR-146a is downregulated in the circulation of T2D patients [179]. Decreased miR-146a correlates with escalated inflammation [180]. In STZ rats, intraocular

injection of miR-146a suppresses the diabetes-induced increase of the pro-inflammatory intercellular adhesion molecule 1 (ICAM1) and mitigates the damage to retinal light response and microvascular integrity [181]. MiR-146a also decreases in HG-treated RECs. Overexpression of miR-146a inhibits the inflammatory response in HG-treated RECs by suppressing the expressions of TLR4, phosphorylated NFκB, and TNF-α, and blocking the downstream signaling of TLR4 [182]. MiR-15a decreases in the RECs of diabetic patients compared to the non-diabetic subjects. Overexpression of miR-15a in the mouse retina inhibits the expressions of pro-inflammatory factors including IL-1β, IL-6, and TNF-α [183]. MiR-15b and miR-16 decrease while TNF-α increases in the RECs treated with HG. Overexpression of miR-15b and miR-16 mitigates the HG-induced upregulation of TNF-α [184]. MiR-20b decreases in the serum of T2D patients compared to healthy subjects and further decreases in T2DR patients compared to the T2D patients without retinopathy [169]. Overexpressing miR-20b-3p in the eyes of STZ rats alleviates the visual dysfunction, as well as neural and vascular degeneration in DR. MiR-20b-3p reduces apoptosis and BAX while increases BCL-2 in the retina of STZ rats. In addition, the expressions of pro-inflammatory factors (IL-1β and TNF-α) are downregulated by overexpressing miR-20b-3p in the diabetic retina [185]. These microRNAs further exemplify their crucial roles in the development of DR.

1.3.3.3. MicroRNA-150 and Diabetic Retinopathy

1.3.3.3.1. Decreased microRNA-150 Associates with the Development of DR

MicroRNA-150 (miR-150) is downregulated in patients with obesity [186], T1D [187, 188], and T2D [167]. In HFD-induced T2D mice, miR-150 is decreased in the

plasma and retina [189, 190]. Downregulated miR-150 is also observed in the heart of STZ rats [191] and in the ischemic retina of mice [192]. Inhibition of miR-150 promotes apoptosis [193] while overexpression of miR-150 alleviates the apoptosis of cells under hypoxia [194], in which local hypoxia occurs in the diabetic retina [195, 196]. Overexpression of miR-150 also protects the retinal vasculature from degeneration induced by oxygen-induced retinopathy (OIR), a model for hypoxia-induced angiogenesis [197]. Moreover, miR-150 is an intrinsic suppressor of inflammation [198]. Overexpression of miR-150 downregulates TNF-α and NFκB induced by lipopolysaccharide (LPS) in endothelial cells [199]. Deletion of miR-150 (miR-150$^{-/-}$) exacerbates the increase of IL-1β, IL-6, and TNF-α in mice with HFD-induced T2D [198]. In our obesity-associated T2D mouse model induced by HFD, the miR-150 knockout (miR-150$^{-/-}$) mice fed with the HFD showed more severe retinal neural dysfunction and vascular pathologies compared to the wild type (WT) mice fed with the HFD [189]. Therefore, decreased miR-150 associates with diabetes and may facilitate the development of DR by promoting apoptosis and inflammation in the neural and vascular retina.

1.3.3.3.2. The Targets of MiR-150 in Diabetic Retina

MicroRNAs often have many targets, and a single mRNA can also be targeted by multiple microRNAs [158]. Decreased miR-150 may promote apoptosis and inflammation in the diabetic retina by upregulating its downstream target genes. There are confirmed target genes of miR-150 that can regulate inflammation. In HFD-T2D mice, decreased miR-150 upregulates its target genes MYB proto-oncogene (c-*Myb*),

ETS-domain transcription factor 1 (*Elk1*), and eukaryotic translation termination factor 1 (*Etf1*). Knocking down c-*Myb*, *Elk1*, or *Etf1* suppresses the inflammatory response by inhibiting the activation of B cells [198]. Early growth response 1 (*Egr1*) is another target gene of miR-150 [200]. Knocking down *Egr1* alleviates the diabetes-induced inflammation in mouse mesangial cells by downregulating the pro-inflammatory factors (IL-1β, IL-6, and TNF-α) [201, 202]. Moreover, these target genes of miR-150 (c-*Myb*, *Elk1*, *Etf1*, and *Egr1*) are also involved in the regulation of apoptosis. Knocking out c-*Myb* upregulates the apoptosis of mouse colorectal carcinoma cells [203], and overexpressing c-*Myb* decreases the production of ROS and alleviates the apoptosis in cardiomyocytes after hypoxia/reoxygenation injury [204]. Overexpression of ELK1 protein has been found to induce apoptosis in neurons by interacting with the mitochondrial permeability transition pore complex (PTP) [205]. Transfection of *Elk1* in the dendrites of primary neurons induces apoptosis [206], while inhibition of *Elk1* alleviates the apoptosis of neurons under oxygen-glucose deprivation [207]. Upregulated *Etf1* is associated with decreased apoptosis in mouse preosteoblast cells [208]. Increased expression of *Egr1* is associated with the apoptosis of squamous cell carcinoma cells and breast cancer cells, while knocking down *Egr1* mitigates apoptosis [209, 210].

Since the biological processes mediated by miRs and their targets are often tissue- and cell-type-dependent [211, 212], I tested the expression levels of the target genes mentioned above in cultured photoreceptors under palmitic acid (PA) treatment, which generates a high-fat environment for the cells. In this way, I can confirm the functional target genes that respond to the T2D conditions in the neural retina.

1.3.3.4. Hypothesis and Specific Aims

My overarching hypothesis is that diabetic insults due to obesity/T2D cause a decrease of miR-150 and an increase of its downstream target(s), which will exacerbate obesity-associated T2DR by promoting retinal inflammation and apoptosis that leads to neural degeneration and vascular complications in the retina.

Aim 1: Determine the role of miR-150 in the development of obesity-associated T2DR in retinal inflammation and retinal microvascular degeneration using an HFD-induced T2D mouse model.

Aim 2: Determine the mechanistic link between miR-150 and its downstream target(s) of miR-150 that leads to neuronal apoptosis in the retina of HFD-induced T2D mice.

Aim 3: Decipher the relationship between miR-150 and its downstream target(s) that leads to retinal inflammation of HFD-induced T2D mice.

2. DECREASED MIR-150 IN OBESITY-ASSOCIATED TYPE 2 DIABETIC MICE INCREASES INTRAOCULAR INFLAMMATION AND EXACERBATES RETINAL DYSFUNCTION[1]

2.1. Overview

Diabetic retinopathy (DR) is the leading cause of blindness among the working population in the US. Current therapies including anti-vascular endothelial growth factor (VEGF) treatments, cannot reverse the visual defects induced by DR. MicroRNA-150 (miR-150) is a regulator that suppresses inflammation and pathological angiogenesis. In diabetic patients, miR-150 is downregulated. As inflammation is a major contributor to the pathogenesis of DR, whether the diabetes-associated decrease of miR-150 is merely associated with the disease progression or decreased miR-150 causes retinal inflammation and pathological angiogenesis is still unknown. We used high-fat diet (HFD)-induced type 2 diabetes (T2D) in both wild type (WT) and miR-150 knockout (miR-150$^{-/-}$) mice as our experimental models. We compared the retinal function and microvasculature morphology among different experimental groups. We found that deletion of miR-150 exacerbated HFD-induced retinal dysfunction and retinal inflammation. MiR-150$^{-/-}$ mice also had increased numbers of degenerated retinal capillaries compared to WT mice. Our findings indicate that deletion of miR-150 exacerbates DR by promoting retinal inflammation and microvascular degeneration.

[1] Yu, F., et al., *Decreased miR-150 in obesity-associated type 2 diabetic mice increases intraocular inflammation and exacerbates retinal dysfunction.* BMJ Open Diabetes Res Care, 2020. **8**(1).

2.2. Introduction

The incidence of diabetes is projected to rise to 33% of the US population by 2050 owing to the obesity epidemic [31], of which 95% of diabetic patients will have type 2 diabetes (T2D) [213]. More than 85% of T2D patients have diabetes-related eye disorders, and 60% develop diabetic retinopathy (DR), the leading cause of blindness in US adults age 20 to 74 [32, 213]. Clinically, DR has been diagnosed and treated as a vascular disease. While anti-vascular endothelial growth factor (VEGF) treatments significantly improve the outcomes of DR, nearly 30% of patients do not respond to anti-VEGFs [214], making development of new treatment strategies imperative. Chronic inflammation is a hallmark of obesity and T2D [215] and a well-accepted major contributor to DR [216-218]. While anti-inflammatory agents have been used to manage intraocular inflammation associated with DR, chronic administrations of anti-inflammatory agents systemically or intravitreally further cause ophthalmic complications such as cataract or steroid-induced glaucoma [102]. Thus, finding other alternatives to mitigate the progression of DR is an imperative medical need.

MicroRNAs (miRs) are short non-coding RNAs that form complexes with RNA binding proteins to suppress the expression of targeted genes through post-transcriptional mechanisms [156]. They represent a set of modulators that can regulate metabolism, inflammation, and angiogenesis [198] and have been linked to DR [189, 191, 219-222]. Among them, there is a strong inverse correlation between miR-150 and patients with diabetes, and DR. Serum miR-150 is decreased in patients with obesity [168, 186], T1D [187, 223], or T2D [168, 224], which is correlated with increased inflammation and

upregulation of angiogenic factors. We and others have reported that miR-150 is significantly decreased in the blood, heart, and retina in experimental animals with streptozotocin-induced T1D [191, 221] or obesity-associated T2D [189]. MiR-150 exhibits dual anti-inflammatory [198] and anti-angiogenic [189, 197, 225] actions. Overexpression of miR-150 suppresses the expression of pro-inflammatory factors including NF-κB, tumor necrosis factor-α (TNF-α), interleukin-1β (IL-1β), and IL-6 [198, 226, 227]. MiR-150 dampens the expression of several angiogenic factors as well as VEGF receptor 2 (VEGFR2) [189, 197, 225], the major VEGFR that promotes angiogenesis and DR [228-230]. Deletion of miR-150 augments lipopolysaccharide-stimulated inflammatory responses [198]. Intraocular injection of miR-150-mimics significantly reduces retinal angiogenesis and pathological neovascularization in animals with oxygen-induced retinopathy (OIR) and laser-induced choroidal neovascularization [192, 197]. These data support the anti-angiogenic and anti-inflammatory roles of miR-150. However, whether the diabetes-associated decrease of miR-150 contributes to the DR pathogenesis or it is merely in parallel with inflammation and microvascular complications in DR remains unclear.

We and others previously used a high-fat diet (HFD)-induced T2D mouse model to mimic human obesity-associated T2D [74, 189, 198, 231]. Mice fed with a diet with 60% calories from fat quickly become obese and further develop hyperglycemia, insulin resistance, and glucose-intolerance, hallmarks of T2D, compared to the control mice fed with normal chow (14% fat calories) [74, 198, 232-234]. These mice have intraocular inflammation with elevated NFκB (pP65) and other pro-inflammatory factors (including IL6, IL12, G-CSF, MCP-1, VEGF) [74] in addition to the commonly observed systemic

inflammation [198, 233, 234]. In pre-diabetic and early diabetic humans and rodents, reduced electroretinogram oscillatory potentials (ERG OPs) are the first sign of troubled retinas [235, 236]. Interestingly, we found that these HFD (60% fat calories)-mice exhibit decreased ERG OPs that precede the development of T2D [74] and resembles pre-diabetic patients. These HFD-mice further develop T2D and have decreased ERG a- and b-waves [74, 231]. After 6 to 7 months of HFD regimens, microvascular complications with degenerated capillaries are apparent in these mice [74, 231], a sign of early DR [237]. Thus, this HFD-induced T2D model is a suitable model to study obesity-associated T2DR. In this report, we used a loss-of-function strategy with miR-150 knockout (miR-$150^{-/-}$) mice to determine the functional role of miR-150 in the pathogenesis of obesity-associated T2DR. If global deletion of miR-150 further exacerbates retinal dysfunction, inflammation, and microvascular complications in high-fat diet-induced T2DR, it will further strengthen the idea that decreased miR-150 under diabetic conditions may contribute to the pathogenesis of DR.

2.3. Materials and Methods

2.3.1. Animals

Four-week-old male C57BL/6J mice (wild type; WT) were purchased from the Jackson Laboratory (Bar Harbor, ME, USA). B6(C)-*Mir150*^{tm1Rsky}/J (miR-$150^{-/-}$) mice were originally purchased from the Jackson Laboratory, and a colony was bred and maintained at Texas A&M University. Only male miR-$150^{-/-}$ mice were used in this study. All animal experiments were approved by the Institutional Animal Care and Use Committee of Texas A&M University. Mice were housed under temperature and

humidity-controlled conditions with 12:12 hour light-dark cycles. All mice were given food and water *ad libitum*. To induce T2D, five-week-old male mice (WT and miR-150$^{-/-}$) were fed with an HFD (60% fat calories, 20% protein calories, and 20% carbohydrates calories; #D12492; Research Diets, New Brunswick, NJ, USA) for up to 24 weeks. Mice fed with a standard laboratory chow (controls; 10% fat calories, 20% protein calories, and 70% carbohydrates calories; #D12450J; Research Diets) were used as the control. The body weights and food intakes of the mice were recorded weekly. The T1D mouse blood was collected from mice used in a previous study, in which the blood was collected at four months after being given intraperitoneal injections of streptozotocin (STZ) [238]. Mice that received injections of citric buffer were used as nondiabetic controls.

2.3.2. Quantitative PCR

Blood was taken via the mouse ocular vein and allowed clotting at room temperature for 30 minutes. After centrifuging at 2000 g for 10 minutes at 4°C, 400–500 μl serum was collected and used for the purification of miRNAs (Direct-zol™ RNA Kit; Zymo Research, Irvine, CA, USA). Quantitative PCR (qPCR) was performed using TaqMan miRNA assay kits (Thermo Fisher Scientific, Waltham, MA, USA) and Taqman qPCR master mix (Thermo Fisher Scientific). Specific primers and probes for mmu-miR-150-5p (5’ UCUCCCAACCCUUGUACCAGUG 3’) were purchased from Life Technologies/Thermo Fisher Scientific. Cel-miR-39 (Life Technologies/Thermo Fisher Scientific) was used as the spike-in control. A standard curve of the cycle values with the corresponding quantities of miRNA was generated using the serial dilutions of

miRNA (1 ×, 2 ×, 4 ×, 5 ×, 8 ×, and 10 ×). The quantities of sample miRNAs were generated by fitting their cycle values into the standard curve.

2.3.3. *In situ* Hybridization

The eye sections from a patient with proliferative DR (PDR) and an age-matched donor without DR were provided by Dr. Robert Rosa Jr. at Baylor Scott and White Health (Temple, TX). The miRCURY LNA miRNA detection probes (Qiagen; Germantown, USA) were used to detect miR-150 according to the manufacturer's instructions. Briefly, the sections were deparaffinized and incubated with proteinase K at 37°C for 10 minutes. The digoxigenin (DIG)-labeled miR-150 probes (1-5nM) in incubation buffer (2xSSC, 1XDenhardt's solution, 1mg/ml yeast tRNA, 50% formamide, 10% Dextran) were hybridized with the sections at 55°C for 1 hour, the sections were washed with a series of saline-sodium citrate (SSC) buffer (2x, 1x and 0.1x), blocked and incubated with alkaline phosphatase (AP) conjugated anti-DIG antibodies (1/1000, Roche, Mannheim, Germany). The signal was visualized by 4-nitro-blue tetrazolium (NBT) and 5-bromo-4-chloro-3'-indolylphosphate (BCIP) (Roche, Mannheim, Germany) according to the manufacturer's manual. The nuclei were counterstained with nuclear fast red. The slides were then dehydrated and mounted. The images were taken using a Zeiss Axioplan microscope (Carl Zeiss Microscopy, White Plains, NY, USA).

2.3.4. Glucose Tolerance and Insulin Resistance Tests

Mice were fasted for 8 hours and given D-glucose (Sigma-Aldrich Corp., St. Louis, MO, USA) at a dosage of 2 g/Kg bodyweight or insulin (Life Technologies/Thermo Fisher Scientific) at a dosage of 1 U/Kg of bodyweight through

intraperitoneal injections. Blood glucose levels were measured from the tail vein using Clarity Plus blood glucose monitoring system (Diagnostic Test Group/VWR, Radnor, PA, USA) at 0, 30, 60, 90, and 120 minutes following the glucose injection and at 0, 15, 30, 45, 60 minutes following the insulin injection.

2.3.5. Electroretinogram (ERG)

Mice were kept in darkness for at least 6 hours before the ERG recordings. Mice were anesthetized with an intraperitoneal injection of Avertin (2% 2,2,2-tribromoethanol, 1.25% tert-amyl alcohol; Thermo Fisher Scientific) solution (12.5 mg/ml) at a dosage of 20 μl/g bodyweight and placed on a heating pad to maintain body temperature. Pupils of the mice were dilated by applying a drop of 1% tropicamide/2.5% phenylephrine mixture on the eyes for 5 minutes. The ground electrode was placed on the tail, the reference electrodes were placed under the skin below the eyes, and the recording electrodes conjugated with the mini contact lenses (OcuScience, Henderson, NV, USA) were placed on the cornea. A drop of Goniovisc (Hub Pharmaceuticals, Rancho Cucamonga, CA, USA) was applied to the cornea to maintain proper contact between the cornea and the recording electrode. A portable ERG device (OcuScience) was used for the ERG recordings. The retinal light responses were recorded after four repeated light flashes at lower intensities (0.1, 0.3, 1.0, and 3.0 cds/m^2) and after a single light flash at higher intensities (10 and 25 cds/m^2). There was a 1-minute recovery period between different light intensities. The amplitudes and implicit times of a-wave, b-wave, and oscillatory potentials (OPs) were analyzed by using the ERGView 4.4 software (OcuScience).

2.3.6. Immunohistological Staining

Mouse eyes were collected and fixed with 4% paraformaldehyde and processed for paraffin-embedded sectioning after 24 weeks of the food regimen. Paraffin sections (4 μm) of the mouse eyes from all four experimental groups were mounted on the same slide. After deparaffinization, sections were permeabilized in citrate buffer (pH 6.0) at 80° for 1 hour. Sections were then blocked with 10% goat serum for 2 hours at room temperature and incubated with anti-phospho ERK (cat. 4370, Cell Signaling, Danvers, MA, USA) or anti-phospho NFκB P65 (cat. 3033, Cell Signaling) overnight at 4°C. After washing with PBS, sections were incubated with Alexa Fluor 488/568 goat anti-rabbit IgG (1:50 dilution; Molecular Probes/Life Technologies/Thermo Fisher Scientific, Grand Island, NY, USA) for 2 hours at room temperature and mounted with ProLong Gold antifade reagent containing 4′,6′-diamidino-2-phenylindole (DAPI; Invitrogen/Life Technologies/Thermo Fisher Scientific). Images were obtained using a Zeiss Stallion digital imaging workstation equipped with a Zeiss Axiovert 200M microscope under identical settings. The average fluorescence intensity was measured in the outer and inner segments of photoreceptors by ImageJ (National Institutes of Health, Bethesda, MD, USA).

2.3.7. Retinal Vasculature Morphological Analysis

Mouse eyes were collected and fixed with 4% paraformaldehyde at 4°C for 20 hours. The whole retinas were excised and kept in distilled water with gentle rocking overnight at room temperature. The retinas were then incubated with 3% trypsin (BD Biosciences, Franklin Lakes, NJ, USA) for 1.5 hours at 37°C, followed by washing with

distilled water by gentle pipetting to remove the neural tissue. The remaining network of retinal vasculature was carefully transferred to a glass slide and flattened. After staining with hematoxylin and eosin (H&E), the images of the retinal vasculature were taken using a Zeiss Axioplan microscope. The numbers of degenerated vessels were counted within 3-4 randomly chosen regions from each retina. The vascular areas were analyzed using AngioTool [239].

2.3.8. Statistical Analysis

All data are presented as mean ± SE of the mean (SEM). Student's *t*-test, one-way, or two-way analysis of variance (ANOVA) followed by Fisher's *post hoc* test was used for statistical analyses among groups whenever appropriate. Throughout, $p < 0.05$ was regarded as significant. Origin 8.6 (OriginLab, Northampton, MA, USA) was used for statistical analyses.

2.4. Results

2.4.1. Decreased microRNA-150 in the Retina is Associated with Diabetes

Using *in situ* hybridization, the retina from a patient with PDR had decreased miR-150 qualitatively compared to the age-appropriated donor without DR (Fig. 2-1A). This indicates that either decreased miR-150 is associated with DR, or decreased miR-150 might contribute to the pathogenesis of DR. We next used both T2D and T1D mouse models to determine if miR-150 would be decreased in the retinas. We compared the levels of miR-150 in WT mice fed with the HFD (60% fat calories) and the control fed with normal chow. One month after the diet regimen, miR-150 was significantly

decreased in the blood circulation and neural retina of HFD-mice compared to the control (Fig. 2-1B), but by this time, HFD-mice were only obese but not diabetic, since

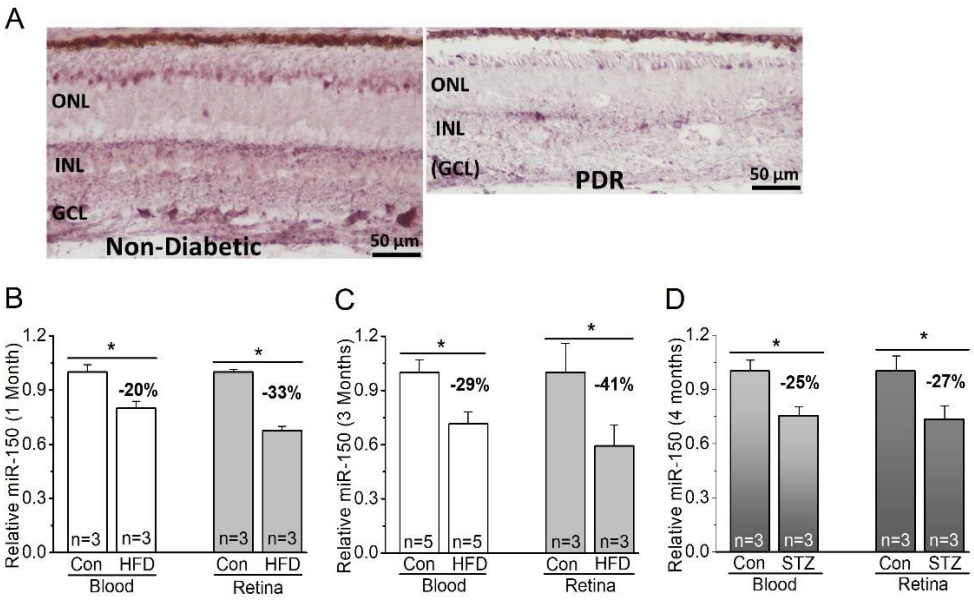

Figure 2-1 MiR-150 is decreased in the diabetic eyes.
(A) The *in situ* hybridization of miR-150 on retinal sections from a non-diabetic age-matched donor (left) and from a patient with PDR (right) shows a qualitative decrease of miR-150 in the retina of PDR. (B-D) The blood serum (blood) and retina were collected from mice to detect the levels of miR-150. (B and C) MiR-150 is decreased in the serum and retina of mice fed with a high-fat diet (HFD) compared to the control mice fed with a normal chow (Con) for 1 month (B) or for 3 months (C). (D) Using the STZ-induced T1D mouse model, 4 months after the STZ-injections, the STZ-T1D mice (STZ) also have decreased miR-150 in the serum and retina compared to the control mice injected with the citric buffer (Con). Student's t-test, *$p < 0.05$. ONL, outer nuclear layer. INL, inner nuclear layer. GCL, ganglion cell layer.

their blood glucose levels were still normal as the control [74] (Fig. 2-2). Three months after the diet regimen, miR-150 was further decreased in the HFD-mice (Fig. 2-1C), and HFD-mice started to display characteristic T2D (Fig. 2-2). We noticed that the HFD-induced decrease of miR-150 in the retina was more severe than that in the blood circulation. As a comparison, we also induced T1D in mice by STZ injections. Four months after STZ-injections, mice with T1D also showed decreased miR-150 in both

blood circulation and the retina (Fig. 2-1D). Hence, the decrease of miR-150 is associated with obesity and diabetic conditions. To further determine whether decreased miR-150 contributed to obesity-associated T2D, we examined if global deletion of miR-150 might exacerbate obesity-associated T2D and DR.

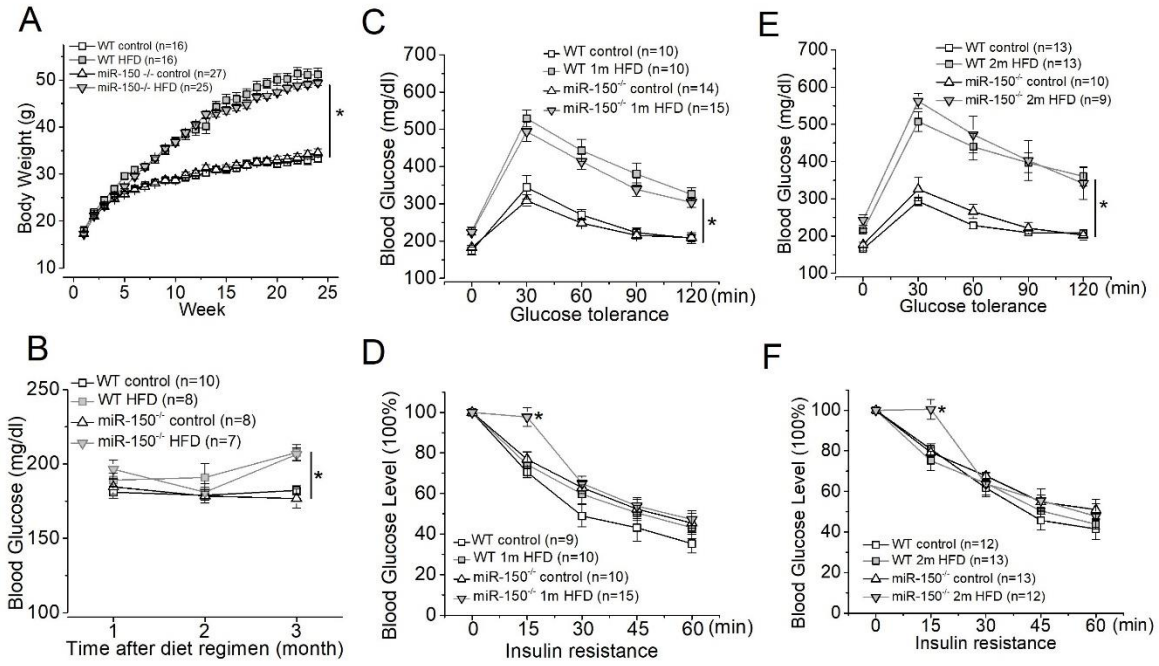

Figure 2-2 Systemic evaluations and comparisons of WT and miR-150$^{-/-}$ mice after the diet regimen.

Both WT and miR-150$^{-/-}$ mice were divided into two groups: the control group (control) fed with the normal chow, and the other group fed with the high-fat diet (HFD). (A) The body weights of mice fed with the HFD (WT HFD and miR-150$^{-/-}$ HFD) have significant weight gain compared to mice fed with the normal chow (WT control and miR-150$^{-/-}$ control). (B) The system blood glucose levels of mice fed with the HFD (WT HFD and miR-150$^{-/-}$ HFD) are significantly higher and above 200 mg/dl compared to the control (WT control and miR-150$^{-/-}$ control) only after 3 months of diet regimen. (C) One month after the diet regimen, mice were tested for glucose tolerance. Mice fed with the HFD (WT 1m HFD and miR-150$^{-/-}$ 1m HFD) have a significantly higher glucose intolerance compared to mice fed with the normal chow (WT control and miR-150$^{-/-}$ control). (D) One month after the diet regimen, mice were tested for insulin resistance. MiR-150$^{-/-}$ mice fed with the HFD (miR-150$^{-/-}$ 1m HFD) show a significant difference in insulin resistance only at 15 min after insulin injections. (E) Two months after the diet regimen, mice were tested for glucose tolerance. Mice fed with the HFD (WT 2m HFD and miR-150$^{-/-}$ 2m HFD) have a significantly higher glucose intolerance compared to mice fed with the normal chow (WT control and miR-150$^{-/-}$ control). (F) Two months after the diet regimen, mice were tested for insulin resistance. MiR-150$^{-/-}$ mice fed with the HFD (miR-150$^{-/-}$ 2m HFD) show a significant difference in insulin resistance only at 15 min after insulin injections. Open square:

WT fed with the normal chow (control); shaded square: WT fed with the HFD; open triangle: miR-150$^{-/-}$ fed with the normal chow (control); shaded triangle: miR-150$^{-/-}$ fed with the HFD. One-way ANOVA with Fisher's post hoc tests, *p < 0.05.

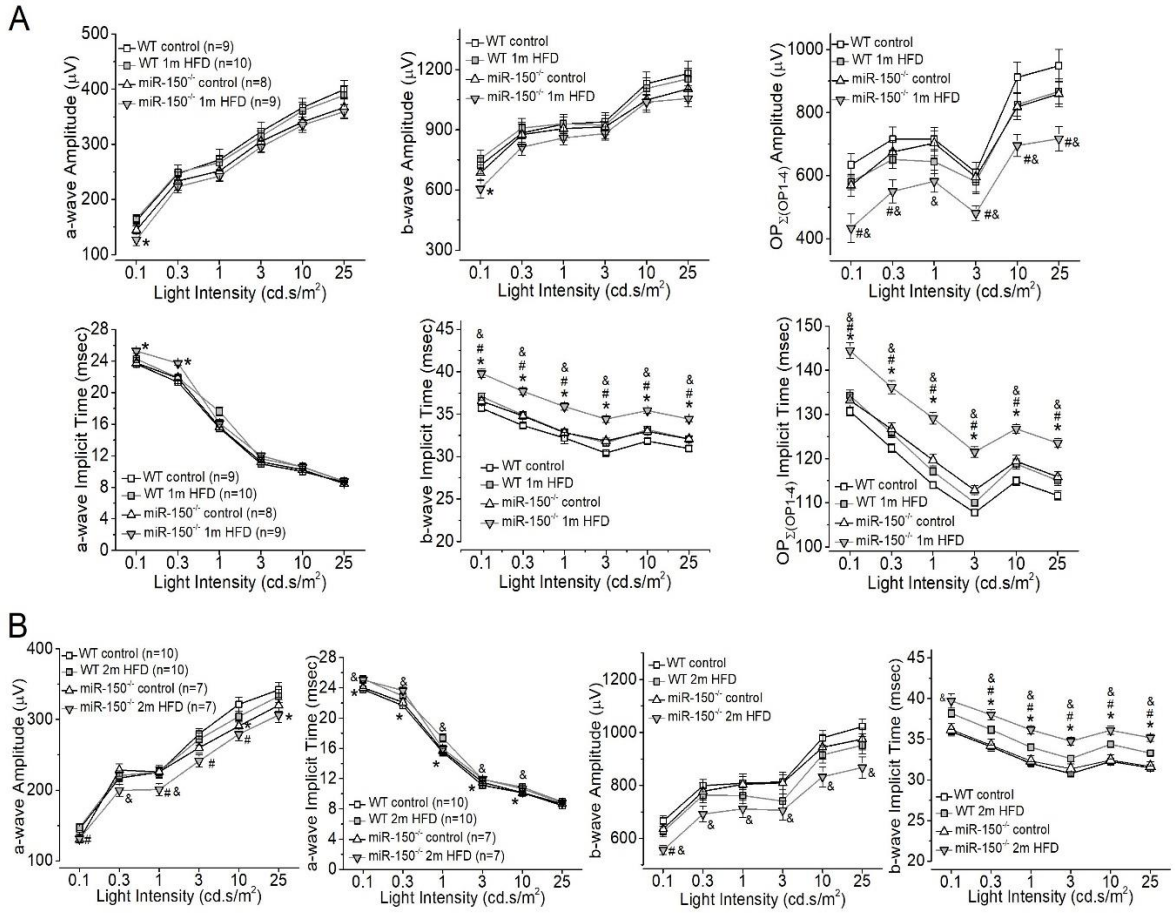

Figure 2-3 MiR-150$^{-/-}$ mice fed with the HFD for only one or two months have compromised retinal light responses.

After 6 hours in complete darkness, dark-adapted ERGs with series of flashlights (0.1, 0.3, 1, 3, 10, and 25 cd.s/m^2) were recorded from all four experimental groups. The amplitudes and implicit times of ERG a-wave, b-wave, and oscillatory potentials (OP1 to OP4) were measured and analyzed. (A) The ERG amplitudes (upper panel) and implicit times (lower panel) of a-wave, b-wave, and summation (∑) of OP1-OP4 from mice after one month of the diet regimen are shown. (B) Two months after the diet regimen, the ERG amplitudes and implicit times of a-wave and b-wave are shown. * indicates a significant difference between the WT HFD group and the miR-150$^{-/-}$ HFD group; # indicates a significant difference between the miR-150$^{-/-}$ control group and the miR-150$^{-/-}$ HFD group; & indicates a significant difference between the WT control group and the WT HFD group; $ indicates a significant difference between the miR-150$^{-/-}$ control group and the WT control group. One-way ANOVA with Fisher's *post hoc* tests, *p < 0.05. ERG, electroretinogram; HFD, high-fat diet.

We monitored WT and miR-150$^{-/-}$ mice fed with the HFD and found that 1 month after the diet HFD regimen, obese WT, and miR-150$^{-/-}$ mice already developed glucose intolerance compared to the mice fed with normal chow (control; Fig. 2-2). The insulin resistance was not developed after 2 months of the HFD. Deletion of miR-150 did not cause significantly higher hyperglycemia or worse glucose intolerance. The glucose intolerance was caused by the HFD alone at this time (two-way ANOVA analysis). Thus, the global deletion of miR-150 did not further exacerbate obesity-associated pre-diabetes at the system level. As we previously reported, mice fed with an HFD (60% fat calories) for 3 months develop T2D-like syndromes [74, 198, 231], including hyperglycemia, glucose intolerance, and insulin resistance. After 3 months of the HFD regimen, mice with whole-body knockout of miR-150 (miR-150$^{-/-}$) have significantly higher glucose intolerance, insulin resistance, as well as systemic inflammation, compared to the WT with an HFD [198], indicating that miR-150 regulates obesity-induced inflammation. However, the biological processes mediated by microRNAs and their targets are often cell type or tissue-dependent [211, 212]. While miR-150 is abundant in circulating blood, it is also expressed in the neural retina [219, 240]. It is possible that the deletion of miR-150 might impact various tissues and organs differently. We next examined whether deletion of miR-150 might affect the function of the neural retina early in mice fed with an HFD.

2.4.2. The Retinal Light Responses are Compromised in miR-150$^{-/-}$-HFD Mice

One month after the diet regimen, mice were examined with a series of light flashes after they were dark-adapted for a few hours. Regardless of mice fed with an HFD or

normal chow (control), WT and miR-150$^{-/-}$ mice have similar amplitudes in light responses shown in both a-wave and b-wave ERG amplitudes in all four groups (Fig. 2-3). However, there was a significant delay in the light responses from miR-150$^{-/-}$ mice fed with the HFD for 1 month (miR-150$^{-/-}$ 1m HFD), as the b-wave implicit times of miR-150$^{-/-}$-HFD mice were significantly higher than the other three groups. After two months of the diet regimen, miR-150$^{-/-}$-HFD mice had significantly decreased ERG a-wave and b-wave amplitudes. We further analyzed the oscillatory potentials (OPs) and found that the OP amplitudes and implicit times were recorded from miR-150$^{-/-}$ mice fed with the HFD for one month (miR-150$^{-/-}$ 1m HFD) were significantly aggravated compared to the other three groups (Fig. 2-3). As a delayed OP latency (higher implicit time) is the first sign of dysfunction in prediabetic/early diabetic retinas in both rodents and humans [236, 241], our data suggest that deletion of miR-150, especially in the neural retina, might have detrimental impacts in obese and pre-diabetic animals that potentially lead to the development of T2DR.

2.4.3. Deletion of miR-150 Exacerbates Retinal Inflammation in Obesity-associated type 2 diabetic (T2D) mice

We previously showed that mice fed with the HFD for 6 months have a significant increase in intraocular inflammation [74, 231]. Since miR-150 is a suppressor of pro-inflammatory factors [198, 226, 227, 242-244], we postulated that deletion of miR-150 would further increase inflammation in the retina. MiR-150$^{-/-}$ mice fed with the HFD (miR-150$^{-/-}$ HFD) for 6 months had the highest signal of activated/phosphorylated P65 (pP65), a subunit of NFκB transcription complex and a biomarker for inflammation [245], compared to the mice fed with normal chow or WT mice fed with the HFD (Fig. 2-4). Similarly, the

signal of activated/ phosphorylated extracellular signal-regulated kinase (ERK), upstream signaling of NFκB leading to inflammation, was also highest in the retina of miR-150$^{-/-}$ mice fed with the HFD (miR-150$^{-/-}$ HFD). These data echoed previously published results that miR-150$^{-/-}$ mice fed with the HFD for 3 months have the highest systemic inflammation [198]. Inflammation is a major culprit contributing to vascular problems of DR, and if deletion of miR-150 caused higher inflammation in obese-T2D mice, we hypothesized that HFD-induced DR in miR-150$^{-/-}$ mice would develop more severe microvascular complications compared to that in the WT.

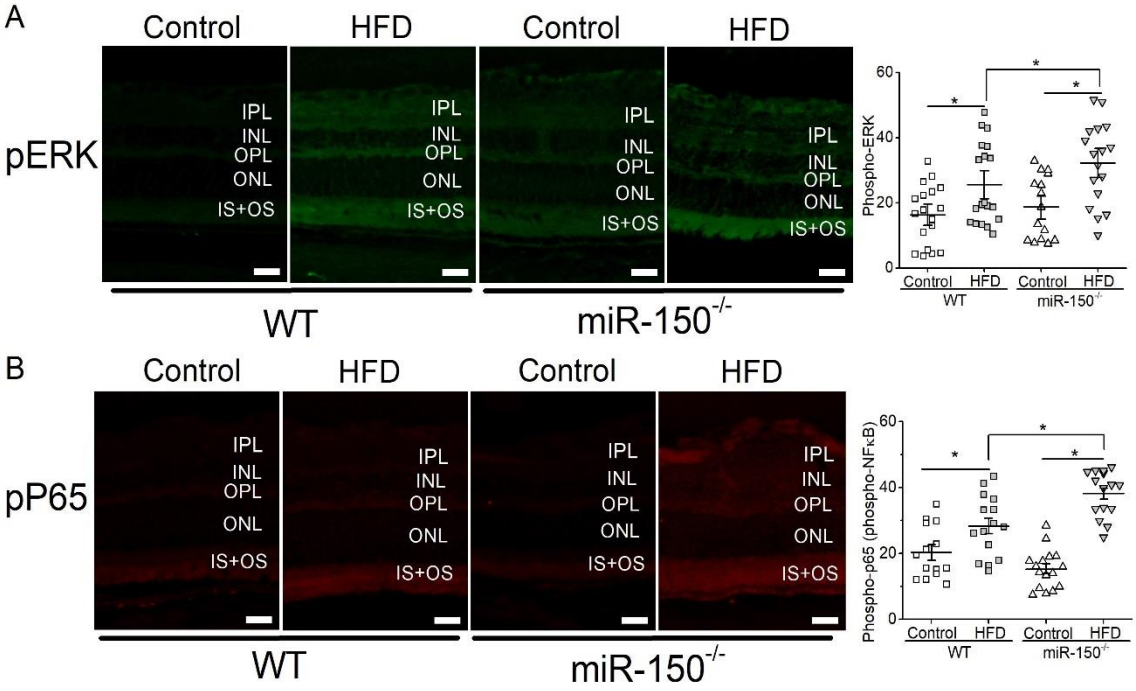

Figure 2-4 MiR-150 knockout exacerbates HFD-induced retinal inflammation.
Six months after the diet regimen, the retinal sections were processed for immunostaining of phosphorylated ERK (pERK; A) and phosphorylated NFκB subunit P65 (pP65; B). Mice fed with the high-fat diet (HFD) have significantly elevated pERK and pP65 compared to mice fed with the normal chow (Control). In addition, the miR-150$^{-/-}$ -HFD mice have significantly higher pERK and pP65 signals compared to the WT-HFD mice. Each data point represents one area of measurement. n=3 mice for each group; scale bar=20 μm. Two-way ANOVA with Tukey *post hoc* tests, *$p < 0.05$. ERK, extracellular signal-regulated kinase; NF-kB, nuclear factor kappa B

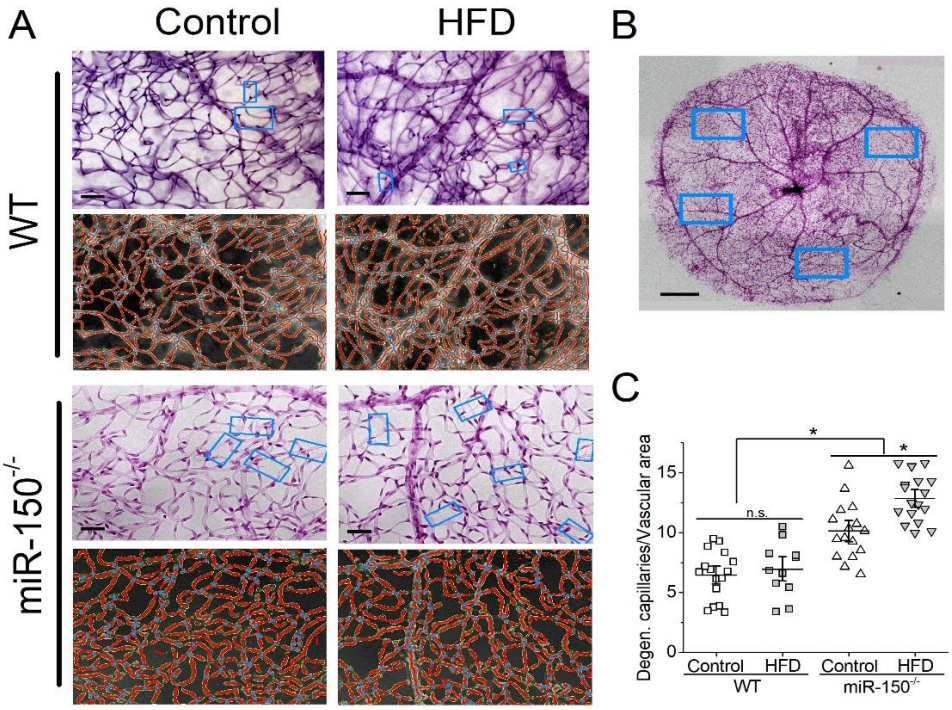

Figure 2-5 Global knockout of miR-150 further promotes degeneration of retinal capillaries.

Six months after the diet regimen, the whole mount retinas were processed and analyzed for microvasculature morphology. (A) Representative images from trypsin-digested and stained retinal vasculature (rows 1 and 3) with AngioTool rendered images (rows 2 and 4) from the WT (rows 1 and 2) and miR-150$^{-/-}$ (rows 3 and 4) fed with the normal chow (Control) or the high-fat diet (HFD) are shown. The light blue rectangular boxes indicate the degenerated/acellular capillaries. scale bar=20 µm. (B) A representative image of a whole-mount retina after trypsin digestion and staining is displayed. The blue rectangular boxes represent randomly selected areas from the whole-mount retina that were used for analyses. scale bar=50 µm. (C) There is no significant difference between the WT fed with the normal chow (Control) or the HFD (HFD), even though the HFD group has a slightly higher density of degenerated capillaries. The miR-150$^{-/-}$ mice have significantly higher densities of degenerated capillaries compared to the WT mice, and the miR-150$^{-/-}$ mice fed with the HFD have even more degenerated capillaries compared to the miR-150$^{-/-}$ mice fed with the normal chow (Control). Each data point represents one analyzed area. Each whole-mount retina has 3-4 randomly chosen areas. The vascular area was measured using the AngioTool. Each group has n=3 mice analyzed. Two-way ANOVA with Fisher's *post hoc* tests, * $p < 0.05$.

2.4.4. Deletion of miR-150 Causes Increased Degeneration in Retinal Microvasculature

We previously showed that the retinal dysfunction occurs after one month of HFD [74] (Fig. 2-3), but it takes at least 6 months of the HFD regimen to induce microvascular

complications in this obesity-associated T2DR animal model shown as mice fed with the HFD having a higher fluorescent leakage [74]. After mice were fed with the HFD for 6 months, we examined retinal capillaries and found that miR-150$^{-/-}$ mice had higher densities of degenerated retinal capillaries compared to the WT regardless of the diets (Fig. 2-5), which is a surprise. This data indicates that miR-150 might contribute to maintaining the health of retinal microvasculature. Furthermore, miR-150$^{-/-}$-HFD mice had significantly higher densities of degenerated capillaries compared to the miR-150$^{-/-}$ mice fed with the normal chow (miR-150$^{-/-}$, control). Using two-way ANOVA analysis, both HFD and deletion of miR-150 had significant impacts on retinal capillary degeneration, and there was an interaction between HFD and miR-150 deletion. Thus, deletion of miR-150 further exacerbates obesity-associated T2DR microvascular complications.

2.5. Discussion

While DR is diagnosed and treated as a chronic vascular disease, the neural retina displays changed physiology in the pre-diabetic or early diabetic stage with one of the earliest signs being altered ERG OPs [236, 241]. We previously demonstrated that one month after the HFD regimen, these obese mice already have decreased OP amplitudes and increased OP implicit times, even though their blood glucose levels are normal [74]. In this report, we showed that after one month of HFD, while the WT-HFD mice also showed decreased OP amplitudes and increased OP implicit times, miR-150$^{-/-}$-HFD mice had further changed OPs, even though there was no significant difference in systemic metabolic measures (glycemia, glucose-intolerance, and insulin-resistance) between WT-HFD and miR-150$^{-/-}$-HFD mice. MiR-150 is present abundantly in the blood circulation and is

expressed in the retina. However, compared to the WT-HFD mice, data from miR-150$^{-/-}$-HFD mice after one month of HFD suggest that decreased miR-150 might already contribute to the retinal dysfunction at obese and pre-diabetic stages. The adverse impact of decreased miR-150 might be greater locally in the retina than globally in the whole body in obesity-associated T2D.

MiR-150 has both anti-inflammatory [198, 226, 227, 242-244] and anti-angiogenic [189, 197, 225] actions, as overexpression of miR-150 dampens the expression of several pro-inflammatory and pro-angiogenic factors. In a mouse model of oxygen-induced retinopathy (OIR), the intraocular injection of miR-150 mimics suppresses the pathological ocular neovascularization [197]. The importance of miR-150 in anti-inflammation and anti-angiogenesis is further verified in miR-150$^{-/-}$ mice with obesity-associated T2D after several months of HFD. These miR-150$^{-/-}$-HFD mice have significantly higher systemic [198] and retinal (Fig. 2-4) inflammation compared to the WT-HFD mice, and they also have significantly more degenerated capillaries compared to the WT-HFD mice (Fig. 2-5). These data suggest that the diabetes-caused decrease of miR-150 is not simply associated with the disease progression, decreased miR-150 in diabetic insults might contribute to the development of DR. Thus, the next step is to determine whether administration with miR-150 might alleviate or dampen the progression of DR.

MicroRNAs regulate the downstream targets by binding to their 3'-untranslated regions (3'-UTRs), degrading, and preventing the translation of target genes. Decreased miR-150 will cause the increase of its target genes, such as *c-Myb*, *Etf1*, and *Elk1*, that promote the expression of inflammatory factors including tumor necrosis factor-α (TNFα)

and interleukin-1β [198]. In addition, miR-150 can suppress the expression of angiogenic genes, including *Cxcr4*, *Dll4*, and *Fzd4* [197]. We previously showed that miR-150 down-regulates the VEGF receptor 2 (VEGFR2) expression in cultured endothelial cells [189]. However, there is no match in sequences between miR-150 and 3'-UTR of VEGFR2, so the action of miR-150 in inhibiting VEGFR2 expression might be indirectly through other factors, possibly *c-Myb*. Therefore, increased miR-150 may inhibit the vascular pathologies of DR by downregulating the angiogenic genes. By targeting the pro-inflammatory and angiogenic genes, miR-150 may alleviate the progression of DR.

MicroRNAs have been indicated as possible biomarkers for diseases or potential therapeutic targets to treat diseases including diabetes and DR. While many miRs are associated with disease conditions, very few are investigated in the mechanistic studies of disease pathogenesis. In addition to miR-150, both miR-15a and miR-146a are downregulated in the retinal endothelial cells isolated from diabetic patients [246, 247]. Overexpression of endothelial miR-15a or miR-146a in mice significantly dampens diabetes-induced inflammation in the retina and prevents vascular damages [247, 248]. Thus, we postulate that overexpression of miR-150 might be able to dampen diabetes-caused vascular complications similar to that of miR-15a and miR-146a because miR-150 is also expressed in the endothelial cells [197]. On the contrary, miR-21 is upregulated in the diabetic retina [249], and downregulation of miR-21 has been shown to dampen diabetes-associated inflammation [250]. MicroRNAs normally form complex networks to regulate physiology, metabolism, and biological processes [212], so obesity or pre-diabetic conditions can dysregulate multiple miRs that leads to the progression of DR. We cannot

rule out the possibility that miR-150 might synergistically act together with other miRs such as miR-15a and miR-146a and antagonistically with miR-21 to maintain the health of retina and vasculature. As we showed that even in obese and pre-diabetic conditions, miR-150 was already decreased in the retina and blood circulation, and decreased miR-150 was strongly correlated with retinal dysfunction and vascular pathology, our results suggest that early intervention with miR-150 might alleviate or slow down the burden of DR progression. The idea of using miR-150 or multiple miRs for therapeutics to treat or prevent DR is worth future investigation.

3. DECREASED MICRORNA-150 EXACERBATES NEURONAL APOPTOSIS IN THE DIABETIC RETINA[2]

3.1. Overview

Diabetic retinopathy (DR) is a chronic complication associated with diabetes and the number one cause of blindness in working adults in the US. More than 90% of diabetic patients have obesity-associated type 2 diabetes (T2D), and 60% of T2D patients will develop DR. Photoreceptors undergo apoptosis shortly after the onset of diabetes, which contributes to retinal dysfunction and microvascular complications leading to vision impairment. However, how diabetic insults cause photoreceptor apoptosis remains unclear. In this study, obesity-associated T2D mice and cultured photoreceptors were used to investigate how decreased microRNA-150 (miR-150) and its downstream target were involved in photoreceptor apoptosis. In the T2D retina, miR-150 was decreased with its target ETS-domain transcription factor (ELK1) and phosphorylated ELK1 at threonine 417 ($pELK1_{T417}$) upregulated. In cultured photoreceptors, treatments with palmitic acid (PA), to mimic a high-fat environment, decreased miR-150 but upregulated ELK1, $pELK1_{T417}$, and the translocation of $pELK1_{T417}$ from the cytoplasm to the cell nucleus. Deletion of miR-150 ($miR\text{-}150^{-/-}$) exacerbates T2D- or PA-induced photoreceptor apoptosis. Blocking the expression of ELK1 with small interfering RNA (siRNA) for *Elk1* did not rescue PA-induced

[2] Yu, F., M.L. Ko, and G.Y.P. Ko, *Decreased MicroRNA-150 Exacerbates Neuronal Apoptosis in the Diabetic Retina*. Biomedicines, 2021. **9**(9).

photoreceptor apoptosis. Translocation of pELK1$_{T417}$ from cytoplasm to nucleus appears to be the key step of diabetic insult-elicited photoreceptor apoptosis.

3.2. Introduction

Diabetic retinopathy (DR) is a chronic complication associated with type 1 and type 2 diabetes (T1D, T2D). It impacts 4.2 million people in the US and 93 million people worldwide [29]. About 95% of diabetic patients have T2D, and 60% of T2D patients develop DR in their lifetime [32]. Patients with DR have impaired neural retinas and vascular integrity, which leads to vision loss and blindness [34]. Intraocular injections of anti-vascular endothelial growth factor (VEGF) agents are currently the most effective therapy for inhibiting the angiogenesis seen in DR [251], but less than 50% of patients have improved vision after 1–2 years of anti-VEGF injections [39]. In general, the current therapies for DR mainly target the ocular neovascularization at the later stages of DR when the visual function is already damaged and difficult to restore [252]. Therefore, it is important to investigate the pathological process in the neural retina at the early stages of DR to develop new therapeutic strategies in the future.

In the diabetic retina, neural dysfunction and degeneration occur early in the development of DR. Patients with T1D have thinner neural layers in the retina and visual dysfunction before the diagnostics of DR [60]. Adolescents with T2D for an average of two years have reduced retinal thickness and dampened light responses [61]. The loss of retinal neurons starts from 10 weeks after streptozotocin (STZ)-induced T1D in mice [70], and neuronal apoptosis in the retina occurs in T2D (db/db) mice from 20 weeks of age [78]. Among retinal neurons, photoreceptors undergo apoptosis shortly after the

onset of diabetes [76, 253]. Apoptotic photoreceptors can be detected in STZ rats 4 weeks after the onset of diabetes [76]. In addition, the dysfunction of photoreceptors in STZ mice is associated with the reduced thickness of the outer nuclear layer (ONL) [254]. Furthermore, diabetic patients with retinitis pigmentosa (RP), a genetic disease with loss of photoreceptors, rarely develop DR, even though these patients develop other diabetes-related vascular diseases [255, 256]. In a mouse model of RP, during the period when photoreceptors are undergoing apoptosis, the retinal vasculature is also degenerating. Once the photoreceptors are completely lost, the vascular degeneration stops [257]. Hence, photoreceptor apoptosis not only contributes to the neural dysfunction under diabetes but may also adversely impact diabetic microvascular complications [257]. However, how diabetic insults cause photoreceptor apoptosis remains unclear.

MicroRNAs (miRs) represent a set of regulators that impact cell proliferation and apoptosis, and diabetes-associated changes in miR levels have been linked to the development of DR [187]. Among them, downregulation of miR-150 is observed in diabetic patients with DR [167], as well as in the plasma and retina of diabetic animals [190]. Inhibition of miR-150 promotes apoptosis [193], while overexpression of miR-150 alleviates the apoptosis of cells under hypoxia [194], and local hypoxia also occurs in the diabetic retina [195, 196]. ETS-domain transcription factor (*Elk1*) is a confirmed target gene of miR-150 that is linked to apoptosis since overexpression of ELK1 protein has been found to promote apoptosis in neurons [205]. Transfection of *Elk1* in the dendrites of primary neurons induces apoptosis [206], while inhibition of *Elk1* alleviates

the apoptosis of neurons under oxygen-glucose deprivation [207]. In addition, phosphorylated ELK1 at threonine 417 ($pELK1_{T417}$) is essential for ELK1-mediated neuronal apoptosis [258]. However, it is unclear whether miR-150 and *Elk1* mediate neural apoptosis in the diabetic retina.

In our obesity-associated T2D mouse model induced by a high-fat diet (HFD), the miR-150 knockout ($miR\text{-}150^{-/-}$) mice fed with the HFD showed more severe retinal neural dysfunction compared with the wild-type (WT) mice fed with the HFD [189, 190]. In this study, we compared WT and $miR\text{-}150^{-/-}$ mice fed with the HFD (60% fat calories) and determined the role of miR-150 and *Elk1* in photoreceptor apoptosis induced by obesity-associated T2DR. We further used cultured 661W cells, a mouse photoreceptor cell line [259], to decipher the relationship between miR-150, *Elk1*, ELK1, and photoreceptor apoptosis. We delineated the critical cellular localization of $pELK1_{T417}$ and photoreceptor apoptosis under palmitic acid (PA), which mimics a high-fat environment for cells. Our data suggest that the cytoplasm-to-nucleus translocation of $pELK1_{T417}$ could be the key step for photoreceptor apoptosis in obesity-associated T2DR.

3.3. Materials and Methods

3.3.1. Animals

Four-week-old male C57BL/6J mice (wild type, WT) were purchased from the Jackson Laboratory (Bar Harbor, ME, USA). B6(C)-$Mir150^{tm1Rsky}$/J ($miR\text{-}150^{-/-}$) mice were originally purchased from the Jackson Laboratory, and a colony was bred and maintained at Texas A&M University (College Station, TX, USA). Only male mice were

used in this study. All animal experiments were approved by the Institutional Animal Care and Use Committee of Texas A&M University and were performed in compliance with the Association for Research in Vision and Ophthalmology (ARVO, Rockville, MD, USA) Statement for the Use of Animals in Ophthalmic and Vision Research. Mice were housed under temperature- and humidity-controlled conditions with 12:12 h of light-dark cycles. All mice were given food and water *ad libitum*. At 5 weeks of age (body weight, 20 g), mice were fed a high-fat diet (HFD; 60% fat calories, 20% protein calories, and 20% carbohydrate calories; #D12492; Research Diets, New Brunswick, NJ, USA) or a control diet (standard laboratory chow; 10% fat calories, 20% protein calories, and 70% carbohydrate calories; #D12450J; Research Diets) for up to 24 weeks. Bodyweight and food intake were measured weekly. Non-fasting blood glucose levels and glucose tolerance were measured monthly by taking blood from the tail vein. Glucose levels were measured using a Clarity BG1000 blood glucose monitoring system (Clarity Diagnostics, Boca Raton, FL, USA).

3.3.2. Cell Culture

The 661W cells [259] were originally obtained from Dr. Al-Ubaidi (University of Houston, Houston, TX, USA) and cultured in Dulbecco's modified Eagle medium (DMEM; #12-614Q, Lonza, Portsmouth, NH, USA) containing 10% fetal bovine serum (FBS; #S11550, R&D Systems, Minneapolis, MN, USA), 2 mM Glutamax (#35050-061, Gibco/ThermoFisher, Waltham, MA, USA), 100 μg/mL penicillin and 100 μg/mL streptomycin (#15140-148, Gibco/Thermo Fisher, Waltham, MA, USA), and 1 mM sodium pyruvate (#S8636, Sigma, St. Louis, MO, USA) at 37 °C and 5% CO_2. The

661W cells were treated with 100 μM palmitic acid (PA, #P5585-10G, Sigma, St. Louis, MO, USA) dissolved in 10% bovine serum albumin (BSA; #A6003-25G, Sigma, St. Louis, MO, USA) or an equal volume of 10% BSA (vehicle control) for various times as indicated.

3.3.3. Lipofectamine Transfection

Cells were transfected using the Lipofectamine 3000 kit (#L3000015, Invitrogen/Thermo Fisher) according to the manufacturer's instructions. Briefly, the 661W cells were seeded at 30% confluency and allowed to grow for 24 h to reach 50% confluency. For Western blot and quantitative real-time RT-PCR (qPCR), the cells were seeded in 6-well plates and transfected with 30 pmol/well microRNA (miRNA)/small interfering RNA (siRNA). For terminal deoxynucleotidyl transferase dUTP nick end labeling (TUNEL) and immunofluorescent staining, the cells were seeded on 12 mm circular coverslips in 24-well plates and transfected with 10 pmol/well miRNA/siRNA. After the first exchange to a normal culture medium, some cultures were immediately treated with PA or BSA for various hours. The following miRNAs/siRNAs were used in this study: miRNA negative control (#4464058, Thermo Fisher), miR-150 mimic (Assay MC10070, #4464066, Thermo Fisher), miR-150 inhibitor (Assay MH10070, #4464084, Thermo Fisher), siRNA negative control (#AM4613, Thermo Fisher), and *Elk1* siRNA (Assay 261017, #AM16708, Thermo Fisher).

3.3.4. Terminal Deoxynucleotidyl Transferase dUTP Nick end Labeling (TUNEL)

The TUNEL staining was conducted according to the manufacturer's instructions (#11684795910, Roche, Indianapolis, IN, USA). Briefly, cells cultured on coverslips

were fixed with 4% paraformaldehyde for 1 h and permeabilized with 0.1% Triton X-100 in 0.1% sodium citrate at 4 °C for 5 min. After washing with phosphate-buffered saline (PBS), 50 µL of TUNEL reaction mixture (5 µL enzyme + 45 µL label solution) was added to each coverslip and incubated at 37 °C in a humid dark chamber for 1 h. The slides were then washed with PBS and mounted with ProLong Gold antifade mountant with 4′,6′-diamidino-2-phenylindole (DAPI; #P36935, Thermo Fisher). The number of TUNEL positive ($TUNEL^+$) 661W cells were counted from 10–15 regions for each culture well and normalized to the total number of cells. After deparaffinization, the retinal sections mounted on glass slides were immersed in 0.1 M citrate buffer (pH 6.0) and microwaved at 750 W for 1 min. After blocking the slides with 5% BSA and washing with PBS, TUNEL staining was applied as described above. Images were obtained using a Zeiss Axiovert 200M microscope (Carl Zeiss AG, Oberkochen, Germany). The number of TUNEL positive ($TUNEL^+$) photoreceptors in the outer nuclear layer (ONL) of the retina was counted from 5–10 regions for each section and normalized to the ONL area.

3.3.5. The 3-[4,5-dimethylthiazol-2-yl]-2,5 Diphenyl Tetrazolium Bromide (MTT) Colorimetric Assay

The 661W cells were seeded onto 96-well plates at 5.0×10^3/well and allowed to grow for 24 h. After various experimental treatments, the proliferation/viability of 661W cells was determined by the MTT assay following the manufacturer's protocol (Chem-Impex, Wood Dale, IL, USA). In brief, cells were incubated with the MTT solution (0.5 mg/mL final concentration) for 3 h at 37 °C until a purple precipitate was visible. After

washing with PBS, 100 µL/well dimethylsulfoxide (DMSO) was added, and cells were kept in darkness at room temperature for 2 h to break the plasma membrane. The absorbance at 570 nm and the reference absorbance at 690 nm were measured with a spectrophotometer.

3.3.6. Quantitative Real-Time RT-PCR (qPCR)

After the cells were collected, total ribonucleic acid (RNA) from each sample was prepared by using a commercially available purification kit (miRNeasy mini kit; #217004, Qiagen, Germantown, MD, USA). From each sample, 500 ng of total RNA was used to quantify miR-150 or messenger RNAs (mRNAs) by qPCR using a TaqMan MicroRNA Reverse Transcription Kit (#4366596, Thermo Fisher) and SYBR green supermix ROX (#95055-500, QuantaBio, Beverly, MA, USA) with the CFX Connect Real-Time PCR Detection System (Bio-Rad, Hercules, CA, USA). The primers (Bioneer, Oakland, CA, USA) of *Elk1* (Forward 5′-GCC GGG CCT TGC GGT ACT ACT ATG A-3′, Reverse 5′-GGG TAG GAC ACA AAC TTG TAG AC-3′) and *β-actin* (Forward 5′-CAA CGG CTC CGG CAT GTG C-3′, Reverse 5′-GTA CAT GGC TGG GGT GTT GAA GGT C-3′) were used in this study.

For each experiment, a standard curve was generated with known quantities of RNAs loaded in curved dilutions (i.e., 2×, 1×, 1/2, 1/4, 1/8, 1/16, and 1/32). The cycle values, corresponding to the log values of the standard curve quantities, were used to generate a linear regression formula. The amplification efficiency of the qPCR reactions (90–100%) was calculated using the standard curve. The quantification of sample RNA was calculated by the $2^{(-\Delta\Delta Ct)}$ method [260] using *β-actin* as the internal control.

3.3.7. Western Blot

Samples for Western blots were collected, prepared, and analyzed as described previously [238, 261]. Briefly, 661W cells were harvested and lysed in a Tris lysis buffer (in mM): 50 Tris, 1 EGTA, 150 NaCl, 1% Triton X-100, 1% β-mercaptoethanol, 50 NaF, and 1 Na_3VO_4, pH 7.5. Samples were separated on 10% sodium dodecyl sulfatepolyacrylamide gels by electrophoresis and transferred to nitrocellulose membranes. The membranes were blocked in 3% BSA in tris buffered saline Tween 20 (TBST) at room temperature for 1 h and incubated in primary antibodies overnight at 4 °C. After washing with TBST, the membranes were incubated in anti-rabbit IgG horseradish peroxidase (HRP)-linked secondary antibody (1:1000, #7074S, Cell Signaling, Beverly, MA, USA) at room temperature for 1 h. The blots were visualized using Super Signal West Pico/Femto chemiluminescent substrate (#34078/#34096, ThemoFisher). Band intensities were quantified using Image J (National Institutes of Health; NIH, Bethesda, MA, USA). The primary antibodies used in this study were anti-ELK1 (1:500, #9182S, Cell Signaling) and anti-β-actin (1:2000, #8457L, Cell Signaling). The band intensities of ELK1 were normalized to those of β-actin.

3.3.8. Immunofluorescent Staining (Retina and Cultured Cells)

Mouse eyes were collected, fixed with 4% paraformaldehyde, and processed for paraffin-embedded sectioning after 24 weeks of the diet regimen. Paraffin sections (4 μm) of the mouse eyes from all four experimental groups were mounted on the same glass slide. The retina sections were deparaffinized by heating at 57 °C followed by washing with xylene and serial dilutions of ethanol. Sections were then permeabilized in

sodium citrate buffer (10 mM sodium citrate, 0.05% Tween 20, pH 6.0) at 80 °C for 1 h. The 661W cells cultured on coverslips were fixed with 4% paraformaldehyde at room temperature for 1 h and permeabilized with 0.1% Triton X-100 in 0.1% sodium citrate at 4 °C for 10 min.

Eye sections or coverslips were then blocked with 10% goat serum in PBS for 2 h at room temperature and incubated with primary antibodies overnight at 4 °C. After washing with PBS, sections or coverslips were incubated with secondary antibodies for 2 h at room temperature and mounted with ProLong Gold antifade mounted with DAPI. Images were obtained using a Zeiss Axiovert 200M microscope (Carl Zeiss AG, Jena, Germany). All fluorescent images were taken under identical settings including light intensity, exposure time, and magnification [74, 190, 238].

The fluorescent intensity was measured in the inner and outer segments of photoreceptors (IS + OS) and in the outer nuclear layer (ONL) for mouse retina sections or in the nuclear and cytoplasmic areas of 661W cells using ImageJ (NIH, Bethesda, MA, USA). The DAPI stain was used to identify the nuclear regions of the cells. The intensity of pELK1 in the cytoplasm was measured at the processes of photoreceptors that were 10 μm from the nucleus. The intensity of pELK1 in the nucleus was measured within the DAPI-stained area. We analyzed 10–15 regions for each culture well. The intensities of the ELK1/pELK1 signal in the IS + OS and ONL were measured from 5–10 regions for each retinal section.

The following primary antibodies were used: anti-ELK1 (1:50, #ab131465, abcam, Waltham, MA, USA) and anti-phospho-ELK1 (T417; 1:50, #ab194795, abcam).

The following secondary antibodies were used: goat anti-rabbit IgG (Alexa Fluor 488; 1:50, #ab150077, abcam, Irving, TX, USA) and goat anti-rabbit IgG (Alexa Fluor 568, 1:50, # ab175471, abcam).

3.3.9. Statistical Analysis

All data are presented as mean ± standard error of the mean (SEM). Student's *t*-test or one-way analysis of variance (ANOVA) followed by Tukey's *post hoc* tests were used for statistical analyses among groups. Throughout, $p < 0.05$ was regarded as significant. Origin 9.0 (OriginLab, Northampton, MA, USA) was used for statistical analyses.

3.4. Results

3.4.1. MicroRNA-150 Knockout (miR-150$^{-/-}$) Exacerbates Apoptosis in the Diabetic Retina

We previously showed that mice develop obesity-associated T2D after 3 months under the HFD [74, 190] and that these mice further develop diabetic vascular leakage and microvascular degeneration after 6 months of HFD [190, 237, 262], thus making our HFD (with 60% fat calories) mouse model suitable to study obesity-associated T2DR. As retinal neurodegeneration occurs early in the development of DR [61, 78], photoreceptors undergo apoptosis shortly after the onset of diabetes [76]. Inhibition of miR-150 is known to promote apoptosis of cells under hypoxia [193], a condition also occurs in the early diabetic retina [195]. Since miR-150 is expressed in the retina, especially in photoreceptors, and since it is decreased in early diabetic retina and blood

circulation [190], we postulated that decreased miR-150 might exacerbate the apoptosis of photoreceptors in the diabetic retina.

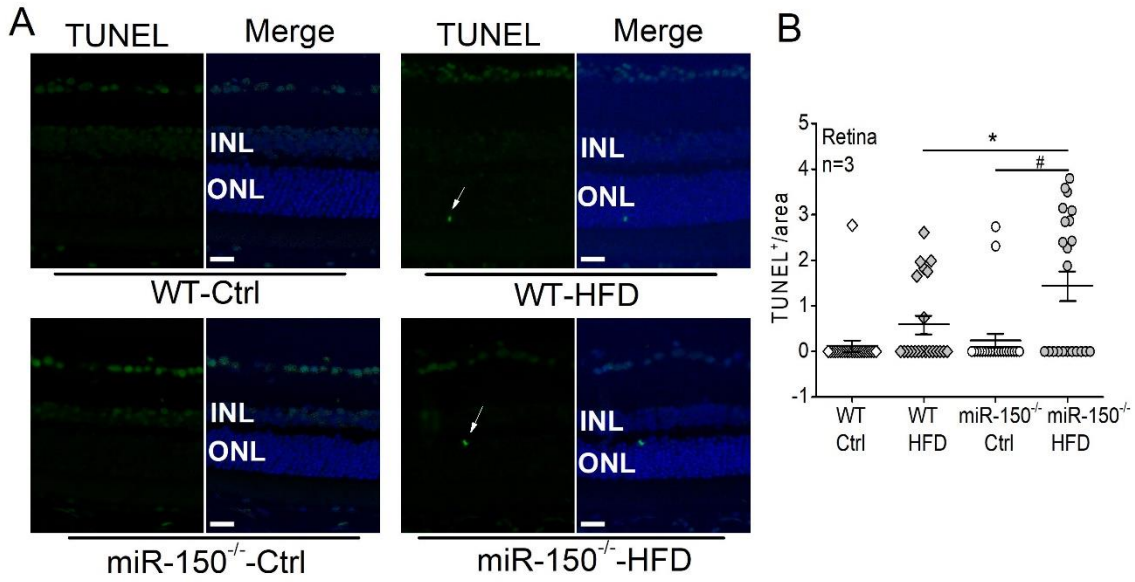

Figure 3-1 MicroRNA-150 knockout (miR-150$^{-/-}$) exacerbates apoptosis in the diabetic retina.
(**A**) Wild-type (WT) and miR-150$^{-/-}$ mice were fed on normal chow (Ctrl) or high-fat diet (HFD) for 6 months. Terminal deoxynucleotidyl transferase dUTP nick end labeling (TUNEL) staining of mouse retinal sections shows TUNEL positive (TUNEL^{+}) apoptotic cells in green fluorescence. The arrows indicate apoptotic photoreceptors in the outer nuclear layer (ONL). The 4′,6′-diamidino-2-phenylindole (DAPI; blue) stains the cell nuclei. Scale bar: 20 μm. (**B**) The number of TUNEL^{+} photoreceptors was counted and normalized to the ONL area. Each data point represents one area of measurement. * and # indicate statistical significances specified with a horizontal line. Each group has $n = 3$ (mice). $p < 0.05$, one-way ANOVA.

Six months after the diet regimen, the wild-type (WT)-HFD mice had more TUNEL positive (TUNEL^{+}) photoreceptors measured in the outer nuclear layer (ONL) than the WT mice with normal chow (WT-Ctrl; 0.59 ± 0.20 vs. 0.12 ± 0.12), even though there was no statistical significance (Fig. 3-1). However, the miR-150$^{-/-}$-HFD mouse retinas had significantly more TUNEL^{+} photoreceptors than the WT-HFD mice and mice under the normal diet (Ctrl; Fig. 3-1). These results indicate that HFD induces

more severe apoptosis of photoreceptors in the miR-150$^{-/-}$ mice than in the WT mice, so photoreceptor apoptosis under T2D conditions was exacerbated by miR-150 knockout.

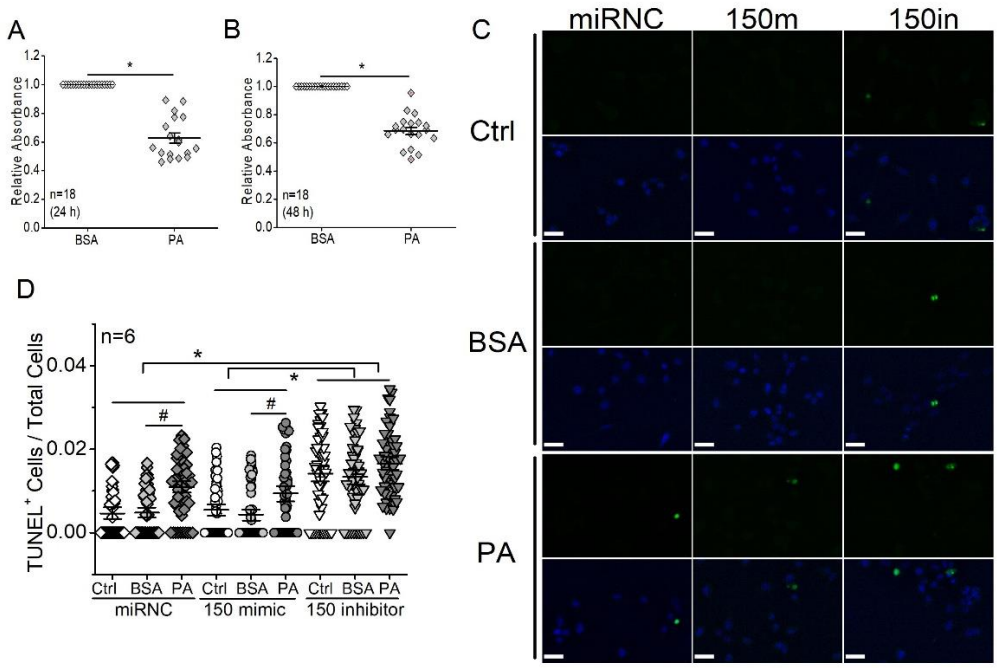

Figure 3-2 MicroRNA-150 knockdown exacerbates palmitic acid (PA)-elicited apoptosis in cultured 661W cells.
The 661W cells were treated with 100 μM PA or BSA (vehicle control) for 24 h (**A**) or 48 h (**B**). and tested cell viability with the 3-[4,5-dimethylthiazol-2-yl]-2,5 diphenyl tetrazolium bromide (MTT) colorimetric assays. n = 18 for each group. *: $p < 0.05$, Student's t-test. (**C**) The 661W cells were transfected with a microRNA negative control (miRNC), miR-150 mimic (150 m), or miR-150 inhibitor (150 in) and then treated with culture medium (Ctrl), BSA (vehicle control), or 100 μM PA (PA) for 24 h. Green fluorescence indicates TUNEL positive (TUNEL$^+$), and the blue fluorescence is DAPI staining for cell nuclei. Scale bar: 30 μm. (**D**) The number of TUNEL$^+$ 661W cells was counted and normalized to the total number of cells. Each data point represents one area of measurement**.** * indicates a statistical difference between 150 inhibitor and miRNC, as well as 150 inhibitor and 150 mimic. n = 6 for each experimental group. $p < 0.05$, one-way ANOVA.

3.4.2. MicroRNA-150 Knockdown Exacerbates Palmitic Acid (PA)-Elicited Apoptosis in Cultured 661W Cells

We next applied PA to cultured photoreceptors to mimic a high-fat environment in vitro and used MTT assays to examine the viability of cells. The 661W cells were

originally derived from a mouse retinal tumor and characterized as a cone-photoreceptor cell line for expressing opsins, transducin, and arrestin [259]. The 661W cells treated with PA (100 μM) for 24 or 48 h showed decreased viability in MTT assays compared with cells treated with bovine serum albumin (BSA; vehicle control; Fig. 3-2A, B). The decreased viability suggests increased apoptosis elicited by PA treatments.

As inhibition of miR-150 promotes cell apoptosis, we then tested whether knocking down miR-150 would exacerbate PA-elicited apoptosis in 661W cells. The 661W cells were first transfected with a miR negative control (miRNC), miR-150 mimic (150 m), or miR-150 inhibitor (150 in), then treated with culture medium (Ctrl), BSA (vehicle), or 100 μM PA for 24 h. Consistent with the earlier results (Fig. 3-2A, B), cells treated with PA had increased apoptosis compared with the BSA- or Ctrl-treated cells transfected with 150 mimic and miRNC (Fig. 3-2C, D). Interestingly, knocking down miR-150 in 661W cells (150 inhibitor) caused a significant increase in apoptosis regardless of the treatments (Fig. 3-2D). However, transfection with miR-150 mimic did not attenuate the PA-induced apoptosis. These data suggest that overexpressing miR-150 in photoreceptors alone might not be enough to overturn the PA-induced apoptosis but that an adequate level of miR-150 is necessary for the survival of photoreceptors.

3.4.3. ETS-Domain Transcription Factor 1 (*Elk1*) is a Direct Target of miR-150 and Contributes to T2D-Induced Apoptosis in Photoreceptors

We then determined how miR-150 and its target genes regulate apoptosis in photoreceptors. MicroRNAs and their targets regulate bioactivities in a cell type- and

tissue-specific manner [156, 212]. Among the major targets of miR-150 expressed in photoreceptors, *Elk1* is known to promote apoptosis in neurons [205, 206]. When 661W cells were transfected with a miR-150 mimic (150 m), the mRNA expression and protein level of *Elk1* were significantly decreased, while knocking down miR-150 (150 in) significantly increased the mRNA and protein of *Elk1* (Fig. 3-3). We further examined the protein level of ELK1 and its phosphorylation at threonine 417 ($pELK1_{T417}$) in the retinas from mice with six months of diet regimens since $pELK1_{T417}$ (the active form of ELK1) is essential for the pro-apoptotic function of ELK1 [258].

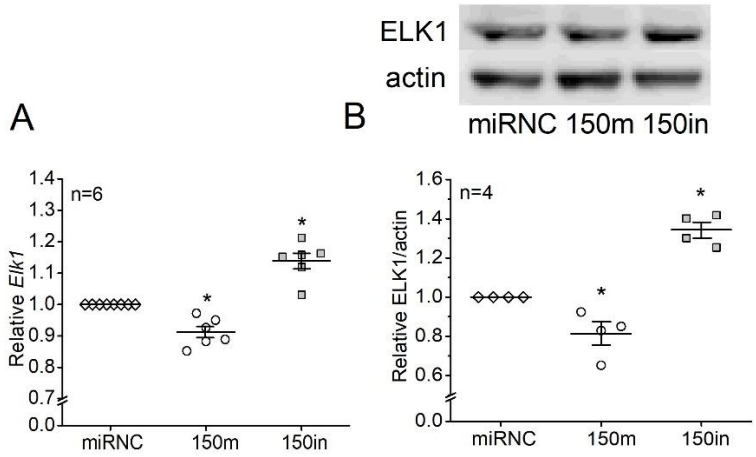

Figure 3-3 ETS-domain transcription factor 1 (*Elk1*) is a direct target of miR-150 in photoreceptors.
The 661W cells were transfected with negative control (miRNC; open diamond), miR-150 mimic (150 m; open circle), or miR-150 inhibitor (150in; gray square) and collected to determine the levels of (**A**) *Elk1* mRNA using qPCR and (**B**) ELK1 protein using Western blots. * indicates statistical significance from the miRNC. $p < 0.05$, one-way ANOVA.

We specifically analyzed the levels of ELK1 and $pELK1_{T417}$ in the inner and outer segments of photoreceptors (IS + OS) as well as in the outer nuclear layer (ONL). We found that the HFD regimen significantly increased the levels of ELK1 in the cytoplasm (IS + OS) and nuclei (ONL) of photoreceptors in WT and miR-$150^{-/-}$ mice

(Fig. 3-4). Knockout of miR-150 (miR-150$^{-/-}$) upregulated pELK1$_{T417}$ in the IS + OS of photoreceptors, while HFD increased pELK1$_{T417}$ in the ONL (Fig. 3-4). It is possible that the HFD-induced apoptosis in photoreceptors (Fig. 3-1) is mediated by an increase in nuclear pELK1$_{T417}$ and that the upregulated cytoplasmic pELK1$_{T417}$ caused by miR-150 knockout exacerbates the HFD-induced apoptosis (Fig. 3-1).

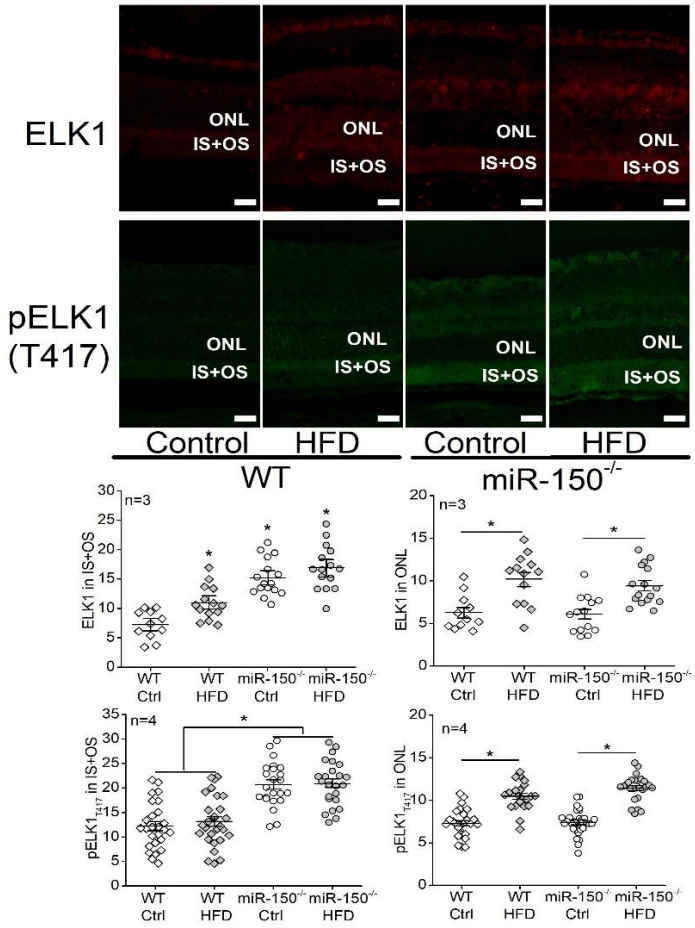

Figure 3-4 High-fat diet (HFD) and microRNA-150 knockout (miR-150$^{-/-}$) altered the levels of ELK1 and phosphorylated ELK1 at T417 (pELK1$_{T417}$) in mouse retina. The high-fat diet (HFD) increases ELK1 (red) and phosphorylated ELK1 at T417 (pELK1$_{T417}$; green) in the outer nuclear layer (ONL), while microRNA-150 knockout (miR-150$^{-/-}$) upregulates ELK1 and pELK1$_{T417}$ in the inner and outer segments of photoreceptors (IS + OS) after the WT and miR-150$^{-/-}$ mice were fed a normal chow (Ctrl) or a high-fat diet (HFD) for 6 months. The signal intensities of ELK1 and pELK1$_{T417}$ in the IS + OS and the ONL were

measured. Each data point represents one area of measurement. * $p < 0.05$, one-way ANOVA. Scale bar: 20 μm.

3.4.4. Treatment with PA Increases ELK1 and Nuclear pELK1$_{T417}$, and Knocking Down miR-150 Upregulates ELK1 and Cytoplasmic pELK1$_{T417}$ in 661W Cells

We further examined how ELK1 and pELK1$_{T417}$ were altered by miR-150 and PA treatments in 661W cells. After cells were treated with PA, the levels of ELK1 were significantly increased in a time-dependent manner, compared with cells treated with BSA (vehicle; Fig. 3-5A). The 661W cells were first transfected with microRNA negative control (miRNC), miR-150 mimic (150 m), or miR-150 inhibitor (150 in), and then treated with 100 μM PA for 24 h. As treatments with PA (24 h) significantly increased ELK1 in all cells, knocking down miR-150 (150 in) further elevated the PA-elicited increase in ELK1 (Fig. 3-5B). Although transfection with miR-150 mimic (150 m) decreased ELK1 in cells treated with BSA (vehicle), it did not attenuate the PA-induced increase in ELK1 (Fig. 3-5B), which suggests that overexpression of miR-150 is not sufficient to downregulate PA-stimulated ELK1.

Hence, the PA treatments elicited ELK1 upregulation (Fig. 3-5A, B) and induced apoptosis (Fig. 3-2) in 661W cells. Knocking down miR-150 further increased ELK1 (Fig. 3-5B) and exacerbated the PA-induced apoptosis (Fig. 3-2). However, transfection with miR-150 mimics did not attenuate the PA-induced increase in ELK1 (Fig. 3-5B), and it did not overturn the PA-induced apoptosis (Fig. 3-2). Using immunostaining, we found that cytoplasmic pELK1$_{T417}$ was decreased in cells transfected with miR-150 mimic (150 m) but increased in cells transfected with miR-150 inhibitor (150 in)

compared with the control (miRNC; Fig. 3-5C). The PA-treated cells had increased nuclear pELK1$_{T417}$ and nuclear/cytoplasmic (N/C) ratio of pELK1$_{T417}$ compared with the BSA or control (Ctrl) group (Fig. 3-5C).

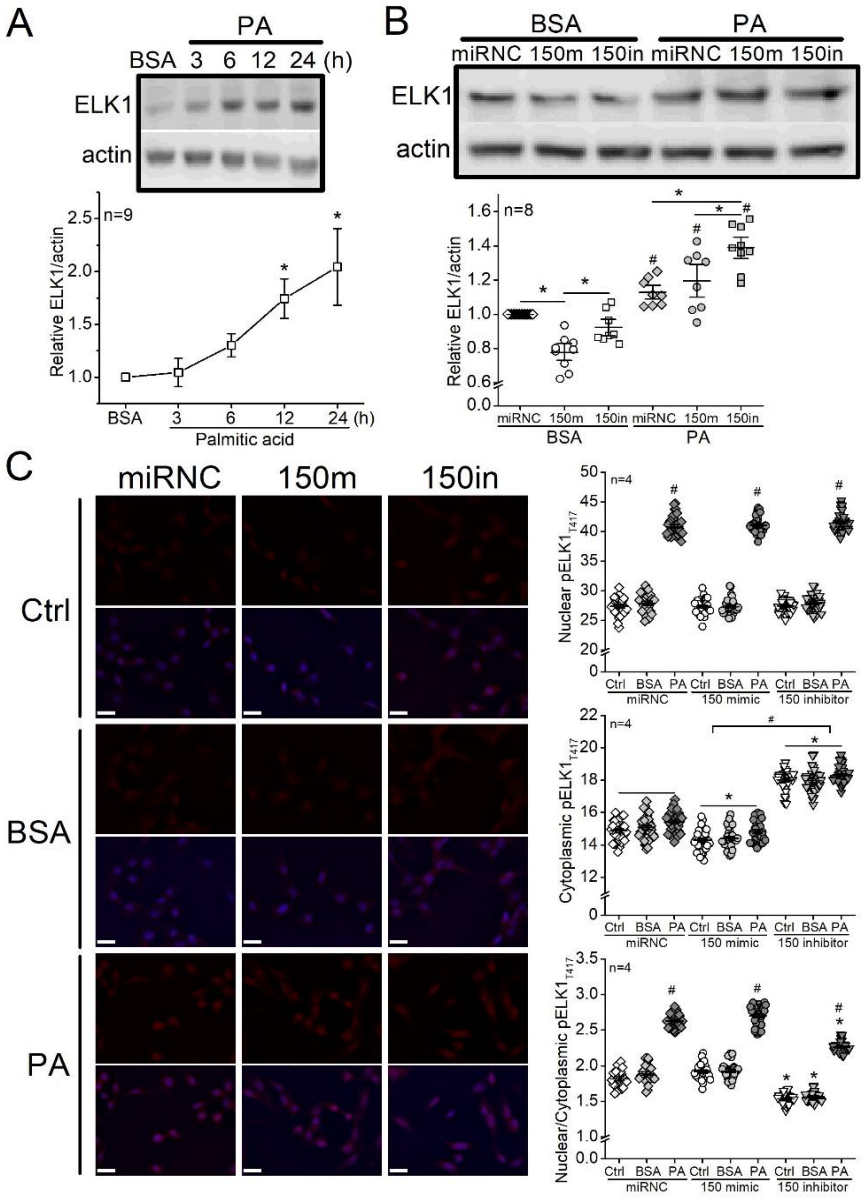

Figure 3-5 Palmitic acid (PA) increases ELK1 and nuclear pELK1$_{T417}$ and miR-150 knockdown upregulates ELK1 and cytoplasmic pELK1$_{T417}$ in 661W cells.
(**A**) The 661W cells were treated with 100 μM PA or BSA (vehicle) for 3–24 h and then harvested to determine the protein levels of ELK1 via Western blots. * indicates a statistical

significance from the BSA. $p < 0.05$, one-way ANOVA. (**B**) The 661W cells were first transfected with microRNA negative control (miRNC), miR-150 mimic (150 m), or miR-150 inhibitor (150 in) and then treated with BSA (vehicle) or 100 μM PA for 24 h. The ELK1 levels were determined by Western blots. * indicates a statistical significance when comparing among miRNC, 150m, and 150in. # indicates a statistical difference between PA and BSA. $p < 0.05$, one-way ANOVA. (**C**) The 661W cells were first transfected with microRNA negative control (miRNC), miR-150 mimic (150 m), or miR-150 inhibitor (150 in) and then treated with culture medium (Ctrl), BSA (vehicle), or 100 μM PA (PA) for 24 h. Cells were fixed and immunostained with $pELK1_{T417}$ (red) and DAPI (blue). The fluorescent intensities of $pELK1_{T417}$ in the nucleus or cytoplasm were quantified with ImageJ, and the intensity ratios of nuclear/cytoplasmic $pELK1_{T417}$ were calculated. For nuclear $pELK1_{T417}$, # indicates a statistical significance when compared with BSA. For cytoplasmic $pELK1_{T417}$, * indicates a statistical significance when compared with miRNC, and # indicates a statistical significance between 150 mimic and 150 inhibitor. For nuclear/cytoplasmic $pELK1_{T417}$ ratio, # indicates a statistical significance when compared with BSA, and * indicates a statistical difference when compared with miRNC. Each data point represents one area of measurement**.** $p < 0.05$, one-way ANOVA. Scale bar: 30 μm.

3.4.5. Knocking Down *Elk1* Decreases PA-Elicited Increases in Total ELK1 and $pELK1_{T417}$ but Does Not Alleviate PA-Elicited Apoptosis in 661W Cells

In order to verify the functions of ELK1 and $pELK1_{T417}$ in regulating apoptosis in photoreceptors, we knocked down *Elk1* in 661W cells by transfecting them with the small interfering RNA (siRNA) of *Elk1* (si*Elk1*). Cells transfected with si*Elk1* had decreased ELK1 expression compared with the cells transfected with a siRNA negative control (siNC). The PA-elicited increase in ELK1 was blocked by si*Elk1* (Fig. 3-6A). In addition, knocking down *Elk1 (*si*Elk1)* decreased the cytoplasmic $pELK1_{T417}$ and also arrested the PA-induced increase in nuclear $pELK1_{T417}$ (Fig. 3-6B). Thus, knocking down *Elk1* effectively inhibits the PA-elicited increase in ELK1 and $pELK1_{T417}$. As we examined whether downregulation of *Elk1* could alleviate PA-induced apoptosis, we found that PA-induced increase in $TUNEL^+$ cells was not dampened by transfection with si*Elk1* (Fig. 3-7). The results indicate that knocking down *Elk1* did not attenuate PA-induced apoptosis.

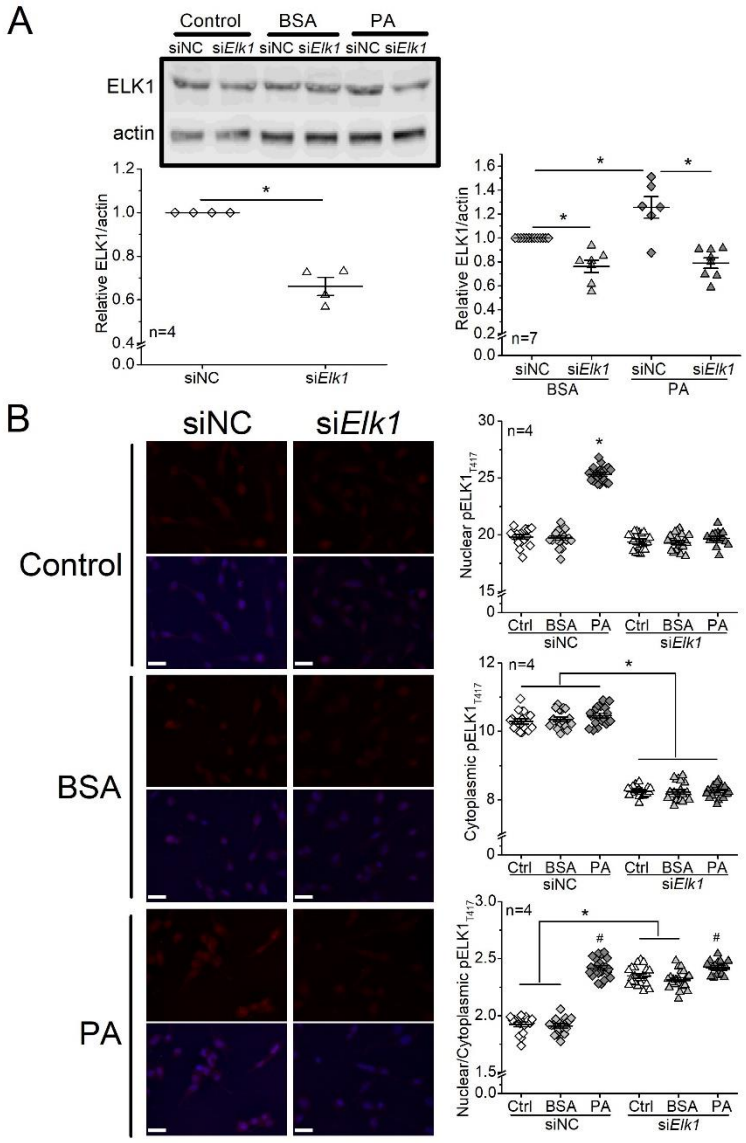

Figure 3-6 Knocking down *Elk1* decreases PA-elicited increases in total ELK1 and pELK1$_{T417}$ in 661W cells.

(**A**) The 661W cells were transfected with siRNA negative control (siNC) or *Elk1* siRNA (siElk1) and treated with culture medium (Ctrl), BSA, or 100 μM PA (PA) for 24 h. The ELK1 levels were determined by Western blots. The left panel * indicates a statistical significance between siNC and si*Elk1*; $p < 0.05$; Student's *t*-test. The right panel * indicates a statistical significance between groups specified with a horizontal line; $p < 0.05$, one-way ANOVA. (**B**) The 661W cells were cultured on coverslips and transfected with siRNA negative control (siNC) or *Elk1* siRNA (si*Elk1*) and treated with culture medium (Ctrl), BSA, or 100 μM PA (PA) for 24 h. Cells were fixed and immunostained with pELK1$_{T417}$ (red) and DAPI (blue). The fluorescent intensities of pELK1$_{T417}$ in the nucleus or cytoplasm were quantified with ImageJ, and the intensity ratios of nuclear/cytoplasmic pELK1$_{T417}$ were calculated. For nuclear pELK1$_{T417}$, * indicates a statistical significance when compared with siNC-BSA. For cytoplasmic pELK1$_{T417}$,

* indicates a statistical significance between siNC and si*Elk1* regardless of treatments (Ctrl, BSA, or PA). For nuclear/cytoplasmic pELK1$_{T417}$ ratio, # indicates a statistical significance when compared with the BSA within siNC or si*Elk1*. * indicates a statistical significance between si*Elk1* and siNC specified with a horizontal line. Each data point represents one area of measurement**.** $p < 0.05$, one-way ANOVA. Scale bar: 30 μm.

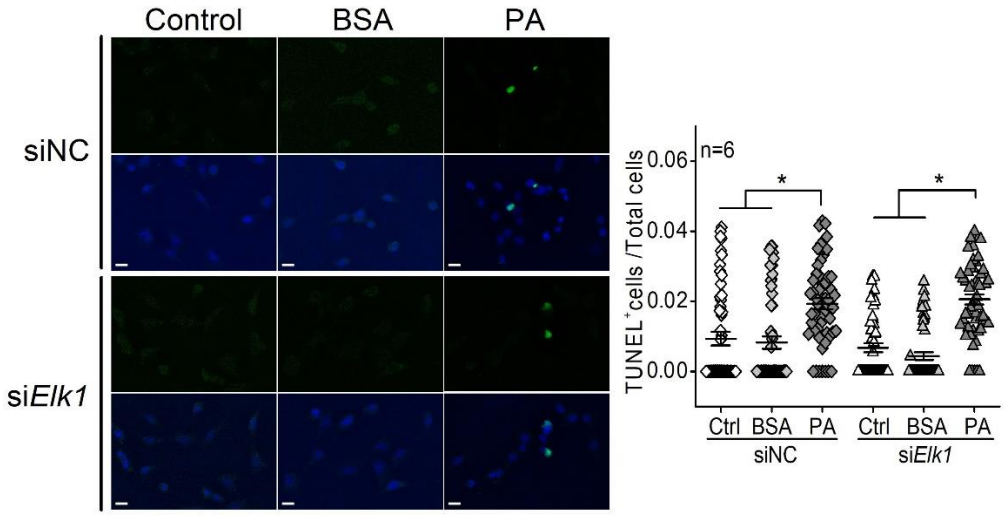

Figure 3-7 Knocking down *Elk1* does not alleviate PA-elicited apoptosis in 661W cells.
The 661W cells were first transfected with siRNA negative control (siNC) or *Elk1* siRNA (si*Elk1*) and treated with culture medium (Ctrl), BSA, or 100 μM PA (PA) for 24 h. The TUNEL$^+$ cells are green, and DAPI stained nuclei are blue. The ratio of TUNEL$^+$ cells/total cells within each defined field was calculated. * indicates a statistical significance. Each data point represents one area of measurement**.** $n = 6$ experimental trials for each group. $p < 0.05$, one-way ANOVA. Scale bar: 30 μm.

3.5. Discussion

We previously found that miR-150 knockout exacerbated retinal neural dysfunction and vascular degeneration in obesity-associated T2DR in mice [189, 190]. MiR-150 is decreased in the retina of DR patients and diabetic mice [190], but how this decrease contributes to the pathogenesis of DR is unknown. The neural retina has the highest oxygen consumption rate among all tissues, including the brain [263], thus making it (especially the retinal photoreceptors) prone to hypoxia-induced apoptosis.

There is local hypoxia in the diabetic retina, and apoptosis of photoreceptors occurs shortly after the onset of diabetes and may contribute to neural dysfunction and vascular degeneration [254, 257]. Inhibition of miR-150 is known to promote apoptosis [193, 264] while overexpressing miR-150 can reduce the apoptosis of cells under hypoxia/ischemia conditions [194, 265]. However, some cancer or endothelial cells with miR-150 overexpression have increased apoptosis under different treatments [266, 267]. Thus, the function of miR-150 in regulating apoptosis might be tissue-specific and treatment-dependent, which might also be associated with its direct downstream targets. In this study, we report that the miR-150$^{-/-}$-HFD mice had more severe apoptosis of photoreceptors than the WT-HFD mice (Fig. 3-1), and knocking down miR-150 exacerbated the PA-induced apoptosis in 661W cells (Fig. 3-2C, D). These results imply that decreased miR-150 exacerbates the apoptosis of photoreceptors under T2D conditions. Interestingly, knocking down miR-150 in 661 W cells caused a significant increase in apoptosis regardless of treatments (Fig. 3-2D). This is partly different from the TUNEL staining results in the mouse retina, where the deletion of miR-150 (miR-150$^{-/-}$) did not increase apoptosis without the HFD regimen (Fig. 3-1). Since other cell types (e.g., Möller glial cells) in the retina may play a role in neuroprotection under stress, the retinal photoreceptors could be more resilient to the miR-150$^{-/-}$ condition in vivo compared with isolated photoreceptors in culture. Alternatively, there might be some compensatory mechanisms against photoreceptor apoptosis during the development of T2DR in miR-150$^{-/-}$ mice. This might require further investigations using conditional knockout animal models.

Elk1 is a *bona fide* target of miR-150 [198]. We found that *Elk1* (mRNA) and ELK1 (protein) were decreased with miR-150 overexpression and increased with miR-150 knockdown in 661W cells (Fig. 3-3A, B). The ELK1 expression was increased by T2D conditions (HFD or PA) in the mouse retina and 661W cells and was further increased by knocking down miR-150 (Fig. 3-4 and 3-5A, B). Overexpression of ELK1 is known to promote apoptosis in neurons [205, 206], but apoptosis in most cancer cells is reduced by ELK1 overexpression [268-270]. As a transcription factor, ELK1 might regulate different downstream molecules in different types of cells/tissues and elicit paradoxical responses. We found that increased ELK1 (Fig. 3-4 and 3-5B) positively correlates with the increased apoptosis in photoreceptors of HFD mice (Fig. 3-1) and in PA-treated 661W cells (Fig. 3-2D), similar to neurons [205, 206]. Knocking down *Elk1* was able to reduce the expression of ELK1 in PA-treated 661W cells (Fig. 3-6A) but did not alleviate the PA-induced apoptosis (Fig. 3-7). Thus, it is possible that the function of ELK1 in regulating apoptosis could be cell-type dependent. In retinal photoreceptors, downregulation of ELK1 might not be sufficient to completely overcome T2D-elicited apoptosis.

Phosphorylated/activated ELK1 has a positive correlation with increased apoptosis in neurons, but it is phosphorylation site-dependent [258]. Overexpression of WT *Elk1* or mutated *Elk1* (S383A) induced apoptosis in cultured primary neurons, but overexpression with a different mutated *Elk1* (T417A) does not induce apoptosis, which indicates that $pELK1_{T417}$ is the active form of ELK1 that mediates neuronal apoptosis [258]. We found that the HFD regimen or PA treatments increased nuclear $pELK1_{T417}$

and that miR-150 knockout or knockdown increased cytoplasmic pELK1$_{T417}$ in mouse retinal photoreceptors or cultured 661W cells, respectively (Fig. 3-4 and 3-5C). There is a positive correlation between the HFD- or PA-elicited increase in nuclear pELK1$_{T417}$ and increased photoreceptor apoptosis (Fig. 3-1B and 3-2D), which suggests that the T2D-induced increase in nuclear pELK1$_{T417}$ could contribute to retinal photoreceptor apoptosis. Downregulation of miR-150 not only increases cytoplasmic pELK1$_{T417}$ but also promotes apoptosis.

Apoptosis can be mediated by the mitochondrial permeability transition pore complex (PTP) that initiates mitochondrial swelling and membrane potential depolarization that leads to cell death [53]. There is a protein-protein interaction between ELK1 and PTP in the brain, and cytoplasmic ELK1 can be isolated from purified mitochondrial fractions. Furthermore, cell apoptosis induced by *Elk1* overexpression can be blocked by a PTP inhibitor in cultured primary neurons [205]. Thus, under T2D conditions, upregulated cytoplasmic pELK1$_{T417}$ would have increased interactions with mitochondrial PTP, which might further accelerate photoreceptor apoptosis. However, while transfection with miR-150 mimics decreased cytoplasmic pELK1$_{T417}$, it did not reduce nuclear pELK1$_{T417}$ or overcome PA-elicited apoptosis. We noticed that the nuclear/cytoplasmic (N/C) ratio of pELK1$_{T417}$ remained comparable between the 150m-PA and the miRNC-PA cells (Fig. 3-5B) and between the si*Elk1*-PA and siNC-PA cells (Fig. 3-6B). The N/C ratio represents the cytoplasm-to-nucleus translocation of pELK1$_{T417}$, which is important for transactivating the downstream targets of *Elk1* and regulating apoptosis [271, 272], as the translocation of ELK1 to the cell nucleus

correlates with increased apoptosis in neurons [271]. Fos proto-oncogene (*c-Fos*) and myeloid cell leukemia 1 (*Mcl1*) are downstream targets of ELK1 that also mediate apoptosis [273, 274]. Upregulated *c-Fos* promotes pathology-induced apoptosis in neurons, while downregulation of *c-Fos/Mcl1* alleviates apoptosis [273, 274]. Therefore, blocking the translocation of $pELK1_{T417}$ to the nucleus may be necessary to mitigate diabetes-associated apoptosis in photoreceptors.

4. MICRORNA-150 AND ITS TARGET ETS-DOMAIN TRANSCRIPTION FACTOR 1 CONTRIBUTE TO INFLAMMATION IN DIABETIC PHOTORECEPTOR

4.1. Overview

Obesity-associated type 2 diabetes (T2D) is on the rise in the US due to the obesity epidemic, and 60% of T2D patients might develop diabetic retinopathy (DR) in their lifetime. Chronic inflammation is a hallmark of obesity and T2D and a well-accepted major contributor to DR. Retinal photoreceptors are a major source of intraocular inflammation and directly contribute to vascular abnormalities in diabetes. However, how diabetic insults cause photoreceptor inflammation is not well known. In this study, we used a high-fat diet (HFD)-induced T2D mouse model and cultured photoreceptors treated with palmitic acid (PA) to decipher major players that mediated high-fat-induced photoreceptor inflammation. We found that PA elicited decreased miR-150 with a consistent upregulation of *Elk1*, a downstream target of miR-150 in PA-elicited photoreceptor inflammation. We compared the wild type (WT) and miR-150$^{-/-}$ mice fed with the HFD and found that deletion of miR-150 exacerbated HFD-induced photoreceptor inflammation in correlation with upregulated ELK1. We further delineated the critical cellular localization of phosphorylated ELK1 at serine 383 (pELK1$_{S383}$) and found that decreased miR-150 exacerbated the T2D-induced inflammation in photoreceptors by upregulating ELK1 and pELK1$_{S383}$. Further, knocking down ELK1 alleviated PA-elicited photoreceptor inflammation.

4.2. Introduction

The incidence of diabetes is projected to rise to 33% of the US population by 2050 owing to the obesity epidemic [31], of which 95% of diabetic patients will have type 2 diabetes (T2D) [213]. More than 85% of T2D patients have diabetes-related eye disorders, and 60% develop diabetic retinopathy (DR), the leading cause of blindness in US adults age 20 to 74 [32, 213]. While anti-vascular endothelial growth factor (VEGF) treatments significantly improve the outcomes of DR, nearly 30% of patients do not respond to anti-VEGFs [275, 276], making the development of new treatment strategies imperative. Chronic inflammation is a hallmark of obesity and T2D [277, 278] and a well-accepted major contributor to DR [102, 279], but numerous studies have indicated that intraocular rather than systemic inflammation is more closely associated with vascular complications in DR [280, 281]. Interestingly, diabetic patients who also have retinitis pigmentosa (RP), congenital blindness with initial degeneration of rod photoreceptors, rarely develop DR [282, 283]. In mice, genetic deletion of rod photoreceptors or pharmacological inhibition of photoreceptors reduces retinal inflammation and alleviates progression of DR [217, 284]. Therefore, retinal photoreceptors are a major source of intraocular inflammation and directly contribute to vascular abnormalities in diabetes. However, how photoreceptors contribute to intraocular inflammation and vascular complications under T2D is still not well elucidated.

MicroRNAs (miRs) represent a set of modulators that regulate metabolism, inflammation, and angiogenesis [247, 285, 286] and have been linked to DR [221, 222]. Among them, there is a strong correlation between miR-150 downregulation and patients

with diabetes and DR. Retinal miR-150 is decreased in the eyes under ischemic insults [192] and in patients with proliferative DR [190]. Serum miR-150 is decreased in patients with obesity [186], T1D [187, 188], or T2D [168, 224], in association with increased inflammation and upregulation of angiogenic factors. We and others have reported that miR-150 is significantly decreased in the blood, heart, and retina in animals with a high-fat diet (HFD)-induced T2D [189] or streptozotocin (STZ)-induced T1D [191, 221]. Deletion of miR-150 in mice (miR-150$^{-/-}$) further exacerbates obesity-associatedT2D and T2DR compared to the wild type (WT) mice, including significantly elevated systemic insulin resistance, glucose intolerance, and inflammation, worsened retinal light responses, and more severe retinal microvascular degeneration and leakage [190]. Thus, downregulation of miR-150 correlates with the progression of diabetes and DR.

In addition, miR-150 is an intrinsic suppressor of inflammation [198]. Overexpression of miR-150 downregulates TNF-α and nuclear factor kappa B (NF-κB) induced by Lipopolysaccharide (LPS) in endothelial cells [199]. Deletion of miR-150 (miR-150$^{-/-}$) exacerbates the increase of TNF-α and IL-1β in mice with an HFD-induced T2D [198]. We previously showed that the miR-150$^{-/-}$-HFD mice have more severe inflammation in photoreceptors and exacerbated vascular degeneration compared to the WT-HFD mice [190]. Overexpression of miR-150 protects the retinal vasculature from degeneration induced by oxygen-induced retinopathy (OIR), a well-established model for pathological angiogenesis [197]. Moreover, overexpressing miR-150 restores the endothelial cell functions including proliferation and migration [287]. Therefore, miR-150 could restrain the development of DR by mitigating the inflammation in the neural

retina especially in photoreceptors. However, how miR-150 and its downstream targets contribute the diabetes-induced inflammation in photoreceptors remains unclear.

The biological processes mediated by miRs and their targets are often tissue- and cell-type-dependent [211, 212]. We screened the top 30 predicted target genes of miR-150 by combining computational analyses, transcriptome profiles, and reporter assays [198, 226], and identified new *bona fide* targets that are pro-inflammatory [198]. Among them, multiple transcription factors including the eukaryotic translation termination factor 1 (*Etf1*), early growth response 1 (*Egr1*), MYBproto-oncogene (c-*Myb*), and*ETS-domain transcription factor 1 (Elk1)* are expressed in photoreceptors and retinal endothelial cells. In this study, we used a functional assay with cultured photoreceptors treated with palmitic acid (PA) to generate a high-fat environment for cells. We found that PA elicited decreased miR-150 with a consistent upregulation of *Elk1* but not others, so we focused on *Elk1* and its associated signaling in promoting retinal inflammation in T2DR using *in vitro* and *in vivo* assays. We compared WT and miR-150$^{-/-}$ mice fed with the HFD and determined the role of miR-150 and *Elk1* in mediating inflammation in photoreceptors under T2D. We further used cultured 661W cells, a mouse photoreceptor cell line [259], to decipher the relationship between miR-150, *Elk1*, ELK1 protein, and inflammation in the photoreceptors. We delineated the critical cellular localization of phosphorylated ELK1 at serine 383 (pELK1$_{S383}$) and HFD- or PA-associated inflammation in photoreceptors. Our data indicate that decreased miR-150 exacerbates the T2D-induced inflammation in photoreceptors by upregulating ELK1 and pELK1$_{S383}$ and knocking down *Elk1* alleviates the inflammation and reduces pELK1$_{S383.}$

4.3. Materials and Methods

4.3.1. Animals

Four-week-old male C57BL/6J mice (wild type, WT) were purchased from the Jackson Laboratory (Bar Harbor, Maine, USA). B6(C)-*Mir150*^{tm1Rsky}/J (miR-150$^{-/-}$) mice were originally purchased from the Jackson Laboratory, and a colony was bred and maintained at Texas A&M University. Only male mice were used in this study. All animal experiments were approved by the Institutional Animal Care and Use Committee of Texas A&M University and were performed in compliance with the Association for Research in Vision and Ophthalmology (ARVO) Statement for the Use of Animals in Ophthalmic and Vision Research. Mice were housed under temperature and humidity-controlled conditions with 12:12 hours of light-dark cycles. All mice were given food and water *ad libitum*. At 5 weeks of age (body weight, 20 g), mice were fed a high-fat diet (HFD; 60% fat calories, 20% protein calories, and 20% carbohydrates calories; #D12492; Research Diets, New Brunswick, NJ, USA) or a control diet (standard laboratory chow; 10% fat calories, 20% protein calories, and 70% carbohydrates calories; #D12450J; Research Diets) for up to 24 weeks. Bodyweight and food intake were measured weekly. Glucose levels were measured monthly by taking blood from the tail vein using Clarity BG1000 blood glucose monitoring system (Clarity Diagnostics, Boca Raton, FL, USA).

4.3.2. Cell Culture

The 661W cells [259] were originally obtained from Dr. Al-Ubaidi (University of Houston) and cultured in Dulbecco's modified Eagle medium (DMEM; #12-614Q,

Lonza, Portsmouth, NH, USA) containing 10% fetal bovine serum (FBS; #S11550, R&D Systems, Minneapolis, MN, USA), 2 mM Glutamax (#35050-061, Gibco/ThermoFisher, Waltham, MA, USA), 100 μg/mL penicillin and 100 μg/mL streptomycin (#15140-148, Gibco/ThermoFisher), and 1 mM sodium pyruvate (#S8636, Sigma, St. Louis, MO, USA) at 37 °C and 5% CO_2. The 661W cells were treated with 100 μM palmitic acid (PA, #P5585-10G, Sigma) dissolved in 10% bovine serum albumin (BSA; #A6003-25G, Sigma) or an equal volume of 10% BSA (vehicle control) for various times as indicated.

4.3.3. Lipofectamine Transfection

Transfection was conducted using the Lipofectamine 3000 (#L3000015, Invitrogen/ThermoFisher) according to the manufacturer's instructions. Briefly, the 661W cells were seeded at 30% confluency and allowed to grow for 24 hours to reach 50% confluency. For Western blot and qPCR, the cells were seeded in 6-well plates and transfected with 30 pmol/well microRNA (miRNA)/ siRNA. For Terminal deoxynucleotidyl transferase dUTP nick end labeling (TUNEL) and immunofluorescent staining, the cells were seeded on 12 mm circular coverslips in 24-well plates and transfected with 10 pmol/well miRNA/siRNA. After the first exchange to the normal cultural medium, some cultures were immediately treated with PA or BSA for various hours. The following miRNAs/ siRNAs were used in this study: miRNA negative control (#4464058, ThermoFisher), miR-150 mimic (Assay MC10070, #4464066, ThermoFisher), miR-150 inhibitor (Assay MH10070, #4464084, ThermoFisher), siRNA

negative control (#AM4613, ThermoFisher), and Elk1 siRNA (Assay 261017, #AM16708, ThermoFisher).

4.3.4. Quantitative real-time RT-PCR (qPCR)

After the cells were collected, total RNA from each sample was prepared by using a commercially available purification kit (miRNeasy mini kit; #217004, Qiagen, Germantown, MD, USA). From each sample, 500 ng of total RNA was used to quantify miR-150 or mRNAs by qPCR using TaqMan MicroRNA Reverse Transcription Kit (#4366596, ThermoFisher) and SYBR green supermix ROX (#95055-500, QuantaBio, Beverly, MA, USA) with the CFX Connect Real-Time PCR Detection System (Bio-Rad, Hercules, CA, USA). The primers (Bioneer, Oakland, CA, USA) of *Elk1* (Forward 5'-GCC GGG CCT TGC GGT ACT ACT ATG A-3', Reverse 5'-GGG TAG GAC ACA AAC TTG TAG AC-3'), *Etf1* (Forward 5'-TTG AAC CTT TCA AAC CAA TTA ATA C-3', Reverse 5'-CAG TGA ATT TGT GCA GGA CTT CTC T-3'), *Egr1* (Forward 5'-GCA ACG GGG CTC CCC AGT TCC TCG G-3', Reverse 5'-AAG CGG CCA GTA TAG GTG ATG GG-3'), *c-Myb* (Forward 5'-CCA GCA AGG TGC ATG ATC GTC CAC C-3', Reverse 5'-AGA ATT CAA AAC TGC TGA GAT CAC A-3'), and *β-actin* (Forward 5'-CAA CGG CTC CGG CAT GTG C-3', Reverse 5'-GTA CAT GGC TGG GGT GTT GAA GGT C-3') were used in this study. The hsa-miR-150 assay (Assay 000473, #4440887, ThermoFisher) and U6 snRNA assay (Assay 001973, #4440887, ThermoFisher) were used to test the level of miR-150.

For each individual experiment, a standard curve was generated with known quantities of RNAs loaded in curved dilutions (i.e., 2×, 1×, 1/2, 1/4, 1/8, 1/16, and 1/32).

The cycle values, corresponding to the log values of the standard curve quantities, were used to generate a linear regression formula. The amplification efficiency of the qPCR reactions (90%-100%) was calculated using the standard curve. The quantification of sample RNA was calculated by the $2^{(-\Delta\Delta Ct)}$ method [260] using U6 (for miR-150) or *β-actin* (for other genes) as the internal control.

4.3.5. Western Blot

Samples for Western blots were collected, prepared, and analyzed as described previously [238]. Briefly, 661W cells were harvested and lysed in a Tris lysis buffer (in mM): 50 Tris, 1 EGTA, 150 NaCl, 1% Triton X-100, 1% β-mercaptoethanol, 50 NaF, and 1 Na3VO4, pH 7.5. Samples were separated on 10% sodium dodecyl sulfate-polyacrylamide gels by electrophoresis and transferred to nitrocellulose membranes. The membranes were blocked in 3% BSA in TBST at room temperature for 1 hour and incubated in primary antibodies overnight at 4 °C. After washing with TBST, the membranes were incubated in anti-rabbit IgG HRP-linked secondary antibody (1:1000, #7074S, Cell Signaling) at room temperature for 1 hour. The blots were visualized using Super Signal West Pico/Femto chemiluminescent substrate (#34078/ #34096, ThemoFisher). Band intensities were quantified using Image J (NIH, Bethesda, MA, USA). The primary antibodies used in this study were: anti-ELK1 (1:500, #9182S, Cell Signaling, Beverly, MA, USA), anti-phospho NFκB P65 (1:1000, #3033, Cell Signaling), anti-NFκB P65 (1:1000, #8242S, Cell Signaling), and anti-β-actin (1:2000, #8457L, Cell Signaling). The band intensities of ELK1 were normalized to those of β-

actin. The band intensities of phosphorylated NFκB P65 (pP65) were normalized to those of total NFκB P65 (P65) and β-actin.

4.3.6. Immunofluorescent Staining

Mouse eyes were collected, fixed with 4% paraformaldehyde, and processed for paraffin-embedded sectioning after 24 weeks of the diet regimen. Paraffin sections (4 μm) of the mouse eyes from all four experimental groups were mounted on the same glass slide. The retina sections were deparaffinized by heating at 57°C followed by washing with xylene and serial dilution of ethanol. After deparaffinization, sections were permeabilized in sodium citrate buffer (10 mM sodium citrate, 0.05% Tween20, pH 6.0) at 80°C for 1 hour. The 661 cells cultured on coverslips were fixed with 4% paraformaldehyde at room temperature for 1 hour and permeabilized with 0.1% Triton X-100 in 0.1% sodium citrate at 4 °C for 10 minutes.

Eye sections or coverslips were then blocked with 10% goat serum in PBS for 2 hours at room temperature and incubated with primary antibodies overnight at 4 °C. After washing with PBS, sections or coverslips were incubated with secondary antibodies for 2 hours at room temperature and mounted with ProLong Gold antifade mountant with 4′,6′-diamidino-2-phenylindole (DAPI) (#P36935, ThermoFisher). Images were obtained using a Zeiss Axiovert 200M microscope (Carl Zeiss AG, Oberkochen, Germany). Each fluorescent image was taken under identical settings, including light intensity, exposure time, and magnification [190, 238].

The fluorescent intensity was measured in the inner and outer segments of photoreceptors (IS/OS) and in the outer nuclear layer (ONL) for mouse retina sections or

in the nuclear and cytoplasmic areas of 661W cells by Image J (NIH, Bethesda, MA, USA). DAPI staining was used to identify the nuclear regions of the cells. The intensity of pELK1 in the cytoplasm was measured at the processes of photoreceptors that are 10 μm from the nucleus. The intensity of pELK1 in the nucleus was measured within the DAPI-stained area. We analyzed 10-15 regions for each culture well. The intensities of the pP65/ pELK1 signal in the IS/OS and ONL were measured from 5-10 regions for each retinal section.

The following primary antibodies were used: anti-phospho NFκB P65 (1:50, #3033, Cell Signaling) and anti-phospho-ELK1(S383) (1:50, #ab218133, abcam, Waltham, MA, USA). The following secondary antibodies were used: goat anti-rabbit IgG (Alexa Fluor 488) (1:50, #ab150077, abcam) and goat anti-rabbit IgG (Alexa Fluor 568) (1:50, # ab175471, abcam).

4.3.7. Statistical Analysis

All data are presented as mean ± standard error of the mean (SEM). Student's *t*-test or one-way analysis of variance (ANOVA) followed by Tukey's *post hoc* test was used for statistical analyses among groups. $p<0.05$ was regarded as significant. Origin 9.0 (OriginLab, Northampton, MA, USA) was used for statistical analyses.

4.4. Results

4.4.1. Deletion of miR-150 (miR-150$^{-/-}$) Exacerbates Inflammation in the Obesity-Associated T2D Retina

Inflammation is a major culprit in the pathogenesis of DR [102, 288]. We previously showed that mice fed with an HFD develop obesity-associated T2D, in which

inflammation is detected in the vitreous and neural retina, and phosphorylated NFκB P65 (pP65), a biomarker for inflammation, is significantly increased in the whole retina [74].

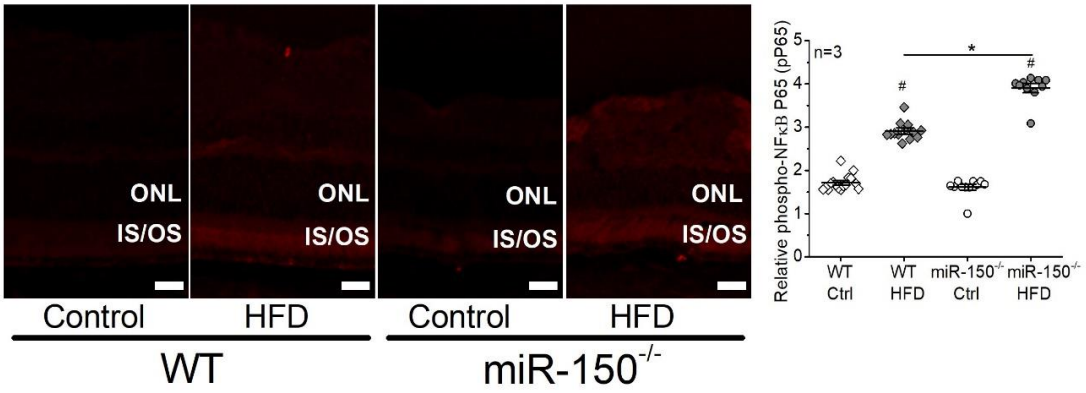

Figure 4-1 Deletion of miR-150 (miR-150$^{-/-}$) exacerbates inflammation in the obesity-associated T2D retina.
Wildtype (WT) and miR-150$^{-/-}$ mice were fed a normal chow (Ctrl) or high-fat diet (HFD) for 6 months. Retinal sections were immunostained with phosphorylated NFκB P65 (pP65; red). The fluorescent intensities in the retinal outer nuclear layer (ONL) were quantified using ImageJ. # indicates a statistical significance when compared to WT-Ctrl and miR-150$^{-/-}$-Ctrl; * indicates a statistical significance between the two HFD groups. Each data point represents one area of measurement**.** *n*=3 mice for each group; * #: $p<0.05$, one-way ANOVA. Scale bar: 20 μm.

Using immunostaining, we found that deletion of miR-150 (miR-150$^{-/-}$) further exacerbates retinal inflammation in obesity-associated T2DR [190] especially in the photoreceptors (Fig. 4-1). The HFD-T2D mice (WT and miR-150$^{-/-}$) had increased pP65 in the outer nuclear layer (ONL), as well as the inner and outer segments of photoreceptors (IS/OS), compared to the mice fed with normal chow. In addition, the miR-150$^{-/-}$-HFD mice had further increased pP65 than the WT-HFD mice (Fig. 4-1). The results demonstrate that miR-150 knockout exacerbates the HFD-induced retinal inflammation, especially in photoreceptors.

4.4.2. MiR-150 Knockdown Exacerbates Palmitic Acid (PA)-Elicited Inflammation in Cultured 661W Cells

As miR-150 is decreased in the blood and retina of diabetic patients [187, 190, 289] and animals with streptozotocin-induced T1D or HFD-associated T2D [190], there is a correlation between decreased miR-150 and diabetes. We next tested whether decreased miR-150 directly triggered inflammatory responses, or if miR-150 is a medium linking diabetic insults and inflammation using cultured 661W cells [259]. The 661W cells are originally derived from a mouse retinal tumor and characterized as a cone-photoreceptor cell line for expressing opsins, transducin, and arrestin [259], and they are widely used in photoreceptor research. We found that cultured cells treated with palmitic acid (PA, 100 μM) had significantly increased levels of pP65, indicating that PA triggered inflammatory responses in 661W cells (Fig. 4-2A). We transfected cells with miR-150 mimics (150m), miR-150 inhibitor (anti-miR-150 antagomir; 150in), or a nonspecific miR as a negative control (miRNC). While cells transfected with miR-150 mimics had decreased pP65, knocking down miR-150 (150in) in cultured cells did not alter the pP65 level (Fig. 4-2B). This indicates that miR-150 has intrinsic anti-inflammatory properties as previously reported [198, 199], but decreasing miR-150 alone does not cause inflammation. However, if transfected cells were treated with PA for 24 hr regardless of whether they were transfected with 150m or 150in, they all had significantly increased pP65 compared to cells treated with the vehicle control (BSA). Cells with miR-150 knockdown (150in) further exacerbated the increase of PA-elicited pP65 compared to cells transfected with miRNC and miR-150 mimics (150m; Fig. 4-2B). These results show that miR-150

knockdown exacerbates the PA-elicited inflammation in cultured 661W cells while overexpressing miR-150 is not sufficient to overturn PA-elicited inflammation. Thus, the diabetic insults elicit inflammation responses, and decreased miR-150 further aggravates the retinal inflammation.

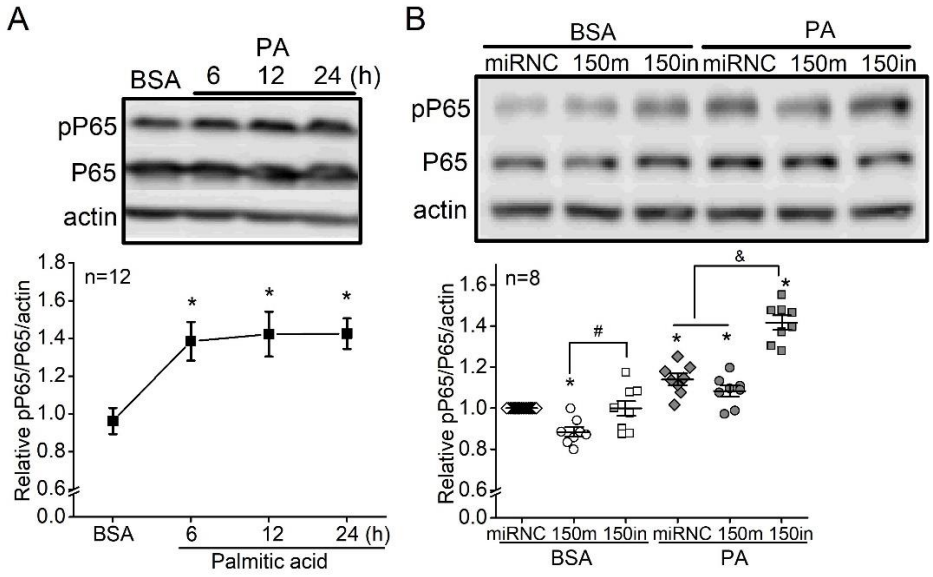

Figure 4-2 MiR-150 knockout exacerbates palmitic acid (PA)-elicited inflammation in cultured 661W cells.
(A) The 661W cells were treated with 100 μM PA or BSA (vehicle) for 6-24 hours. The protein levels of P65, pP65, and actin (loading control) were determined by Western blots. * indicates a statistical significance when compared to BSA. N=12 experimental trials. $p<0.05$, one-way ANOVA. **(B)** The 661W cells were first transfected with a microRNA negative control (miRNC), miR-150 mimic (150m), or miR-150 inhibitor (150in) and then treated with BSA or PA for 24 hours. The protein levels of P65, pP65, and actin (loading control) were determined by Western blots. * indicates statistical significance when comparing miRNC-BSA with miRNC-BSA, and comparing PA-treated cells with BSA-treated cells. # indicates a statistical difference between 150m-BSA and 150in-BSA. & indicates statistical difference when compared 150in-PA with miRNC-PA and 150m-PA. $p<0.05$, one-way ANOVA.

4.4.3. *Elk1*, but Not *c-Myb*, *Etf1*, or *Egr1*, is the Direct Target of miR-150 in Responses to PA Treatments in 661W Cells

There are several *bona fide* targets of miR-150 known to be pro-inflammatory including *c-Myb*, *Etf1*, *Egr1*, and *Elk1* [198]. In cultured adipose B lymphocytes, LPS

induces inflammatory responses corresponding with decreased miR-150 and upregulated *c-Myb*, *Etf1*, *Egr1*, and *Elk1*, and knocking down miR-150 further increases the expression of these genes and escalates LPS-elicited inflammation [198]. Because miRs and their downstream targets have tissue- and cell type-specific bioactivities [156, 212], we set forth to determine the downstream target(s) of miR-150 that is responsible for diabetes-associated inflammation in retinal photoreceptors.

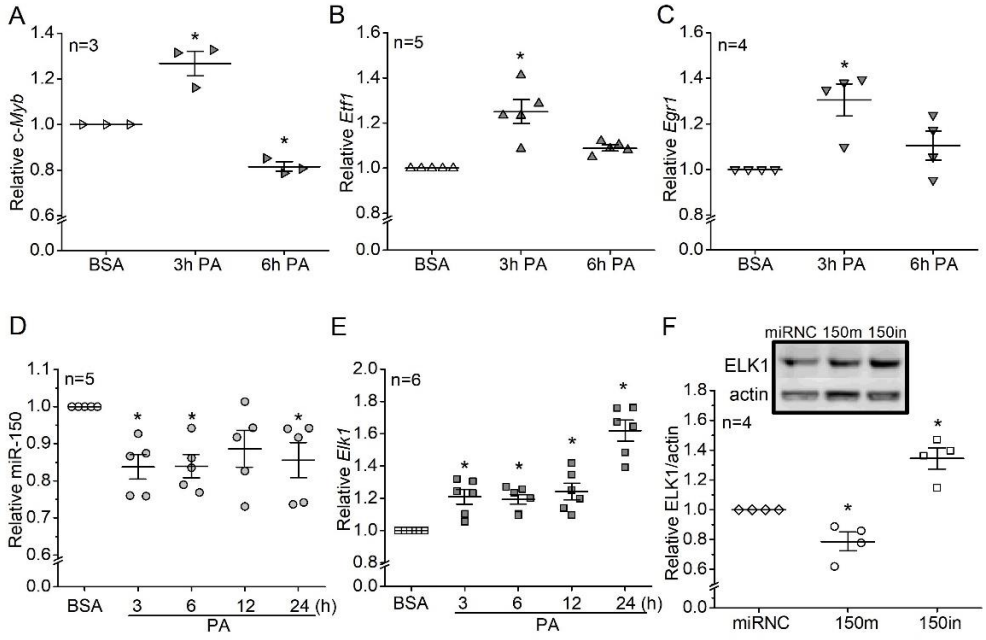

Figure 4-3 *Elk1*, but not *c-Myb*, *Etf1*, or *Egr1*, is the direct target of miR-150 in responses to PA treatments in 661W cells.
(**A-E**) The 661W cells were treated with BSA (vehicle) or 100 μM PA (PA) for various times. The mRNA or miR levels of c-*Myb* (**A**), *Elf1* (**B**), *Egr1* (**C**), miR-150 (**D**), and *Elk1* (**E**) were carried out using qPCR. * indicates a statistical difference when compared to the BSA treatment. (**F**) The 661W cells were transfected with a microRNA negative control (miRNC), miR-150 mimic (150m), or miR-150 inhibitor (150in). The ELK1 levels were measured using Western blots. * indicates a statistical difference when compared to the miRNC. $p<0.05$, one-way ANOVA.

Using cultured 661W cells treated with 100 μM PA, we found that cells treated with PA for 3 hours had a transient increase of *c-Myb*, *Etf1*, and *Egr1* (Fig. 4-3A-C),

even though miR-150 was decreased consistently in the presence of PA (3 to 24 hours; Fig. 4-3D). *Elk1* was the only downstream target that was consistently increased in the presence of PA (3 to 24 hours; Fig. 4-3E). In addition, ELK1 protein was decreased in cells transfected with a miR-150 mimic (150m) but increased in cells transfected with the miR-150 inhibitor (150in; Fig. 4-3F). The result confirms that *Elk1* is a direct target of miR-150 in 661W cells in responding to PA.

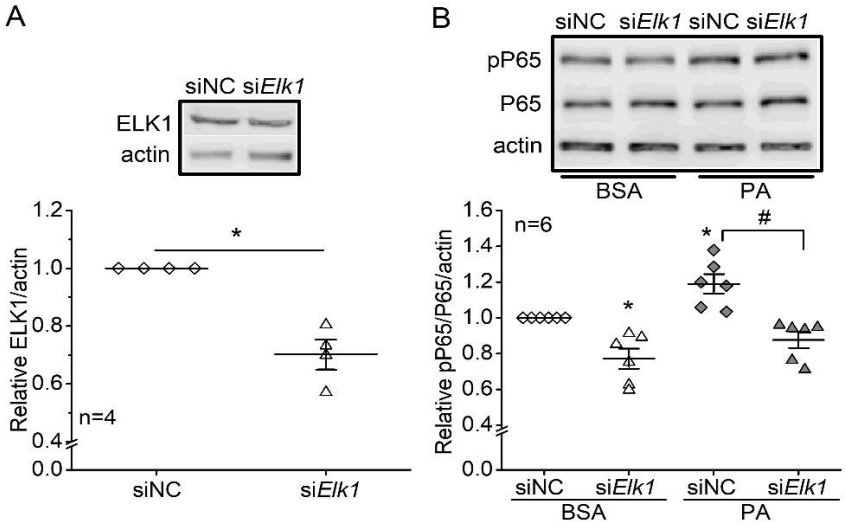

Figure 4-4 Knocking down *Elk1* alleviates PA-induced inflammation in 661W cells. The 661W cells were transfected with siRNA negative control (siNC) or *Elk1* siRNA (si*Elk1*). (**A**) After transfections, cells were harvested, and the ELK1 protein levels were measured with Western blots. * indicates a statistical significance between siNC (open diamond) and si*Elk1* (open triangle) groups. $p<0.05$, student's *t*-test. **(B)** After transfections, 661W cells were treated with BSA or 100 μM PA (PA) for 24 hours. Cells were harvested and the protein levels of P65, pP65, and actin (loading control) were measured using Western blots. * indicates a statistical significance when compared to siNC-BSA. # indicates a statistical significance between siNC-PA and siNC-*Elk1* groups. $p<0.05$, one-way ANOVA.

4.4.4. Knocking Down *Elk1* Alleviates PA-Induced Inflammation in 661W Cells

We then tested whether *Elk1* could regulate PA-induced inflammation in 661W cells. The 661W cells were first transfected with the siRNA of *Elk1* (si*Elk1*) to knock down the ELK1 protein (Fig. 4-4A) or negative control (siNC) and then treated with 100

μM PA or BSA (vehicle). As PA-treated cells had a significant increase of pP65, transfection with si*Elk1* blocked the PA-elicited increase of pP65 (Fig. 4-4B). The results indicate that knocking down *Elk1* alleviates PA-induced inflammation in 661W cells.

4.4.5. Cytoplasmic Versus Nuclear Phosphorylated ELK1 at S383 (pELK1$_{S383}$) in Retinal Photoreceptors: Differential Effects of HFD and Deletion of miR-150

Phosphorylated ELK1 at serine 383 (pELK1$_{S383}$) promotes inflammation as an activated transcription factor [290, 291]. As we showed in Figure 4-1 that six months after the HFD regimen, pP65 was significantly increased in the retinal photoreceptors, and deletion of miR-150 (miR-150$^{-/-}$) further exacerbated HFD-induced photoreceptor inflammation. This HFD-induced photoreceptor inflammation correlated with an increase of pELK1$_{S383}$ in the retinal outer nuclear layer (ONL; Fig. 4-5). Deletion of miR-150 (miR-150$^{-/-}$) significantly increased pELK1$_{S383}$ in the inner and outer segments of photoreceptors (IS/OS) regardless of the diet regimen (Fig. 4-5). These data imply that the HFD-induced inflammation in photoreceptors (Fig. 4-1) could be mediated by the increase of nuclear pELK1$_{S383}$ (Fig. 4-5), and the upregulated cytoplasmic pELK1$_{S383}$ by miR-150 knockout (Fig. 4-5) could exacerbate the HFD-induced inflammation (Fig. 4-1).

4.4.6. Knocking Down miR-150 Increases Cytoplasmic pELK1$_{S383}$, while PA Treatments Increase Nuclear pELK1$_{S383}$ in 661W Cells

We next examined the differential effects of PA and miR-150 in regulating pELK1$_{S383}$ (nucleus versus cytoplasm) in 661W cells. After 661W cells were first

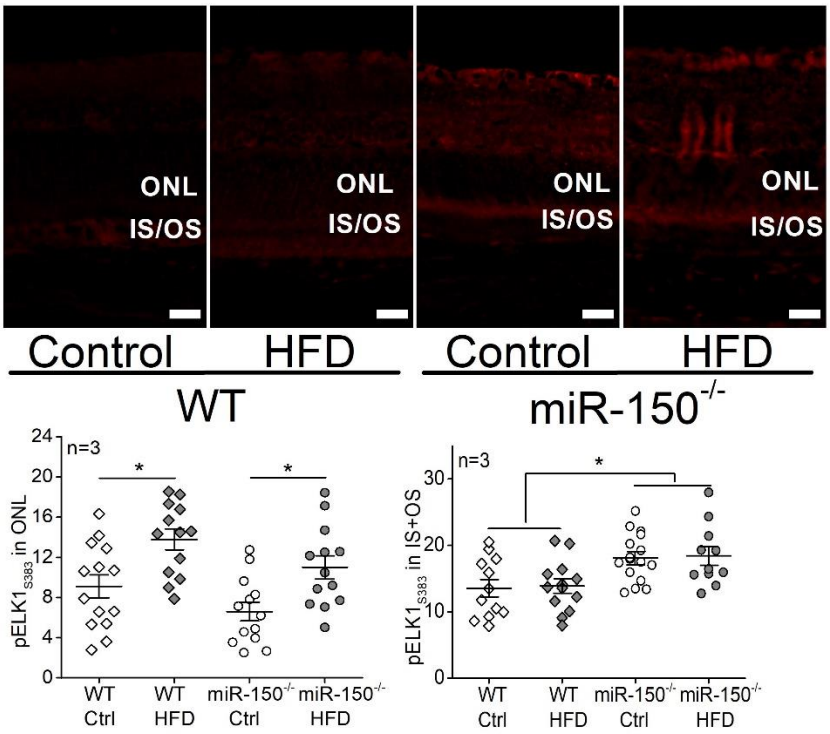

Figure 4-5 MiR-150 knockout (miR-150$^{-/-}$) increases phosphorylated ELK1 at S383 (pELK1$_{S383}$) in the inner and outer segments (IS/OS) of photoreceptors, while HFD-induced T2D increases pELK1$_{S383}$ in the outer nuclear layer (ONL).
Six months after the diet regimens with either the normal chow (Ctrl) or the HFD, the WT and miR-150$^{-/-}$ mouse retinas were fixed, sectioned, and processed for immunostaining of pELK1$_{S383}$ (red). The fluorescent intensities in the ONL and IS/OS were measured using ImageJ. * indicates a statistical significance between the groups specified with horizontal lines. Each data point represents one area of measurement. n=3 mice for each group; p<0.05, one-way ANOVA. Scale bar: 20 µm.

transfected with the miR-150 mimic (150m; 150 mimic), miR-150 inhibitor (150in; 150 inhibitor), or the negative control (miRNC), cells were then treated with 100 µM PA, BSA (vehicle), or cultural medium control (Ctrl) for 24 hours. Treatments with PA significantly increased nuclear pELK1$_{S383}$ regardless of the cellular levels of miR-150 (Fig. 4-6). Overexpression of miR-150 (150 mimic) in BSA- or Ctrl-treated cells significantly decreased cytoplasmic pELK1$_{S383}$, while cells transfected with miR-150 inhibitor had significant increases in cytoplasmic pELK1$_{S383}$ regardless of their

treatments (PA, BSA, or Ctrl; Fig. 4-6). Therefore, the PA treatments increased nuclear pELK1$_{S383}$ (Fig. 4-6) and induced inflammation (Fig. 4-2) in 661W cells. Knocking down miR-150 increased cytoplasmic pELK1$_{S383}$ (Fig. 4-6) and promoted inflammation (Fig. 4-2B).

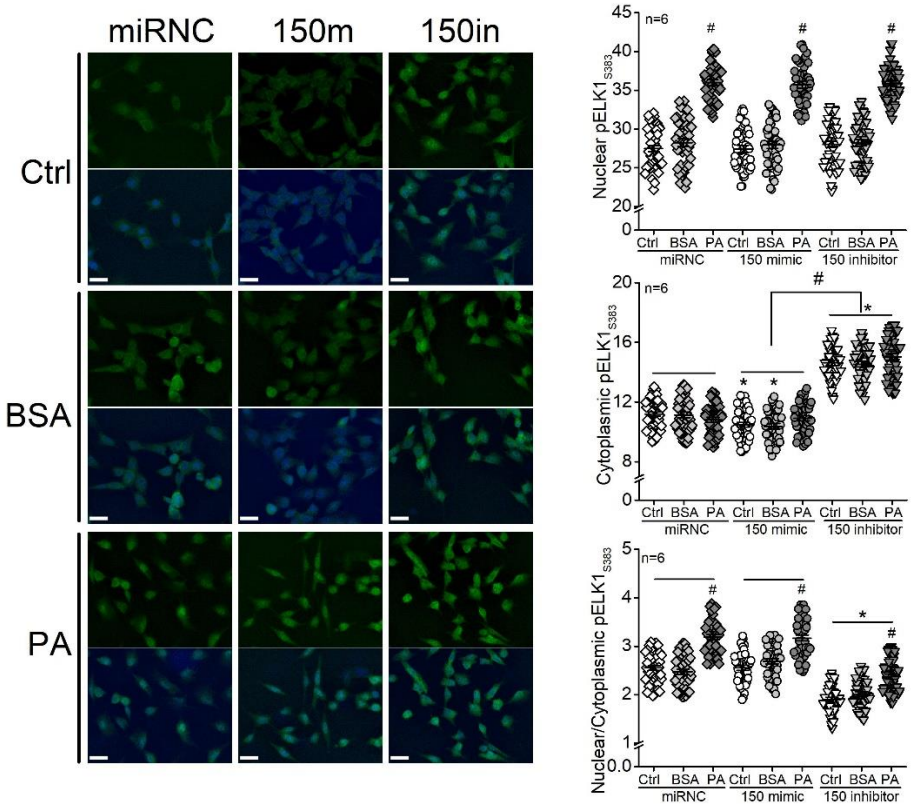

Figure 4-6 Knocking down miR-150 increases cytoplasmic pELK1$_{S383}$, while PA treatments increase nuclear pELK1$_{S383}$ in 661W cells.
The 661W cells were first transfected with microRNA negative control (miRNC), miR-150 mimic (150m; 150 mimic), or miR-150 inhibitor (150in; 150 inhibitor) and then treated with culture medium (Ctrl), BSA (vehicle), or 100 μM PA (PA) for 24 hours. Cells were fixed and processed for fluorescent immunostaining with pELK1$_{S383}$ (green) and DAPI (blue). The fluorescent intensities of pELK1$_{S383}$ in the cell nucleus and cytoplasm were measured using ImageJ, and the nuclear and cytoplasmic pELK1$_{S383}$ ratio was calculated. Nuclear pELK1$_{S383}$: # indicates a statistical significance when comparing PA-treated cells with BSA-treated cells. Cytoplasmic pELK1$_{S383}$: * indicates that all three 150 inhibitor groups are significantly different from miRNC groups, and 150 mimic-Ctrl and 150mimic-BSA are also significantly different from miRNC-Ctrl and miRNC-BSA. # indicates that there is a statistical significance between all 150 inhibitor groups when compared to all 150 mimic groups. Nuclear/Cytoplasmic pELK1$_{S383}$: # indicates a statistical significance when compared to the BSA groups. * indicates a

statistical significance of 150 inhibitor groups when compared to the miRNC and 150 mimic groups. Each data point represents one area of measurement**.** $n = 6$ experimental trials for each group; $p<0.05$, one-way ANOVA. Scale bar: 30 μm.

Overexpression of miR-150 (150 mimic) did not overturn the PA-induced inflammation (Fig. 4-2B), which may be explained by the nuclear pELK1$_{S383}$ level of PA-treated and miR-150 mimic-transfected cells (Fig. 4-6). These data suggest that the PA-induced increase of nuclear pELK1$_{S383}$ (Fig. 4-6) could mediate the inflammation in 661W cells (Fig. 4-2), and the upregulated cytoplasmic pELK1$_{S383}$ in miR-150 knockdown (150in) cells (Fig. 4-6) may promote inflammation (Fig. 4-2B). The overexpression of miR-150 is not sufficient to downregulate pELK1$_{S383}$ under the PA treatment (Fig. 4-6) or overcome PA-induced inflammation (Fig. 4-2B).

4.4.7. Knocking Down *Elk1* Decreases Cytoplasmic pELK1$_{S383}$ and Prevents PA-Elicited Increase of Nuclear pELK1$_{S383}$ in 661W Cells

We showed that knocking down *Elk1* alleviated PA-induced inflammation in 661W cells (Fig. 4-4). In order to understand whether the suppression of inflammation is correlated with the cellular distribution of pELK1$_{S383}$, we used siRNA to knock down *Elk1 (*si*Elk1)* and determine cytoplasmic versus nuclear pELK1$_{S383}$ in 661W cells. While PA treatments elicited significant increases of nuclear pELK1$_{S383}$, transfection with si*Elk1* significantly decreased the cytoplasmic pELK1$_{S383}$ and attenuated the PA-induced increase of nuclear pELK1$_{S383}$, compared to cells transfected with the negative control (siNC; Fig. 4-7). Therefore, knocking down *Elk1* decreased PA-elicited increases of pELK1$_{S383}$ (Fig. 4-7), which implies that downregulation of pELK1$_{S383}$ could dampen PA-induced inflammation (Fig. 4-4).

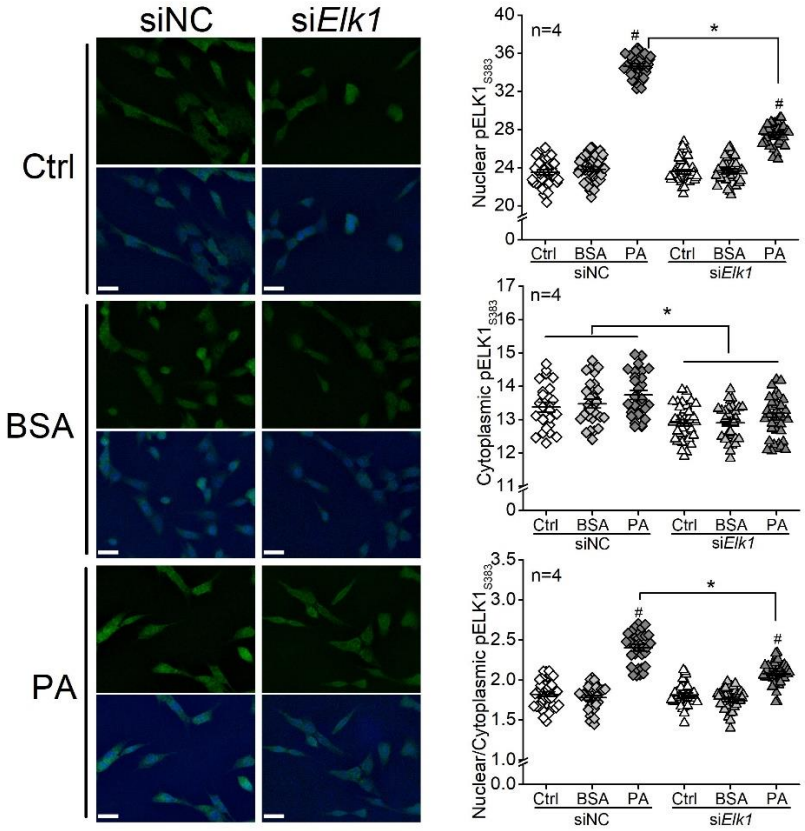

Figure 4-7 Knocking down *Elk1* decreases cytoplasmic pELK1$_{S383}$ and prevents PA-elicited increase of nuclear pELK1$_{S383}$ in 661W cells.
The 661W cells were first transfected with siRNA negative control (siNC) or *Elk1* siRNA (si*Elk1*), and then treated with culture medium (Ctrl), BSA, or 100 µM PA (PA) for 24 hours. Cells were fixed, processed, and immunostained with pELK1$_{S383}$ (green) and DAPI (blue). The fluorescent intensities of pELK1$_{S383}$ in the cell nucleus and cytoplasm were measured using ImageJ, and the nuclear and cytoplasmic pELK1$_{S383}$ ratio was calculated. Nuclear pELK1$_{S383}$: # indicates a statistical significance when comparing PA-treated cells with BSA-treated cells. * indicates a statistical significance between siNC-PA and si*Elk1*-PA. Cytoplasmic pELK1$_{S383}$: * indicates that all si*Elk1* groups are significantly different from all siNC groups. Nuclear/Cytoplasmic ELK1$_{S383}$: # indicates a statistical significance when comparing PA-treated cells with BSA-treated cells. * indicates a statistical significance between siNC-PA and si*Elk1*-PA. Each data point represents one area of measurement**.** n = 4 experimental trials for each group; p<0.05, one-way ANOVA. Scale bar: 30 µm.

4.5. Discussion

Chronic inflammation manifests in the diabetic retina [74, 190, 292]. Diabetic conditions such as hyperlipidemia and hyperglycemia cause increases in pro-

inflammatory molecules in the retinal neurons including photoreceptors [293, 294]. Photoreceptors are major contributors to the inflammation in the diabetic retina [217, 280], but we still do not have a complete picture of how diabetic conditions elicit inflammation in photoreceptors. MiR-150 is a suppressor of inflammation [198, 199, 295]. Under diabetic insults, deletion of miR-150 causes an exacerbated upregulation of pro-inflammatory cytokines [190, 198], and miR-150 overexpression reduces those molecules [296]. We found that pP65, a biomarker of inflammation, increased in both inner and outer segments and the ONL of photoreceptors in the mouse retina under HFD-induced T2D, and deletion of miR-150 further exacerbated the HFD-induced increase of pP65 (Fig. 4-1). Others have shown that overexpression of miR-150 suppresses pP65 by downregulating the target genes of miR-150.

Using cultured 661W cells, we identified that *Elk1* is the direct target of miR-150 that mediates PA-elicited inflammation. The activation and specific function of ELK1 is its phosphorylation site-dependent [297, 298], as phosphorylation of ELK1 on S383 ($pELK1_{S383}$) is known to promote inflammation [290, 291]. Phosphorylation site-dependent functions for a protein are not unique to ELK1. For example, phosphorylation of AMP-activated protein kinase (AMPK) at Ser485/491 facilitates cardiac hypertrophy, while phosphorylated AMPK at Thr172 mediates the antihypertrophic response [299]. The phosphorylated ELK1 at S383 ($pELK1_{S383}$) translocates from the cytoplasm to the nucleus, and nuclear $pELK1_{S383}$ further transactivates its downstream genes to promote inflammation [290, 291]. In this study, we found that the $pELK1_{S383}$ increased in the retinal ONL of the HFD mice (Fig. 4-5)

and the nuclei of PA-treated 661W cells (Fig. 4-6), and the increased nuclear pELK1$_{S383}$ correlates with the upregulated pP65 in photoreceptors under the HFD regimen or PA treatments (HFD/PA). Knocking out miR-150 further upregulated cytoplasmic pELK1$_{S383}$ as well as exacerbated HFD/PA-elicited increase of pP65 (Fig. 4-1 and 4-2). Our results suggest that HFD/PA may induce inflammation in photoreceptors by increasing the nuclear pELK1$_{S383}$, and the upregulated cytoplasmic pELK1$_{S383}$ could further exacerbate the inflammation. While phosphorylated ELK1 promotes the transcription of downstream genes, SUMOylated ELK1 represses the transactivation activity [300, 301]. Stress elevates the phosphorylation of ELK1 while removing the SUMOylation [302, 303]. It is possible that decreased SUMOylated ELK1 in the cytosol partially contributes to the upregulation of cytoplasmic pELK1$_{S383}$ (Fig. 4-5 and 4-6), which may explain the exacerbated inflammation in miR-150-knockdown cells.

As nuclear/cytoplasmic (N/C) ratio represents the cytoplasm-to-nucleus translocation of pELK1$_{S383}$, we showed that the PA treatment increased the N/C ratio of pELK1$_{S383}$ in 661W cells (Fig. 4-6), and knocking down *Elk1* (si*Elk1*) decreased nuclear pELK1$_{S383}$ and the N/C ratio of pELK1$_{S383}$ in PA-treated 661W cells (Fig. 4-7), which correlated with the downregulation of pP65 (Fig. 4-4B). In addition, the cytoplasmic pELK1$_{S383}$ was decreased in the si*Elk1* cells, which may further repress the activity of ELK1. The results imply that knocking down *Elk1* can potentially alleviate diabetes-associated inflammation in retinal photoreceptors.

Inflammation in retinal photoreceptors under diabetes correlates with the dampened light responses of the retina [74, 190]. Although pP65 is not significantly

downregulated by overexpressing of miR-150 (Fig. 4-2B), other pro-inflammatory molecules such as TNF-α are diminished by overexpression of miR-150 [199, 244, 295]. Moreover, miR-150 can reduce the apoptosis of endothelial cells under inflammation [199]. Therefore, overexpressing miR-150 could protect the retinal endothelial cells from diabetic insults. In this study, knocking down *Elk1* reduces pP65 in PA-treated 661W cells, indicating that pP65 is regulated by ELK1, although NFκB is not a direct target of ELK1. Since inhibiting NFκB P65 alleviates the high glucose-induced apoptosis in endothelial cells [304, 305], knocking down *Elk1* could mitigate diabetes-induced damages to the retinal vasculature. Therefore, *Elk1* might be a new target for future therapeutics to treat diabetes-associated inflammation and potentially prevent the development of DR.

5. CONCLUSIONS

5.1. Summary

The results from chapters 2-4 indicate that decreased miR-150 under T2D conditions contribute to the development of DR by promoting the degeneration of the neural retina and retinal vasculature. MiR-150 knockout/knockdown in T2D mice or palmitic acid (PA)-treated photoreceptors exacerbates the apoptosis and inflammation. However, overexpressing miR-150 is not sufficient to overcome the PA-induced apoptosis in photoreceptors. *Elk1* is a functional target of miR-150 in photoreceptors. MiR-150 knockout/knockdown upregulates ELK1 and phosphorylated ELK1 (pELK1) in the cytoplasm of photoreceptors while HFD/PA increases the nuclear ELK1 and pELK1. Overexpressing miR-150 downregulates cytoplasmic ELK1 and pELK1 in photoreceptors. Knocking down *Elk1* decreases ELK1 and cytoplasmic pELK1, and reduces the nuclear pELK1 in PA-treated photoreceptors. Knocking down *Elk1* alleviates PA-elicited inflammation but not apoptosis in photoreceptors, which may be explained by the different cytoplasm-to-nucleus translocations of pELK1 at serine 383 ($pELK1_{S383}$) and pELK1 at threonine 417 ($pELK1_{T417}$).

5.2. Mechanisms for Diabetes-Induced Neural Dysfunction

In chapters 2 and 3, I showed dampened light responses and apoptosis of photoreceptors in the retina of HFD mice. Though neuronal apoptosis in the diabetic retina contributes to neural dysfunction [61, 306], there could be other factors that impair the neural function, such as reduced regeneration of rhodopsin [307]. In STZ rats and mice, the retinal light responses measured by electroretinography (ERG) are dampened

while the levels of rhodopsin and 11-*cis*-retinal (chromophore of rhodopsin) in the retina decrease after 3-4 months of diabetes. Further investigation found that STZ rats had decreased retinal expression of interphotoreceptor retinol-binding protein (IRBP) [308, 309], which is secreted by photoreceptors and facilitates the transportation of 11-*cis*-retinal into photoreceptors [310]. The level of IRBP decreases in the vitreous of DR patients compared to healthy subjects and reduces in the retina of non-proliferative DR (NPDR) patients compared to the PDR patients [311]. The transgenic STZ mice overexpressing IRBP had improved visual function and restored levels of rhodopsin and 11-*cis*-retinal [309]. Interestingly, overexpressing IRBP in photoreceptors alleviates the reduction of retinal thickness in STZ mice [311]. In addition, the IRBP-transgenic STZ mice had alleviated apoptosis, decreased levels of NADPH oxidase 4 (NOX4) and NFκB, and inhibited activation of microglia in the retina compared to the WT STZ mice [309]. The results suggest that the dysfunction of photoreceptors can contribute to apoptosis in the diabetic retina by promoting oxidative stress and inflammation.

5.3. Neuroprotection by miR-150

In chapter 3, I showed that miR-150 knockdown exacerbated the palmitic acid-induced apoptosis in cultured photoreceptors. However, overexpressing miR-150 was not sufficient to reverse the apoptosis. This could be explained by other factors that contribute to neuronal apoptosis but are not regulated by miR-150, such as decreased rhodopsin and IRBP in the diabetic retina. Another possibility is that other cell types in the retina participate in the neuroprotection exerted by miR-150, which can be tested by *in vivo* experiments to see whether overexpressing miR-150 in the mouse retina could

alleviate the T2D-induced neuronal apoptosis. One target gene of miR-150 that may affect various cell types and mediate apoptosis in the diabetic retina is glucose transporter 1 (*Glut1*) [312, 313]. GLUT1 is the primary glucose transporter in the retina and is expressed in the endothelial cells, retinal pigmented endothelium (RPE) [314], and cells in the neural retina including photoreceptors and Müller Glia [315]. Intraocular injection of siRNA of *Glut1* in STZ mice reduced the glucose concentration in the retina and alleviated the neural dysfunction and degeneration of the outer nuclear layer (ONL) induced by diabetes. The levels of pro-inflammatory factors (TNF-α and ICAM-1) were decreased by inhibiting *Glut1* in the retina of STZ mice [316]. Specific knockdown of *Glut1* in the neural retina restored the visual function and reduced the levels of pro-inflammatory factors (IL-1β and TNF-α) [317]. Therefore, overexpressing miR-150 in the retina could protect the neurons from diabetic insults by downregulating *Glut1*.

5.4. MiR-150 May Inhibit Apoptosis Through Other Downstream Targets

In chapter 3, I showed that knocking down *Elk1* did not alleviate the PA-induced apoptosis in photoreceptors. Since ELK1 is a transcription factor and phosphorylated ELK1 at threonine 417 ($pELK1_{T417}$) is the active form of ELK1 that regulates apoptosis, the result can be explained by the similar ratio of nuclear/cytoplasmic $pELK1_{T417}$ in *Elk1* knockdown cells and the control cells. To further evaluate the function of *Elk1* in regulating neuronal apoptosis, we need to test the effect of *Elk1* overexpression in the PA-treated photoreceptors. We have shown that the upregulated ELK1 and $pELK1_{T417}$ correlated with more severe apoptosis of photoreceptors in miR-$150^{-/-}$ mice and miR-150-knockdown cells under T2D conditions. If overexpression of *Elk1* in PA-treated

photoreceptors exacerbates the apoptosis, it is possible that other factors or retinal cell types (as mentioned in the last paragraph) are needed for the neuroprotection exerted by *Elk1* knockdown.

However, there is a possibility that *Elk1* is not the primary downstream target of miR-150 that regulates apoptosis in retinal neurons. MiR-150 has multiple target genes that can regulate apoptosis under hypoxia, which also occurs in the diabetic retina [195, 196]. For example, overexpression of miR-150 alleviated the hypoxia-induced apoptosis in cardiomyocytes by downregulating the pro-apoptotic BCL2 associated X protein (BAX). Inhibiting miR-150 or overexpressing BAX exacerbates apoptosis [318]. The glucose-regulated protein 94 (GRP94) is another target of miR-150 that can regulate apoptosis [194] and is upregulated in T2D patients [319]. Overexpression of miR-150 alleviated the apoptosis of hypoxic cardiomyocytes by downregulating GRP94 [194]. Both BAX and GRP94 are expressed in the retina [320] and could be upregulated by decreased miR-150 under diabetes.

5.5. NFκB Regulates Both Oxidative Stress and Inflammation

In chapter 4, I showed that phosphorylated NFκB P65 (pP65) is upregulated in photoreceptors by miR-150 knockout/knockdown under T2D conditions. Overexpressing miR-150 in BSA-treated photoreceptors downregulated pP65. However, it is not clear whether NFκB is a direct target of miR-150. Other studies have shown the correlation between miR-150 overexpression and reduced level of pP65 in epithelial and endothelial cells under inflammatory stimuli [199, 321]. However, the regulation of pP65 could be mediated through other target genes of miR-150 [322].

NFκB is a transcription factor that is activated upon the stimulation of upstream receptors, such as toll-like receptors (TLRs) and TNF receptors (TNFRs) [323]. The activated NFκB dissociates with IκB, translocates to the nucleus, and regulates the transcription of downstream genes [324]. Phosphorylated NFκB P65 (pP65) increases under inflammatory stimuli and promotes the expression of inflammatory factors [324]. For example, the pP65 increases in the cytosol and nuclei of cells under TNF treatment. Knocking out P65 or blocking the phosphorylation of P65 inhibits the expression of pro-inflammatory factors including vascular cell adhesion molecule (VCAM)-1 [325]. NFκB is also involved in oxidative stress and is activated by reactive oxygen species (ROS) [326]. In STZ rats, oral treatment with antioxidants reduced the activation of NFκB and expression of P65 in the retina [293]. Therefore, NFκB could regulate the diabetes-induced apoptosis in photoreceptors through the signaling of inflammation and oxidative stress. Decreased miR-150 in the diabetic retina could exacerbate apoptosis by upregulating both NFκB and ELK1.

In chapter 4, I showed that knocking down *Elk1* decreased pP65 in photoreceptors under BSA/PA treatments, indicating the NFκB could be a downstream target of ELK1. In the human urothelial carcinoma cell line, knocking down *Elk1* reduced the expression of NFκB P65 [327]. However, ELK1 could also be regulated by NFκB. In the human pancreatic tumor cell line, inhibiting the activation of NFκB reduced the expression of *Elk1* and suppressed the binding activity of ELK1 to its downstream genes [328]. Therefore, ELK1 and NFκB could interact with each other in response to different stimuli. It will be interesting to test whether blocking the activation

of NFκB could decrease the expression of ELK1 or inhibit the cytoplasm-to-nucleus translocation of pELK1 in photoreceptors and alleviate the PA-induced apoptosis.

5.6. MiR-150 in Retinal Neurons and Endothelial Cells

MiR-150 is decreased in the blood circulation and retina of diabetic patients [167, 187] and animals [189, 190]. In chapter 3, I showed that miR-150 decreased in the photoreceptors under palmitic acid (PA) treatment. However, the level of miR-150 is changed differently by PA in retinal endothelial cells (RECs). I found that miR-150 increased while the mRNA and protein levels of *Elk1* decreased in PA-treated human RECs (HRECs) (Fig. 5-1), indicating the regulation of miR-150 expression is different between endothelial cells and photoreceptors.

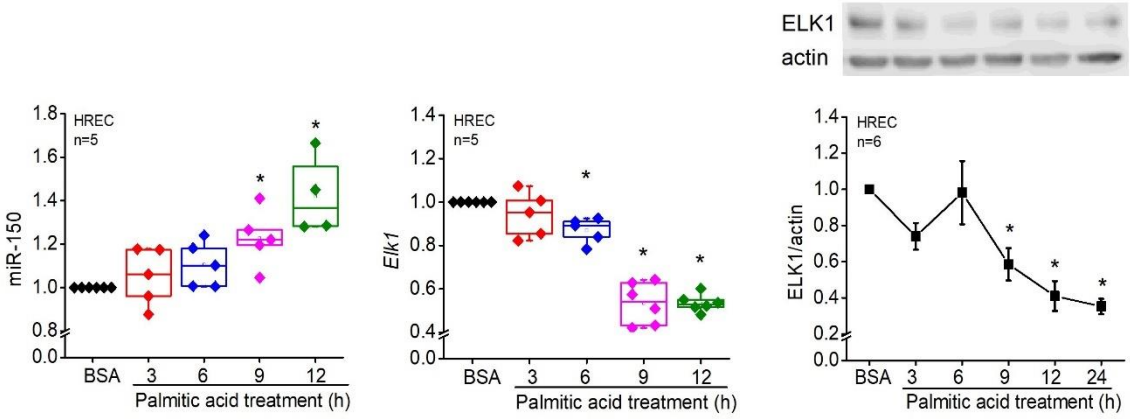

Figure 5-1 MiR-150 increases while mRNA *Elk1* and protein ELK1 decrease in human retinal endothelial cells (HRECs) under palmitic acid (PA) treatment.
The HRECs were treated with BSA (vehicle) or 100 μM PA (PA) for various times. The levels of miR-150 (left) and *Elk1* mRNA (middle) were carried out using qPCR. The protein level of ELK1 (right) was measured using Western blots. * indicates a statistical difference when compared to the BSA treatment. $p<0.05$, one-way ANOVA.

Several microRNAs also have varying expression levels and functions in different tissues under diabetes. As mentioned in chapter 1, miR-29b increases in the

blood of DR patients. Inhibiting miR-29b alleviates the apoptosis of RECs under high glucose (HG) and hypoxia [178]. However, miR-29b has also been found to decrease in the retina of STZ rats after 1-7 months of diabetes while the TUNEL positive cells increase in the inner nuclear layer (INL). Overexpressing miR-29b decreases the caspase-3 activity and the expression of pro-apoptotic BCL2 associated X protein (BAX), and increases the anti-apoptotic B-cell lymphoma protein 2 (BCL2) in HG-treated Müller cells [329]. MiR-145 is upregulated in retinal ganglion cells (RGCs) [330] but downregulated in RECs [173] under high glucose treatment. Inhibiting miR-145 in RGCs alleviated the apoptosis and suppressed the expression of IL-6 and TNF-α induced by HG [330], while overexpressing miR-145 in HG-treated RECs mitigated apoptosis, reduced the production of ROS, and decreased the expressions of NFκB, IL-1β, and TNF-α [173].

Therefore, miR-150 and *Elk1* may function differently in endothelial cells and neurons when regulating apoptosis under diabetic conditions. In chapter 2, I showed that the miR-150$^{-/-}$ mice had more severe degeneration of retinal capillaries, indicating the overall decreased level of miR-150 promotes apoptosis in endothelial cells. If miR-150 increases *in vivo* in the RECs under diabetes as showed in the *in vitro* experiment (Fig. 5-1), it is possible that the decreased miR-150 in neurons or glia influences the vasculature and promotes vascular degeneration in the diabetic retina.

5.7. Future Directions

The level of miR-150 decreases in the retina (Fig. 2-1) and photoreceptors (Fig. 4-3) while increases in REC (Fig. 5-1) under diabetic conditions. The results indicate

that the expression of miR-150 is cell type-dependent. Therefore, it is necessary to clarify the up-/down-regulation of miR-150 in different cell types of the diabetic retina. We can use *in situ* hybridization and cell type-specific markers to show the expression levels of miR-150 in retinal neurons and endothelial cells.

In Figure 2-4, I showed that miR-150$^{-/-}$ mice had an increased number of degenerated capillaries compared to the WT mice, which suggests that decreased miR-150 promotes apoptosis and increased miR-150 suppresses apoptosis in REC. We need to confirm the function of miR-150 in regulating apoptosis of REC by knocking down/overexpressing miR-150 in cultured REC. If knocking down miR-150 in REC promotes apoptosis but the level of miR-150 increases in the REC of the diabetic retina, we can postulate that miR-150 is upregulated in REC as a compensatory mechanism to mitigate the diabetes-induced impairment. However, if overexpressing miR-150 promotes apoptosis in REC, we can postulate that miR-150 functions differently in regulating apoptosis of retinal neurons and endothelial cells. In cultured human umbilical vein endothelial cells (HUVEC) treated with oxidized low-density lipoprotein (ox-LDL), overexpressing miR-150 exacerbated apoptosis while knocking down miR-150 alleviated apoptosis [267]. It is possible that miR-150 targets different sets of downstream target genes in neurons and endothelial cells and regulates apoptosis in a cell type-dependent manner.

In Figure 3-2, I showed that overexpressing miR-150 in cultured photoreceptors did not alleviate apoptosis under PA treatment. However, we cannot exclude the neuroprotective effect of miR-150. Retinal glial cells are involved in neuroprotection.

The Müller glial cells protect retinal neurons from hypoxia [331], and the activated microglia contribute to neuronal apoptosis [23]. Therefore, miR-150 could regulate the apoptosis of retinal neurons by affecting the functions of retinal glia. We can confirm whether miR-150 protects neurons in the diabetic retina by intraocular injection of miR-150. If overexpressing miR-150 preserves neural function and promotes neuronal survival in the diabetic retina, it is possible that the functions of glial cells are under the regulation of miR-150.

Overall, miR-150 alleviates neuroinflammation and suppresses pathological angiogenesis in the retina [197], and could protect retinal neurons from diabetic insults. Therefore, miR-150 is a potential therapeutic target of DR that needs further studies.

REFERENCES

1. Runkle, E.A. and D.A. Antonetti, *The blood-retinal barrier: structure and functional significance.* Methods Mol Biol, 2011. **686**: p. 133-48.

2. Zhang, C., et al., *Establishing Wiring Specificity in Visual System Circuits: From the Retina to the Brain.* Annu Rev Neurosci, 2017. **40**: p. 395-424.

3. Pepe, I.M., *Rhodopsin and phototransduction.* Journal of Photochemistry and Photobiology B: Biology, 1999. **48**(1): p. 1-10.

4. Jindrová, H., *Vertebrate phototransduction: activation, recovery, and adaptation.* (0862-8408 (Print)).

5. Barnstable, C.J., J.-Y. Wei, and M.-H. Han, *Modulation of synaptic function by cGMP and cGMP-gated cation channels.* Neurochemistry International, 2004. **45**(6): p. 875-884.

6. Kefalov, V.J., *Rod and Cone Visual Pigments and Phototransduction through Pharmacological, Genetic, and Physiological Approaches.* Journal of Biological Chemistry, 2012. **287**(3): p. 1635-1641.

7. Baylor, D.A. and M.E. Burns, *Control of rhodopsin activity in vision.* Eye, 1998. **12**(3): p. 521-525.

8. Grünert, U. and P.R. Martin, *Cell types and cell circuits in human and non-human primate retina.* Progress in Retinal and Eye Research, 2020. **78**: p. 100844.

9. Thoreson, W.B. and S.C. Mangel, *Lateral interactions in the outer retina.* Prog Retin Eye Res, 2012. **31**(5): p. 407-41.

10. Barnes, S., et al., *Horizontal Cell Feedback to Cone Photoreceptors in Mammalian Retina: Novel Insights From the GABA-pH Hybrid Model.* Front Cell Neurosci, 2020. **14**: p. 595064.

11. Masland, R.H., *The neuronal organization of the retina.* Neuron, 2012. **76**(2): p. 266-80.

12. Masland, R.H., *The fundamental plan of the retina.* (1097-6256 (Print)).

13. Schiller, P.H., *Parallel information processing channels created in the retina.* Proceedings of the National Academy of Sciences, 2010. **107**(40): p. 17087-17094.

14. Richard, *The Neuronal Organization of the Retina.* Neuron, 2012. **76**(2): p. 266-280.

15. Pereiro, X., et al., *Optimization of a Method to Isolate and Culture Adult Porcine, Rats and Mice Muller Glia in Order to Study Retinal Diseases.* Front Cell Neurosci, 2020. **14**: p. 7.

16. Reichenbach, A. and A. Bringmann, *Glia of the human retina.* Glia, 2020. **68**(4): p. 768-796.

17. Barber, A.J., T.W. Gardner, and S.F. Abcouwer, *The Significance of Vascular and Neural Apoptosis to the Pathology of Diabetic Retinopathy.* Investigative Opthalmology & Visual Science, 2011. **52**(2): p. 1156.

18. Bringmann, A., et al., *Müller cells in the healthy and diseased retina.* Progress in Retinal and Eye Research, 2006. **25**(4): p. 397-424.

19. Fitzgerald, M., et al., *Early events of secondary degeneration after partial optic nerve transection: an immunohistochemical study.* (1557-9042 (Electronic)).

20. Ly, A., et al., *Early Inner Retinal Astrocyte Dysfunction during Diabetes and Development of Hypoxia, Retinal Stress, and Neuronal Functional Loss.* Investigative Opthalmology & Visual Science, 2011. **52**(13): p. 9316.

21. Rungger-Brändle, E., P.M. Dosso Aa Fau - Leuenberger, and P.M. Leuenberger, *Glial reactivity, an early feature of diabetic retinopathy.* (0146-0404 (Print)).

22. Fontainhas, A.M., et al., *Microglial Morphology and Dynamic Behavior Is Regulated by Ionotropic Glutamatergic and GABAergic Neurotransmission.* PLoS ONE, 2011. **6**(1): p. e15973.

23. Langmann, T., *Microglia activation in retinal degeneration.* Journal of Leukocyte Biology, 2007. **81**(6): p. 1345-1351.

24. McCarthy, C.A., et al., *Brain and retinal microglia in health and disease: An unrecognized target of the renin-angiotensin system.* Clinical and Experimental Pharmacology and Physiology, 2013. **40**(8): p. 571-579.

25. Kur, J., E.A. Newman, and T. Chan-Ling, *Cellular and physiological mechanisms underlying blood flow regulation in the retina and choroid in health and disease.* Progress in Retinal and Eye Research, 2012. **31**(5): p. 377-406.

26. Xu, H. and M. Chen, *Diabetic retinopathy and dysregulated innate immunity.* Vision Res, 2017. **139**: p. 39-46.

27. Campbell, M. and P. Humphries, *The blood-retina barrier: tight junctions and barrier modulation.* (0065-2598 (Print)).

28. Li, M., et al., *Occludin downregulation in high glucose is regulated by SSTR2 via the VEGF/NRP1/Akt signaling pathway in RF/6A cells.* Experimental and Therapeutic Medicine, 2017. **14**(2): p. 1732-1738.

29. Barsegian, A., et al., *Diabetic Retinopathy: Focus on Minority Populations.* Int J Clin Endocrinol Metab, 2017. **3**(1): p. 034-45.

30. Barber, A.J., *A new view of diabetic retinopathy: a neurodegenerative disease of the eye.* Progress in Neuro-Psychopharmacology and Biological Psychiatry, 2003. **27**(2): p. 283-290.

31. Boyle, J.P., et al., *Projection of the year 2050 burden of diabetes in the US adult population: dynamic modeling of incidence, mortality, and prediabetes prevalence.* Popul Health Metr, 2010. **8**: p. 29.

32. Wong, T.Y., et al., *Diabetic retinopathy.* Nat Rev Dis Primers, 2016. **2**: p. 16012.

33. Simó-Servat, O., C. Hernández, and R. Simó, *Diabetic Retinopathy in the Context of Patients with Diabetes.* Ophthalmic Research, 2019. **62**(4): p. 211-217.

34. Moran, E.P., et al., *Neurovascular cross talk in diabetic retinopathy: Pathophysiological roles and therapeutic implications.* Am J Physiol Heart Circ Physiol, 2016. **311**(3): p. H738-49.

35. Cheng, R. and J.-X. Ma, *Angiogenesis in diabetes and obesity.* Reviews in Endocrine and Metabolic Disorders, 2015. **16**(1): p. 67-75.

36. Tzekov, R. and G.B. Arden, *The Electroretinogram in Diabetic Retinopathy.* Survey of Ophthalmology, 1999. **44**(1): p. 53-60.

37. Zeng, Y., et al., *Retinal vasculature–function correlation in non-proliferative diabetic retinopathy.* Documenta Ophthalmologica, 2020. **140**(2): p. 129-138.

38. Simo, R., J.M. Sundstrom, and D.A. Antonetti, *Ocular Anti-VEGF therapy for diabetic retinopathy: the role of VEGF in the pathogenesis of diabetic retinopathy.* Diabetes Care, 2014. **37**(4): p. 893-9.

39. Cheung, N., I.Y. Wong, and T.Y. Wong, *Ocular anti-VEGF therapy for diabetic retinopathy: overview of clinical efficacy and evolving applications.* Diabetes Care, 2014. **37**(4): p. 900-5.

40. Lopes De Faria, J.M., H. Russ, and V.P. Costa, *Retinal nerve fibre layer loss in patients with type 1 diabetes mellitus without retinopathy.* British Journal of Ophthalmology, 2002. **86**(7): p. 725-728.

41. Van Dijk, H.W., et al., *Early Neurodegeneration in the Retina of Type 2 Diabetic Patients.* Investigative Opthalmology & Visual Science, 2012. **53**(6): p. 2715.

42. Frydkjaer-Olsen, U., et al., *Structural neurodegeneration correlates with early diabetic retinopathy.* International Ophthalmology, 2018. **38**(4): p. 1621-1626.

43. Curtis, T.M., T.A. Gardiner, and A.W. Stitt, *Microvascular lesions of diabetic retinopathy: clues towards understanding pathogenesis?* Eye, 2009. **23**(7): p. 1496-1508.

44. Carrasco, E., et al., *Lower Somatostatin Expression Is an Early Event in Diabetic Retinopathy and Is Associated With Retinal Neurodegeneration.* Diabetes Care, 2007. **30**(11): p. 2902-2908.

45. Garcia-Ramírez, M., et al., *Interphotoreceptor retinoid-binding protein (IRBP) is downregulated at early stages of diabetic retinopathy.* Diabetologia, 2009. **52**(12): p. 2633-2641.

46. Li, W., et al., *Retinal capillary pericyte apoptosis in early human diabetic retinopathy.* (0366-6999 (Print)).

47. Elmore, S., *Apoptosis: A Review of Programmed Cell Death.* Toxicologic Pathology, 2007. **35**(4): p. 495-516.

48. Xu, X., Y. Lai, and Z.C. Hua, *Apoptosis and apoptotic body: disease message and therapeutic target potentials.* Biosci Rep, 2019. **39**(1).

49. Kurosaka, K., et al., *Silent cleanup of very early apoptotic cells by macrophages.* J Immunol, 2003. **171**(9): p. 4672-9.

50. Zeiss, C.J., *The Apoptosis-Necrosis Continuum: Insights from Genetically Altered Mice.* Veterinary Pathology, 2003. **40**(5): p. 481-495.

51. Trump, B.E., et al., *The Pathways of Cell Death: Oncosis, Apoptosis, and Necrosis.* Toxicologic Pathology, 1997. **25**(1): p. 82-88.

52. Igney, F.H. and P.H. Krammer, *Death and anti-death: tumour resistance to apoptosis.* Nat Rev Cancer, 2002. **2**(4): p. 277-88.

53. Halestrap AP, M.G., Clarke SJ, *The permeability transition pore complex: another view.* Biochimie, 2002. **84**(2-3): p. 14.

54. Saelens, X., et al., *Toxic proteins released from mitochondria in cell death.* Oncogene, 2004. **23**(16): p. 2861-74.

55. Li, L.Y., X. Luo, and X. Wang, *Endonuclease G is an apoptotic DNase when released from mitochondria.* Nature, 2001. **412**(6842): p. 95-99.

56. Locksley, R.M., N. Killeen, and M.J. Lenardo, *The TNF and TNF Receptor Superfamilies.* Cell, 2001. **104**(4): p. 487-501.

57. Falschlehner, C., et al., *TRAIL signalling: Decisions between life and death.* The International Journal of Biochemistry & Cell Biology, 2007. **39**(7-8): p. 1462-1475.

58. Nagata, S., *Apoptotic DNA Fragmentation.* Experimental Cell Research, 2000. **256**(1): p. 12-18.

59. Ndozangue-Touriguine, O., J. Hamelin, and J. Bréard, *Cytoskeleton and apoptosis.* Biochemical Pharmacology, 2008. **76**(1): p. 11-18.

60. van Dijk, H.W., et al., *Association of visual function and ganglion cell layer thickness in patients with diabetes mellitus type 1 and no or minimal diabetic retinopathy.* Vision Res, 2011. **51**(2): p. 224-8.

61. Bronson-Castain, K.W., et al., *Adolescents with Type 2 diabetes: early indications of focal retinal neuropathy, retinal thinning, and venular dilation.* Retina, 2009. **29**(5): p. 618-26.

62. Durham, J.T. and I.M. Herman, *Microvascular Modifications in Diabetic Retinopathy.* Current Diabetes Reports, 2011. **11**(4): p. 253-264.

63. Penn, J.S., et al., *Vascular endothelial growth factor in eye disease.* Progress in Retinal and Eye Research, 2008. **27**(4): p. 331-371.

64. Barber, A.J., et al., *Neural apoptosis in the retina during experimental and human diabetes. Early onset and effect of insulin.* Journal of Clinical Investigation, 1998. **102**(4): p. 783-791.

65. El-Asrar, A.M.A., et al., *Expression of Apoptosis Markers in the Retinas of Human Subjects with Diabetes.* Investigative Opthalmology & Visual Science, 2004. **45**(8): p. 2760.

66. Chhablani, J., et al., *Neurodegeneration in Type 2 Diabetes: Evidence From Spectral-Domain Optical Coherence Tomography.* Investigative Opthalmology & Visual Science, 2015. **56**(11): p. 6333.

67. Tavares Ferreira, J., et al., *Retina and Choroid of Diabetic Patients Without Observed Retinal Vascular Changes: A Longitudinal Study.* American Journal of Ophthalmology, 2017. **176**: p. 15-25.

68. Ning, X., et al., *Neuro-optic cell apoptosis and microangiopathy in KKAY mouse retina.* International Journal of Molecular Medicine, 2004. **13**(1): p. 87-92.

69. Barber, A.J., et al., *The Ins2Akita mouse as a model of early retinal complications in diabetes.* Invest Ophthalmol Vis Sci, 2005. **46**(6): p. 2210-8.

70. Martin, P.M., et al., *Death of retinal neurons in streptozotocin-induced diabetic mice.* Invest Ophthalmol Vis Sci, 2004. **45**(9): p. 3330-6.

71. Ahmadieh, H., S. Behbahani, and S. Safi, *Continuous wavelet transform analysis of ERG in patients with diabetic retinopathy.* Documenta Ophthalmologica, 2021. **142**(3): p. 305-314.

72. Kim, M., et al., *Electroretinography and retinal microvascular changes in type 2 diabetes.* Acta Ophthalmologica, 2020. **98**(7).

73. McAnany, J.J. and J.C. Park, *Cone Photoreceptor Dysfunction in Early-Stage Diabetic Retinopathy: Association Between the Activation Phase of Cone Phototransduction and the Flicker Electroretinogram.* Investigative Opthalmology & Visual Science, 2019. **60**(1): p. 64.

74. Kim, A.J., et al., *The Effects of Metformin on Obesity-Induced Dysfunctional Retinas.* Invest Ophthalmol Vis Sci, 2017. **58**(1): p. 106-118.

75. Karaca, C. and Z. Karaca, *Beyond Hyperglycemia, Evidence for Retinal Neurodegeneration in Metabolic Syndrome.* Invest Ophthalmol Vis Sci, 2018. **59**(3): p. 1360-1367.

76. Park, S.H., et al., *Apoptotic death of photoreceptors in the streptozotocin-induced diabetic rat retina.* Diabetologia, 2003. **46**(9): p. 1260-8.

77. Énzsöly, A., et al., *Pathologic Alterations of the Outer Retina in Streptozotocin-Induced Diabetes.* Investigative Opthalmology & Visual Science, 2014. **55**(6): p. 3686.

78. Yang, Q., et al., *Retinal Neurodegeneration in db/db Mice at the Early Period of Diabetes.* J Ophthalmol, 2015. **2015**: p. 757412.

79. Gábriel, R., *Neuropeptides and diabetic retinopathy.* British Journal of Clinical Pharmacology, 2013. **75**(5): p. 1189-1201.

80. Ou, K., et al., *Treatment of diabetic retinopathy through neuropeptide Y-mediated enhancement of neurovascular microenvironment.* Journal of Cellular and Molecular Medicine, 2020. **24**(7): p. 3958-3970.

81. Beltramo, E. and M. Porta, *Pericyte Loss in Diabetic Retinopathy: Mechanisms and Consequences.* Current Medicinal Chemistry, 2013. **20**(26): p. 3218-3225.

82. Mizutani, M., T.S. Kern, and M. Lorenzi, *Accelerated death of retinal microvascular cells in human and experimental diabetic retinopathy.* Journal of Clinical Investigation, 1996. **97**(12): p. 2883-2890.

83. Kern, T.S., et al., *Response of Capillary Cell Death to Aminoguanidine Predicts the Development of Retinopathy: Comparison of Diabetes and Galactosemia.* Investigative Ophthalmology & Visual Science, 2000. **41**(12): p. 3972-3978.

84. Joussen, A.M., et al., *Suppression of Fas-FasL-induced endothelial cell apoptosis prevents diabetic blood-retinal barrier breakdown in a model of streptozotocin-induced diabetes.* The FASEB Journal, 2003. **17**(1): p. 76-78.

85. Podestà, F., et al., *Bax Is Increased in the Retina of Diabetic Subjects and Is Associated with Pericyte Apoptosis in Vivo and in Vitro.* The American Journal of Pathology, 2000. **156**(3): p. 1025-1032.

86. Sugiyama, T., et al., *Enhancement of P2X7-Induced Pore Formation and Apoptosis: An Early Effect of Diabetes on the Retinal Microvasculature.* Investigative Opthalmology & Visual Science, 2004. **45**(3): p. 1026.

87. Cheung, A.K.H., et al., *Aldose Reductase Deficiency Prevents Diabetes-Induced Blood-Retinal Barrier Breakdown, Apoptosis, and Glial Reactivation in the Retina of db/db Mice.* Diabetes, 2005. **54**(11): p. 3119-3125.

88. Behl, Y., et al., *Diabetes-Enhanced Tumor Necrosis Factor-α Production Promotes Apoptosis and the Loss of Retinal Microvascular Cells in Type 1 and Type 2 Models of Diabetic Retinopathy.* The American Journal of Pathology, 2008. **172**(5): p. 1411-1418.

89. Huang, H., et al., *TNFα Is Required for Late BRB Breakdown in Diabetic Retinopathy, and Its Inhibition Prevents Leukostasis and Protects Vessels and Neurons from Apoptosis.* Investigative Opthalmology & Visual Science, 2011. **52**(3): p. 1336.

90. Kang, Q. and C. Yang, *Oxidative stress and diabetic retinopathy: Molecular mechanisms, pathogenetic role and therapeutic implications.* Redox Biol, 2020. **37**: p. 101799.

91. Letts, J.A. and L.A. Sazanov, *Clarifying the supercomplex: the higher-order organization of the mitochondrial electron transport chain.* Nat Struct Mol Biol, 2017. **24**(10): p. 800-808.

92. Brownlee, M., *The Pathobiology of Diabetic Complications: A Unifying Mechanism.* Diabetes, 2005. **54**(6): p. 1615-1625.

93. Panday, A., et al., *NADPH oxidases: an overview from structure to innate immunity-associated pathologies.* Cellular & Molecular Immunology, 2015. **12**(1): p. 5-23.

94. Kizub, I.V., K.I. Klymenko, and A.I. Soloviev, *Protein kinase C in enhanced vascular tone in diabetes mellitus.* International Journal of Cardiology, 2014. **174**(2): p. 230-242.

95. Zhang, Y., et al., *NADPH oxidases and oxidase crosstalk in cardiovascular diseases: novel therapeutic targets.* Nature Reviews Cardiology, 2020. **17**(3): p. 170-194.

96. Neginskaya, M.A., E.V. Pavlov, and S.S. Sheu, *Electrophysiological properties of the mitochondrial permeability transition pores: Channel diversity and disease implication.* Biochimica et Biophysica Acta (BBA) - Bioenergetics, 2021. **1862**(3): p. 148357.

97. Wakabayashi, Y., et al., *Increased levels of 8-hydroxydeoxyguanosine in the vitreous of patients with diabetic retinopathy.* Diabetes Research and Clinical Practice, 2010. **89**(3): p. e59-e61.

98. Kanwar, M., et al., *Oxidative Damage in the Retinal Mitochondria of Diabetic Mice: Possible Protection by Superoxide Dismutase.* Investigative Opthalmology & Visual Science, 2007. **48**(8): p. 3805.

99. Kowluru, R.A. and S. Odenbach, *Effect of Long-Term Administration of -Lipoic Acid on Retinal Capillary Cell Death and the Development of Retinopathy in Diabetic Rats.* Diabetes, 2004. **53**(12): p. 3233-3238.

100. Sasaki, M., et al., *Neurodegenerative influence of oxidative stress in the retina of a murine model of diabetes.* Diabetologia, 2010. **53**(5): p. 971-979.

101. Moran, E., et al., *Protective and antioxidant effects of PPARalpha in the ischemic retina.* Invest Ophthalmol Vis Sci, 2014. **55**(7): p. 4568-76.

102. Tang, J. and T.S. Kern, *Inflammation in diabetic retinopathy.* Prog Retin Eye Res, 2011. **30**(5): p. 343-58.

103. Yu, Y., H. Chen, and S.B. Su, *Neuroinflammatory responses in diabetic retinopathy.* J Neuroinflammation, 2015. **12**: p. 141.

104. Rübsam, A., S. Parikh, and P. Fort, *Role of Inflammation in Diabetic Retinopathy.* International Journal of Molecular Sciences, 2018. **19**(4): p. 942.

105. Sharma, Y., et al., *Advanced glycation end products and diabetic retinopathy.* J Ocul Biol Dis Infor, 2012. **5**(3-4): p. 63-9.

106. Hammes, H.P., et al., *Differential accumulation of advanced glycation end products in the course of diabetic retinopathy.* Diabetologia, 1999. **42**(6): p. 728-736.

107. Ibrahim, A.S., et al., *Retinal Microglial Activation and Inflammation Induced by Amadori-Glycated Albumin in a Rat Model of Diabetes.* Diabetes, 2011. **60**(4): p. 1122-1133.

108. Mulfaul, K., et al., *Toll-like Receptor 2 Facilitates Oxidative Damage-Induced Retinal Degeneration.* Cell Reports, 2020. **30**(7): p. 2209-2224.e5.

109. Lee, J.-J., et al., *High-Fat Diet Induces Toll-Like Receptor 4-Dependent Macrophage/Microglial Cell Activation and Retinal Impairment.* Investigative Opthalmology & Visual Science, 2015. **56**(5): p. 3041.

110. Grigsby, J.G., et al., *The Role of Microglia in Diabetic Retinopathy.* Journal of Ophthalmology, 2014. **2014**: p. 1-15.

111. Busik, J.V., S. Mohr, and M.B. Grant, *Hyperglycemia-Induced Reactive Oxygen Species Toxicity to Endothelial Cells Is Dependent on Paracrine Mediators.* Diabetes, 2008. **57**(7): p. 1952-1965.

112. Chen, W., et al., *Anti-inflammatory Effect of Docosahexaenoic Acid on Cytokine-Induced Adhesion Molecule Expression in Human Retinal Vascular Endothelial Cells.* Investigative Opthalmology & Visual Science, 2005. **46**(11): p. 4342.

113. Vincent, J.A. and S. Mohr, *Inhibition of Caspase-1/Interleukin-1 Signaling Prevents Degeneration of Retinal Capillaries in Diabetes and Galactosemia.* Diabetes, 2007. **56**(1): p. 224-230.

114. Kowluru, R.A., *Role of interleukin-1 in the pathogenesis of diabetic retinopathy.* British Journal of Ophthalmology, 2004. **88**(10): p. 1343-1347.

115. Joussen, A.M., et al., *TNF-alpha mediated apoptosis plays an important role in the development of early diabetic retinopathy and long-term histopathological alterations.* Molecular vision, 2009. **15**: p. 1418-1428.

116. Sivakumar, V., et al., *Retinal ganglion cell death is induced by microglia derived pro-inflammatory cytokines in the hypoxic neonatal retina.* The Journal of Pathology, 2011. **224**(2): p. 245-260.

117. Syeda, S., et al., *Reduced photoreceptor death and improved retinal function during retinal degeneration in mice lacking innate immunity adaptor protein MyD88.* Experimental Neurology, 2015. **267**: p. 1-12.

118. Shin, E.S., et al., *High Glucose Alters Retinal Astrocytes Phenotype through Increased Production of Inflammatory Cytokines and Oxidative Stress.* PLoS ONE, 2014. **9**(7): p. e103148.

119. Zhang, K. and J. Luo, *Role of MCP-1 and CCR2 in alcohol neurotoxicity.* Pharmacological Research, 2019. **139**: p. 360-366.

120. Gerhardinger, C., et al., *Expression of Acute-Phase Response Proteins in Retinal Müller Cells in Diabetes.* Investigative Opthalmology & Visual Science, 2005. **46**(1): p. 349.

121. Liu, X., et al., *IL-1beta induces IL-6 production in retinal Muller cells predominantly through the activation of p38 MAPK/NF-kappaB signaling pathway.* Exp Cell Res, 2015. **331**(1): p. 223-231.

122. Zhang, S.X., et al., *Pigment epithelium-derived factor (PEDF) is an endogenous antiinflammatory factor.* The FASEB Journal, 2006. **20**(2): p. 323-325.

123. Mu, H., et al., *Effect of high glucose concentration on VEGF and PEDF expression in cultured retinal Müller cells.* Molecular Biology Reports, 2009. **36**(8): p. 2147-2151.

124. Lange, J., et al., *Regulation of Pigment Epithelium–Derived Factor Production and Release by Retinal Glial (Müller) Cells under Hypoxia.* Investigative Opthalmology & Visual Science, 2008. **49**(11): p. 5161.

125. Le, Y.Z., *VEGF production and signaling in Muller glia are critical to modulating vascular function and neuronal integrity in diabetic retinopathy and hypoxic retinal vascular diseases.* Vision Res, 2017. **139**: p. 108-114.

126. Wang, J.J., M. Zhu, and Y.Z. Le, *Functions of Muller cell-derived vascular endothelial growth factor in diabetic retinopathy.* World J Diabetes, 2015. **6**(5): p. 726-33.

127. Thoreson, W., *Glutamate receptors and circuits in the vertebrate retina.* Progress in Retinal and Eye Research, 1999. **18**(6): p. 765-810.

128. Iovino, L., M.E. Tremblay, and L. Civiero, *Glutamate-induced excitotoxicity in Parkinson's disease: The role of glial cells.* Journal of Pharmacological Sciences, 2020. **144**(3): p. 151-164.

129. Ambati, J., *Elevated γ-Aminobutyric Acid, Glutamate, and Vascular Endothelial Growth Factor Levels in the Vitreous of Patients With Proliferative Diabetic Retinopathy.* Archives of Ophthalmology, 1997. **115**(9): p. 1161.

130. Santiago, A.R., et al., *Diabetes changes ionotropic glutamate receptor subunit expression level in the human retina.* Brain Research, 2008. **1198**: p. 153-159.

131. Ma, M., et al., *High Glucose-Induced TRPC6 Channel Activation Decreases Glutamate Uptake in Rat Retinal Muller Cells.* Front Pharmacol, 2019. **10**: p. 1668.

132. Li, Q. and D.G. Puro, *Diabetes-Induced Dysfunction of the Glutamate Transporter in Retinal Müller Cells.* Investigative Ophthalmology & Visual Science, 2002. **43**(9): p. 3109-3116.

133. Rao, V.R. and S. Finkbeiner, *NMDA and AMPA receptors: old channels, new tricks.* Trends in Neurosciences, 2007. **30**(6): p. 284-291.

134. Ureshino, et al., *The Interplay between Ca2+ Signaling Pathways and Neurodegeneration.* International Journal of Molecular Sciences, 2019. **20**(23): p. 6004.

135. Behm-Ansmant, I., J. Rehwinkel, and E. Izaurralde, *MicroRNAs Silence Gene Expression by Repressing Protein Expression and/or by Promoting mRNA Decay.* Cold Spring Harbor Symposia on Quantitative Biology, 2006. **71**(0): p. 523-530.

136. Gong, Q. and G. Su, *Roles of miRNAs and long noncoding RNAs in the progression of diabetic retinopathy.* Bioscience Reports, 2017. **37**(6): p. BSR20171157.

137. Barutta, F., et al., *MicroRNA and Microvascular Complications of Diabetes.* International Journal of Endocrinology, 2018. **2018**: p. 1-20.

138. Bushati, N. and S.M. Cohen, *microRNA Functions.* Annual Review of Cell and Developmental Biology, 2007. **23**(1): p. 175-205.

139. Michlewski, G. and J.F. Cáceres, *Post-transcriptional control of miRNA biogenesis.* RNA, 2019. **25**(1): p. 1-16.

140. Kim, V.N., *MicroRNA precursors in motion: exportin-5 mediates their nuclear export.* Trends in Cell Biology, 2004. **14**(4): p. 156-159.

141. Fareh, M., et al., *TRBP ensures efficient Dicer processing of precursor microRNA in RNA-crowded environments.* Nature Communications, 2016. **7**(1): p. 13694.

142. Krol, J., I. Loedige, and W. Filipowicz, *The widespread regulation of microRNA biogenesis, function and decay.* Nature Reviews Genetics, 2010. **11**(9): p. 597-610.

143. Du, T. and P.D. Zamore, *microPrimer: the biogenesis and function of microRNA.* Development, 2005. **132**(21): p. 4645-4652.

144. Guo, L., et al., *Evolutionary and Expression Analysis of miR-#-5p and miR-#-3p at the miRNAs/isomiRs Levels.* BioMed Research International, 2015. **2015**: p. 1-14.

145. Semler, B.L. and M.L. Waterman, *IRES-mediated pathways to polysomes: nuclear versus cytoplasmic routes.* Trends Microbiol, 2008. **16**(1): p. 1-5.

146. Aitken, C.E. and J.R. Lorsch, *A mechanistic overview of translation initiation in eukaryotes.* Nature Structural & Molecular Biology, 2012. **19**(6): p. 568-576.

147. Humphreys, D.T., et al., *MicroRNAs control translation initiation by inhibiting eukaryotic initiation factor 4E/cap and poly(A) tail function.* Proceedings of the National Academy of Sciences, 2005. **102**(47): p. 16961-16966.

148. Mathonnet, G., et al., *MicroRNA Inhibition of Translation Initiation in Vitro by Targeting the Cap-Binding Complex eIF4F.* Science, 2007. **317**(5845): p. 1764-1767.

149. Chendrimada, T.P., et al., *MicroRNA silencing through RISC recruitment of eIF6.* Nature, 2007. **447**(7146): p. 823-828.

150. Joel and J. Coller, *Pausing on Polyribosomes: Make Way for Elongation in Translational Control.* Cell, 2015. **163**(2): p. 292-300.

151. Nottrott, S., M.J. Simard, and J.D. Richter, *Human let-7a miRNA blocks protein production on actively translating polyribosomes.* Nature Structural & Molecular Biology, 2006. **13**(12): p. 1108-1114.

152. Vislovukh, A., et al., *Proto-oncogenic isoform A2 of eukaryotic translation elongation factor eEF1 is a target of miR-663 and miR-744.* British Journal of Cancer, 2013. **108**(11): p. 2304-2311.

153. Jonas, S. and E. Izaurralde, *Towards a molecular understanding of microRNA-mediated gene silencing.* Nature Reviews Genetics, 2015. **16**(7): p. 421-433.

154. Wu, L., J. Fan, and J.G. Belasco, *MicroRNAs direct rapid deadenylation of mRNA.* Proceedings of the National Academy of Sciences, 2006. **103**(11): p. 4034-4039.

155. Eulalio, A., et al., *Target-specific requirements for enhancers of decapping in miRNA-mediated gene silencing.* Genes & Development, 2007. **21**(20): p. 2558-2570.

156. Bartel, D.P., *MicroRNAs.* Cell, 2004. **116**(2): p. 281-297.

157. Bagga, S., et al., *Regulation by let-7 and lin-4 miRNAs Results in Target mRNA Degradation.* Cell, 2005. **122**(4): p. 553-563.

158. Mohr, A. and J. Mott, *Overview of MicroRNA Biology.* Seminars in Liver Disease, 2015. **35**(01): p. 003-011.

159. Kiriakidou, M., et al., *An mRNA m7G Cap Binding-like Motif within Human Ago2 Represses Translation.* Cell, 2007. **129**(6): p. 1141-1151.

160. Schmitter, D., et al., *Effects of Dicer and Argonaute down-regulation on mRNA levels in human HEK293 cells.* Nucleic Acids Research, 2006. **34**(17): p. 4801-4815.

161. Takimoto, K., M. Wakiyama, and S. Yokoyama, *Mammalian GW182 contains multiple Argonaute-binding sites and functions in microRNA-mediated translational repression.* RNA, 2009. **15**(6): p. 1078-1089.

162. Eulalio, A., E. Huntzinger, and E. Izaurralde, *GW182 interaction with Argonaute is essential for miRNA-mediated translational repression and mRNA decay.* Nature Structural & Molecular Biology, 2008. **15**(4): p. 346-353.

163. Fabian, M.R., et al., *Mammalian miRNA RISC Recruits CAF1 and PABP to Affect PABP-Dependent Deadenylation.* Molecular Cell, 2009. **35**(6): p. 868-880.

164. Behm-Ansmant, I., *mRNA degradation by miRNAs and GW182 requires both CCR4:NOT deadenylase and DCP1:DCP2 decapping complexes.* Genes & Development, 2006. **20**(14): p. 1885-1898.

165. Miao, C., et al., *MicroRNAs in type 1 diabetes: new research progress and potential directions.* Biochem Cell Biol, 2018. **96**(5): p. 498-506.

166. Barutta, F., et al., *MicroRNA-126 and micro-/macrovascular complications of type 1 diabetes in the EURODIAB Prospective Complications Study.* Acta Diabetol, 2017. **54**(2): p. 133-139.

167. Mazzeo, A., et al., *Molecular and functional characterization of circulating extracellular vesicles from diabetic patients with and without retinopathy and healthy subjects.* Exp Eye Res, 2018. **176**: p. 69-77.

168. Zampetaki, A., et al., *Plasma MicroRNA Profiling Reveals Loss of Endothelial MiR-126 and Other MicroRNAs in Type 2 Diabetes.* Circulation Research, 2010. **107**(6): p. 810-817.

169. Shaker, O.G., et al., *Diagnostic and prognostic role of serum miR-20b, miR-17-3p, HOTAIR, and MALAT1 in diabetic retinopathy.* IUBMB Life, 2019. **71**(3): p. 310-320.

170. Zhang, X., Y. Yang, and Z. Feng, *Suppression of microRNA-495 alleviates high-glucose-induced retinal ganglion cell apoptosis by regulating Notch/PTEN/Akt signaling.* Biomed Pharmacother, 2018. **106**: p. 923-929.

171. Wang, H., et al., *MicroRNA-93-5p participates in type 2 diabetic retinopathy through targeting Sirt1.* International Ophthalmology, 2021.

172. Chen, Q., et al., *Pathogenic Role ofmicroRNA-21in Diabetic Retinopathy Through Downregulation of PPARα.* Diabetes, 2017. **66**(6): p. 1671-1682.

173. Hui, Y. and Y. Yin, *MicroRNA-145 attenuates high glucose-induced oxidative stress and inflammation in retinal endothelial cells through regulating TLR4/NF-kappaB signaling.* Life Sci, 2018. **207**: p. 212-218.

174. Rocha, D.M., et al., *Saturated fatty acids trigger TLR4-mediated inflammatory response.* Atherosclerosis, 2016. **244**: p. 211-5.

175. Wallace, D.C., *A mitochondrial paradigm for degenerative diseases and ageing.* (1528-2511 (Print)).

176. Mortuza, R., B. Feng, and S. Chakrabarti, *miR-195 regulates SIRT1-mediated changes in diabetic retinopathy.* Diabetologia, 2014. **57**(5): p. 1037-1046.

177. Zhang, W., et al., *Sirt1 Inhibits Oxidative Stress in Vascular Endothelial Cells.* Oxid Med Cell Longev, 2017. **2017**: p. 7543973.

178. Zeng, Y., et al., *MicroRNA-29b-3p Promotes Human Retinal Microvascular Endothelial Cell Apoptosis via Blocking SIRT1 in Diabetic Retinopathy.* Front Physiol, 2019. **10**: p. 1621.

179. Mensà, E., et al., *Circulating miR-146a in healthy aging and type 2 diabetes: Age- and gender-specific trajectories.* Mechanisms of Ageing and Development, 2019. **180**: p. 1-10.

180. Roganović, J., *Downregulation of microRNA-146a in diabetes, obesity and hypertension may contribute to severe COVID-19.* Medical Hypotheses, 2021. **146**: p. 110448.

181. Zhuang, P., C.K. Muraleedharan, and S. Xu, *Intraocular Delivery of miR-146 Inhibits Diabetes-Induced Retinal Functional Defects in Diabetic Rat Model.* Investigative Opthalmology & Visual Science, 2017. **58**(3): p. 1646.

182. Ye, E.-A. and J.J. Steinle, *miR-146a Attenuates Inflammatory Pathways Mediated by TLR4/NF-κB and TNFαto Protect Primary Human Retinal Microvascular Endothelial Cells Grown in High Glucose.* Mediators of Inflammation, 2016. **2016**: p. 1-9.

183. Wang, Q., et al., *Dual Anti-Inflammatory and Anti-Angiogenic Action of miR-15a in Diabetic Retinopathy.* EBioMedicine, 2016. **11**: p. 138-150.

184. Ye, E.-A. and J.J. Steinle, *miR-15b/16 protects primary human retinal microvascular endothelial cells against hyperglycemia-induced increases in tumor necrosis factor alpha and suppressor of cytokine signaling 3.* Journal of Neuroinflammation, 2015. **12**(1): p. 44.

185. Wang, S., et al., *Elevated microRNA-20b-3p and reduced thioredoxin-interacting protein ameliorate diabetic retinopathy progression by suppressing the NLRP3 inflammasomes.* IUBMB Life, 2020. **72**(7): p. 1433-1448.

186. Yury, O., et al., *Altered levels of circulating cytokines and microRNAs in lean and obese individuals with prediabetes and type 2 diabetes.* Mol. BioSyst., 2017. **13**: p. 106-121.

187. Assmann, T.S., et al., *MicroRNA expression profiles and type 1 diabetes mellitus: systematic review and bioinformatic analysis.* Endocr Connect, 2017. **6**(8): p. 773-790.

188. Wang, G., et al., *Decreased expression of miR-150, miR146a and miR424 in type 1 diabetic patients: Association with ongoing islet autoimmunity.* Biochem Biophys Res Commun, 2017.

189. Shi, L., et al., *Deletion of miR-150 Exacerbates Retinal Vascular Overgrowth in High-Fat-Diet Induced Diabetic Mice.* PLoS One, 2016. **11**(6): p. e0157543.

190. Yu, F., et al., *Decreased miR-150 in obesity-associated type 2 diabetic mice increases intraocular inflammation and exacerbates retinal dysfunction.* BMJ Open Diabetes Res Care, 2020. **8**(1).

191. Duan, Y., et al., *miR-150 regulates high glucose-induced cardiomyocyte hypertrophy by targeting the transcriptional co-activator p300.* Exp Cell Res, 2013. **319**(3): p. 173-84.

192. Shen, J., et al., *MicroRNAs regulate ocular neovascularization.* Mol Ther, 2008. **16**(7): p. 1208-16.

193. Zhu, J., et al., *miR-181a and miR-150 regulate dendritic cell immune inflammatory responses and cardiomyocyte apoptosis via targeting JAK1-STAT1/c-Fos pathway.* J Cell Mol Med, 2017. **21**(11): p. 2884-2895.

194. Ma, J.L., W.L. Guo, and X.M. Chen, *Overexpressing microRNA-150 attenuates hypoxia-induced human cardiomyocyte cell apoptosis by targeting glucose-regulated protein-94.* Mol Med Rep, 2018. **17**(3): p. 4181-4186.

195. Wright, W.S., et al., *Hypoxia and the expression of HIF-1alpha and HIF-2alpha in the retina of streptozotocin-injected mice and rats.* Exp Eye Res, 2010. **90**(3): p. 405-12.

196. Linsenmeier, R.A. and H.F. Zhang, *Retinal oxygen: from animals to humans.* Prog Retin Eye Res, 2017. **58**: p. 115-151.

197. Liu, C.H., et al., *Endothelial microRNA-150 is an intrinsic suppressor of pathologic ocular neovascularization.* Proc Natl Acad Sci U S A, 2015. **112**(39): p. 12163-8.

198. Ying, W., et al., *miR-150 regulates obesity-associated insulin resistance by controlling B cell functions.* Sci Rep, 2016. **6**: p. 20176.

199. Liu, L., L.N. Yan, and Z. Sui, *MicroRNA-150 affects endoplasmic reticulum stress via MALAT1-miR-150 axis-mediated NF-kappaB pathway in LPS-challenged HUVECs and septic mice.* Life Sci, 2021. **265**: p. 118744.

200. Shen, J., et al., *MiR-150-5p retards the progression of myocardial fibrosis by targeting EGR1.* Cell Cycle, 2019. **18**(12): p. 1335-1348.

201. Peng, W., et al., *Long noncoding RNA NONHSAG053901 promotes diabetic nephropathy via stimulating Egr-1/TGF-beta-mediated renal inflammation.* J Cell Physiol, 2019. **234**(10): p. 18492-18503.

202. Zha, F., et al., *Long non-coding RNA MEG3 promotes fibrosis and inflammatory response in diabetic nephropathy via miR-181a/Egr-1/TLR4 axis.* Aging, 2019. **11**(11): p. 3716-3730.

203. Qu, X., et al., *c-Myb promotes growth and metastasis of colorectal cancer through c-fos-induced epithelial-mesenchymal transition.* Cancer Science, 2019. **110**(10): p. 3183-3196.

204. Chen, C., et al., *MiR-195 enhances cardiomyocyte apoptosis induced by hypoxia/reoxygenation injury via downregulating c-myb.* (2284-0729 (Electronic)).

205. Barrett, L.E., et al., *Elk-1 associates with the mitochondrial permeablity transition pore complex in neurons.* PNAS, 2006. **103**(13): p. 6.

206. Barrett, L.E., et al., *Region-directed phototransfection reveals the functional significance of a dendritically synthesized transcription factor.* Nat Methods, 2006. **3**(6): p. 455-60.

207. Lu, Z., et al., *ETS-domain containing protein (Elk1) suppression protects cortical neurons against oxygen-glucose deprivation injury.* Exp Cell Res, 2018. **371**(1): p. 42-49.

208. Park, S.J., et al., *Fibroblast growth factor 2-induced cytoplasmic asparaginyl-tRNA synthetase promotes survival of osteoblasts by regulating anti-apoptotic PI3K/Akt signaling.* Bone, 2009. **45**(5): p. 994-1003.

209. Yoon, T.M., et al., *EGR1 regulates radiation-induced apoptosis in head and neck squamous cell carcinoma.* Oncol Rep, 2015. **33**(4): p. 1717-22.

210. Ding, Y., et al., *Identification of a small molecule as inducer of ferroptosis and apoptosis through ubiquitination of GPX4 in triple negative breast cancer cells.* J Hematol Oncol, 2021. **14**(1): p. 19.

211. Agrawal, S. and B. Chaqour, *MicroRNA signature and function in retinal neovascularization.* World J Biol Chem, 2014. **5**(1): p. 1-11.

212. Bartel, D.P., *MicroRNAs: Target Recognition and Regulatory Functions.* Cell, 2009. **136**(2): p. 215-233.

213. Engelgau, M.M., et al., *The evolving diabetes burden in the United States.* Ann Intern Med, 2004. **140**(11): p. 945-50.

214. Lux, A., et al., *Non-responders to bevacizumab (Avastin) therapy of choroidal neovascular lesions.* Br J Ophthalmol, 2007. **91**(10): p. 1318-22.

215. Lee, Y.S., J. Wollam, and J.M. Olefsky, *An Integrated View of Immunometabolism.* Cell, 2018. **172**(1-2): p. 22-40.

216. Abcouwer, S.F., *Angiogenic Factors and Cytokines in Diabetic Retinopathy.* J Clin Cell Immunol, 2013. **Suppl 1**(11).

217. Du, Y., et al., *Photoreceptor cells are major contributors to diabetes-induced oxidative stress and local inflammation in the retina.* Proc Natl Acad Sci U S A, 2013. **110**(41): p. 16586-91.

218. Semeraro, F., et al., *Diabetic Retinopathy: Vascular and Inflammatory Disease.* J Diabetes Res, 2015. **2015**: p. 582060.

219. Kovacs, B., et al., *microRNAs in Early Diabetic Retinopathy in Streptozotocin-Induced Diabetic Rats.* Investigative Opthalmology & Visual Science, 2011. **52**(7): p. 4402.

220. Joglekar, M.V., et al., *Circulating microRNA Biomarkers of Diabetic Retinopathy.* Diabetes, 2016. **65**(1): p. 22-24.

221. Kovacs, B., et al., *MicroRNAs in early diabetic retinopathy in streptozotocin-induced diabetic rats.* Invest Ophthalmol Vis Sci, 2011. **52**(7): p. 4402-9.

222. Wu, J.H., et al., *Altered MicroRNA Expression Profiles in Retinas with Diabetic Retinopathy.* Ophthalmic Res, 2011. **47**(4): p. 195-201.

223. Estrella, S., et al., *Expression of miR-22 and miR-150 in type 1 diabetes mellitus: Possible relationship with autoimmunity and clinical characteristics.* Med Clin (Barc), 2016. **147**(6): p. 245-7.

224. Pescador, N., et al., *Serum circulating microRNA profiling for identification of potential type 2 diabetes and obesity biomarkers.* PLoS One, 2013. **8**(10): p. e77251.

225. Alhamdoosh, M., et al., *Combining multiple tools outperforms individual methods in gene set enrichment analyses.* Bioinformatics, 2017. **33**(3): p. 414-424.

226. Bousquet, M., et al., *miR-150 blocks MLL-AF9-associated leukemia through oncogene repression.* Mol Cancer Res, 2013. **11**(8): p. 912-22.

227. Zhou, B., et al., *miR-150, a microRNA expressed in mature B and T cells, blocks early B cell development when expressed prematurely.* Proc Natl Acad Sci U S A, 2007. **104**(17): p. 7080-5.

228. Aiello, L.P., et al., *Vascular endothelial growth factor in ocular fluid of patients with diabetic retinopathy and other retinal disorders.* N Engl J Med, 1994. **331**(22): p. 1480-7.

229. Hammes, H.P., et al., *Upregulation of the vascular endothelial growth factor/vascular endothelial growth factor receptor system in experimental background diabetic retinopathy of the rat.* Diabetes, 1998. **47**(3): p. 401-6.

230. Pe'er, J., et al., *Upregulated expression of vascular endothelial growth factor in proliferative diabetic retinopathy.* Br J Ophthalmol, 1996. **80**(3): p. 241-5.

231. Bueno-Silva, B., et al., *Brazilian Red Propolis Attenuates Inflammatory Signaling Cascade in LPS-Activated Macrophages.* PLoS One, 2015. **10**(12): p. e0144954.

232. Chang, R.C.-A., et al., *High-Fat Diet–Induced Retinal Dysfunction.* Investigative Opthalmology & Visual Science, 2015. **56**(4): p. 2367.

233. Woo, S.-L., et al., *Metformin Ameliorates Hepatic Steatosis and Inflammation without Altering Adipose Phenotype in Diet-Induced Obesity.* PLoS ONE, 2014. **9**(3): p. e91111.

234. Zhuang, G., et al., *A Novel Regulator of Macrophage Activation.* Circulation, 2012. **125**(23): p. 2892-2903.

235. Rajagopal, R., et al., *Functional Deficits Precede Structural Lesions in Mice With High-Fat Diet-Induced Diabetic Retinopathy.* Diabetes, 2016. **65**(4): p. 1072-84.

236. Shirao, Y. and K. Kawasaki, *Electrical responses from diabetic retina.* (1350-9462 (Print)).

237. Rithwick Rajagopal, G.W.B., Sheng Zhang, Li Yin, Peter Lukasiewicz, Clay F. Semenkovich, *Functional Deficits Precede Structural Lesions in Mice With High-Fat Diet–Induced Diabetic Retinopathy.* Diabetes, 2016. **65**: p. 13.

238. Chang, J.Y., et al., *Melatonin Affects Mitochondrial Fission/Fusion Dynamics in the Diabetic Retina.* J Diabetes Res, 2019. **2019**: p. 8463125.

239. Zudaire, E., et al., *A computational tool for quantitative analysis of vascular networks.* PLoS One, 2011. **6**(11): p. e27385.

240. Xu, S., et al., *MicroRNA (miRNA) Transcriptome of Mouse Retina and Identification of a Sensory Organ-specific miRNA Cluster.* Journal of Biological Chemistry, 2007. **282**(34): p. 25053-25066.

241. Pardue, M.T., et al., *Rodent Hyperglycemia-Induced Inner Retinal Deficits are Mirrored in Human Diabetes.* Transl Vis Sci Technol, 2014. **3**(3): p. 6.

242. Karkeni, E., et al., *Vitamin D limits inflammation-linked microRNA expression in adipocytes in vitro and in vivo: A new mechanism for the regulation of inflammation by vitamin D.* Epigenetics, 2018. **13**(2): p. 156-162.

243. Slattery, M.L., et al., *The NF-kappaB signalling pathway in colorectal cancer: associations between dysregulated gene and miRNA expression.* J Cancer Res Clin Oncol, 2018. **144**(2): p. 269-283.

244. Xue, H. and M.X. Li, *MicroRNA-150 protects against cigarette smoke-induced lung inflammation and airway epithelial cell apoptosis through repressing p53: MicroRNA-150 in CS-induced lung inflammation.* Hum Exp Toxicol, 2018. **37**(9): p. 920-928.

245. Karin, M. and F.R. Greten, *NF-κB: linking inflammation and immunity to cancer development and progression.* Nature Reviews Immunology, 2005. **5**(10): p. 749-759.

246. Wang, Q., et al., *Regulation of retinal inflammation by rhythmic expression of MiR-146a in diabetic retina.* Invest Ophthalmol Vis Sci, 2014. **55**(6): p. 3986-94.

247. Wang, Q., et al., *Dual Anti-Inflammatory and Anti-Angiogenic Action of miR-15a in Diabetic Retinopathy.* EBioMedicine, 2016. **11**: p. 138-150.

248. Chen, S., et al., *miR-146a regulates glucose induced upregulation of inflammatory cytokines extracellular matrix proteins in the retina and kidney in diabetes.* PLoS One, 2017. **12**(3): p. e0173918.

249. Lu, J.M., et al., *Repression of microRNA-21 inhibits retinal vascular endothelial cell growth and angiogenesis via PTEN dependent-PI3K/Akt/VEGF signaling pathway in diabetic retinopathy.* Exp Eye Res, 2020. **190**: p. 107886.

250. Chen, X., et al., *Down-regulation of microRNA-21 reduces inflammation and podocyte apoptosis in diabetic nephropathy by relieving the repression of TIMP3 expression.* Biomed Pharmacother, 2018. **108**: p. 7-14.

251. Stewart, M.W., *Treatment of diabetic retinopathy: Recent advances and unresolved challenges.* World J Diabetes, 2016. **7**(16): p. 333-41.

252. Cheung, N., P. Mitchell, and T.Y. Wong, *Diabetic retinopathy.* The Lancet, 2010. **376**(9735): p. 124-136.

253. Zhang, J., et al., *Intravitreal injection of erythropoietin protects both retinal vascular and neuronal cells in early diabetes.* Invest Ophthalmol Vis Sci, 2008. **49**(2): p. 732-42.

254. Lv, J., et al., *Sulforaphane delays diabetes-induced retinal photoreceptor cell degeneration.* Cell Tissue Res, 2020. **382**(3): p. 477-486.

255. GB, A., *The absence of diabetic retinopathy in patients with retinitis pigmentosa: implications for pathophysiology and possible treatment.* Br J Ophthalmol, 2001. **85**(3): p. 5.

256. Lahdenranta J, P.R., Schlingemann RO, Hagedorn M, Stallcup WB, Bucana CD, Sidman RL, Arap W, *An anti-angiogenic state in mice and humans with retinal photoreceptor cell degeneration.* Proc Natl Acad Sci U S A, 2001. **98**(18): p. 6.

257. Liu, H., et al., *Photoreceptor Cells Influence Retinal Vascular Degeneration in Mouse Models of Retinal Degeneration and Diabetes.* Invest Ophthalmol Vis Sci, 2016. **57**(10): p. 4272-81.

258. Sharma, A., et al., *A neurotoxic phosphoform of Elk-1 associates with inclusions from multiple neurodegenerative diseases.* PLoS One, 2010. **5**(2): p. e9002.

259. Tan E, D.X., Saadi A, Agarwal N, Naash MI, Al-Ubaidi MR, *Expression of cone-photoreceptor-specific antigens in a cell line derived from retinal tumors in transgenic mice.* Invest Ophthalmol Vis Sci, 2004. **45**(3): p. 5.

260. Livak, K.J. and T.D. Schmittgen, *Analysis of relative gene expression data using real-time quantitative PCR and the 2(-Delta Delta C(T)) Method.* Methods, 2001. **25**(4): p. 402-8.

261. Shi, L., et al., *Peptide Lv augments L-type voltage-gated calcium channels through vascular endothelial growth factor receptor 2 (VEGFR2) signaling.* Biochim Biophys Acta, 2015. **1853**(5): p. 1154-64.

262. Asare-Bediako, B., et al., *Characterizing the Retinal Phenotype in the High-Fat Diet and Western Diet Mouse Models of Prediabetes.* Cells, 2020. **9**(2).

263. Wong-Riley, M.T., *Energy metabolism of the visual system.* Eye Brain, 2010. **2**: p. 99-116.

264. Wan, J., et al., *MicroRNA-150 inhibitors enhance cell apoptosis of melanoma by targeting PDCD4.* Oncol Lett, 2018. **15**(2): p. 1475-1482.

265. Ou H, T.H., Qin Y, Luo X, Yang P, Zhang W, Chen W, Lv D, Tang H, *Extracellular vesicles derived from microRNA-150-5p-overexpressing*

mesenchymal stem cells protect rat hearts against ischemia/reperfusion. Aging (Albany NY), 2020. **12**(13): p. 15.

266. Ling, Z., et al., *MicroRNA-150 functions as a tumor suppressor and sensitizes osteosarcoma to doxorubicin-induced apoptosis by targeting RUNX2.* Exp Ther Med, 2020. **19**(1): p. 481-488.

267. Qin, B., et al., *MicroRNA-150 targets ELK1 and modulates the apoptosis induced by ox-LDL in endothelial cells.* Mol Cell Biochem, 2017. **429**(1-2): p. 45-58.

268. Demir, O., et al., *ETS-domain transcription factor Elk-1 mediates neuronal survival: SMN as a potential target.* Biochim Biophys Acta, 2011. **1812**(6): p. 652-62.

269. Kawahara T, S.H., Aljarah AK, Ide H, Li Y, Kashiwagi E, Netto GJ, Zheng Y, Miyamoto H. , *ELK1 is up-regulated by androgen in bladder cancer cells and promotes tumor progression.* . Oncotarget, 2015. **6**(30): p. 17.

270. Zhao H, C.M., Wang J, Cao G, Chen W, Xu J. , *PCNA-associated factor KIAA0101 transcriptionally induced by ELK1 controls cell proliferation and apoptosis in nasopharyngeal carcinoma: an integrated bioinformatics and experimental study.* . Aging (Albany NY), 2020. **12**(7): p. 26.

271. Lavaur, J., et al., *A TAT-DEF-Elk-1 peptide regulates the cytonuclear trafficking of Elk-1 and controls cytoskeleton dynamics.* J Neurosci, 2007. **27**(52): p. 14448-58.

272. Wu, W., R.D. Mosteller, and D. Broek, *Sphingosine kinase protects lipopolysaccharide-activated macrophages from apoptosis.* Mol Cell Biol, 2004. **24**(17): p. 7359-69.

273. Wu, D.M., et al., *Effects of microRNA-129 and its target gene c-Fos on proliferation and apoptosis of hippocampal neurons in rats with epilepsy via the MAPK signaling pathway.* J Cell Physiol, 2018. **233**(9): p. 6632-6643.

274. Fan, L., L. Jiang, and Z. Du, *Myeloid cell leukemia 1 (Mcl(-1)) protects against 1-methyl-4-phenylpyridinium ion (MPP+) induced apoptosis in Parkinson's disease.* Metab Brain Dis, 2015. **30**(5): p. 1269-74.

275. Gallemore, R.P. and D. Nguyen, *When Anti-VEGF Treatment Fails.* Review of Ophthalmology, 2008. **March**: p. http://www.reviewofophthalmology.com/content/d/retinal_insider/i/1230/c/23141/

276. Palejwala, N.V. and A.K. Lauer, *Aflibercept: an update on recent milestones achieved.* Drugs Today (Barc), 2014. **50**(12): p. 779-90.

277. Agrawal, N.K. and S. Kant, *Targeting inflammation in diabetes: Newer therapeutic options.* World J Diabetes, 2014. **5**(5): p. 697-710.

278. Sell, H., C. Habich, and J. Eckel, *Adaptive immunity in obesity and insulin resistance.* Nat Rev Endocrinol, 2012. **8**(12): p. 709-16.

279. Patel, N., *Targeting leukostasis for the treatment of early diabetic retinopathy.* Cardiovasc Hematol Disord Drug Targets, 2009. **9**(3): p. 222-9.

280. Tonade, D., H. Liu, and T.S. Kern, *Photoreceptor Cells Produce Inflammatory Mediators That Contribute to Endothelial Cell Death in Diabetes.* Invest Ophthalmol Vis Sci, 2016. **57**(10): p. 4264-71.

281. Mima, A., et al., *Retinal not systemic oxidative and inflammatory stress correlated with VEGF expression in rodent models of insulin resistance and diabetes.* Invest Ophthalmol Vis Sci, 2012. **53**(13): p. 8424-32.

282. Arden, G.B., *The absence of diabetic retinopathy in patients with retinitis pigmentosa: implications for pathophysiology and possible treatment.* British Journal of Ophthalmology, 2001. **85**(3): p. 366-370.

283. Arden, G.B., J.E. Wolf, and Y. Tsang, *Does dark adaptation exacerbate diabetic retinopathy? Evidence and a linking hypothesis.* Vision Res, 1998. **38**(11): p. 1723-9.

284. de Gooyer, T.E., et al., *Retinopathy is reduced during experimental diabetes in a mouse model of outer retinal degeneration.* Invest Ophthalmol Vis Sci, 2006. **47**(12): p. 5561-8.

285. Ying, W., et al., *MicroRNA-223 is a crucial mediator of PPARgamma-regulated alternative macrophage activation.* J Clin Invest, 2015. **125**(11): p. 4149-59.

286. Poy, M.N., et al., *A pancreatic islet-specific microRNA regulates insulin secretion.* Nature, 2004. **432**(7014): p. 226-30.

287. Luo, X.Y., et al., *MicroRNA-150 restores endothelial cell function and attenuates vascular remodeling by targeting PTX3 through the NF-kappaB signaling pathway in mice with acute coronary syndrome.* Cell Biol Int, 2018. **42**(9): p. 1170-1181.

288. Esser, N., et al., *Inflammation as a link between obesity, metabolic syndrome and type 2 diabetes.* Diabetes Res Clin Pract, 2014. **105**(2): p. 141-50.

289. Nunez Lopez, Y.O., G. Garufi, and A.A. Seyhan, *Altered levels of circulating cytokines and microRNAs in lean and obese individuals with prediabetes and type 2 diabetes.* Mol Biosyst, 2016. **13**(1): p. 106-121.

290. Lin, C.C., et al., *Endothelin-1 induces VCAM-1 expression-mediated inflammation via receptor tyrosine kinases and Elk/p300 in human tracheal smooth muscle cells.* Am J Physiol Lung Cell Mol Physiol, 2015. **309**(3): p. L211-25.

291. Kasza A, W.P., Horwacik I, Tymoszuk P, Mizgalska D, Palmer K, Rokita H, Sharrocks AD, Jura J. , *Transcription factors Elk-1 and SRF are engaged in IL1-dependent regulation of ZC3H12A expression.* BMC Mol Biol, 2010. **11**(14).

292. Scuderi, S., et al., *Different Retinal Expression Patterns of IL-1alpha, IL-1beta, and Their Receptors in a Rat Model of Type 1 STZ-Induced Diabetes.* J Mol Neurosci, 2015. **56**(2): p. 431-9.

293. Kowluru, R.A., et al., *Diabetes-induced activation of nuclear transcriptional factor in the retina, and its inhibition by antioxidants.* Free Radic Res, 2003. **37**(11): p. 1169-80.

294. Saadane, A., et al., *Photoreceptor cell calcium dysregulation and calpain activation promote pathogenic photoreceptor oxidative stress and inflammation in prodromal diabetic retinopathy.* Am J Pathol, 2021.

295. Wei S, L.Q., *Long noncoding RNA MALAT1 modulates sepsis-induced cardiac inflammation through the miR-150-5p/NF-κB axis.* Int J Clin Exp Pathol, 2019. **12**(9): p. 9.

296. Yan, B., et al., *lncRNA-MIAT Regulates Microvascular Dysfunction by Functioning as a Competing Endogenous RNA.* Circulation Research, 2015. **116**(7): p. 1143-1156.

297. Mylona, A., et al., *opposing effects of Elk-1 multisite phosphorylation shape its response to ERK activation.* science, 2016. **354**(6309): p. 5.

298. Besnard, A., et al., *Elk-1 a transcription factor with multiple facets in the brain.* Front Neurosci, 2011. **5**: p. 35.

299. Pang, T., et al., *Differential AMPK phosphorylation sites associated with phenylephrine vs. antihypertrophic effects of adenosine agonists in neonatal rat ventricular myocytes.* Am J Physiol Heart Circ Physiol, 2010. **298**(5): p. H1382-90.

300. Chowdhury, D., et al., *p38 MAPK pathway-dependent SUMOylation of Elk-1 and phosphorylation of PIAS2 correlate with the downregulation of Elk-1 activity in heat-stressed HeLa cells.* Cell Stress Chaperones, 2019. **24**(2): p. 393-407.

301. Salinas, S., et al., *SUMOylation regulates nucleo-cytoplasmic shuttling of Elk-1.* J Cell Biol, 2004. **165**(6): p. 767-73.

302. Liu, S.Y., et al., *Protein inhibitor of activated STAT1 Ser(503) phosphorylation-mediated Elk-1 SUMOylation promotes neuronal survival in APP/PS1 mice.* Br J Pharmacol, 2019. **176**(11): p. 1793-1810.

303. Yang SH, S.A., *Interplay of the SUMO and MAP kinase pathways.* Ernst Schering Res Found Workshop, 2006. **57**: p. 17.

304. Luo, E., et al., *The NF-kappaB/miR-425-5p/MCT4 axis: A novel insight into diabetes-induced endothelial dysfunction.* Mol Cell Endocrinol, 2020. **500**: p. 110641.

305. Song, G., L. Li, and Y. Yang, *MicroRNA-329-3p alleviates high glucose-induced endothelial cell injury via inhibition of the TLR4/TRAF6/NF-kappaB signaling pathway.* Exp Ther Med, 2021. **21**(1): p. 29.

306. Van Dijk, H.W., et al., *Association of visual function and ganglion cell layer thickness in patients with diabetes mellitus type 1 and no or minimal diabetic retinopathy.* Vision Research, 2011. **51**(2): p. 224-228.

307. Majidi, S.P. and R. Rajagopal, *Photoreceptor responses to light in the pathogenesis of diabetic retinopathy.* Vis Neurosci, 2020. **37**: p. E007.

308. Malechka, V.V., et al., *Impaired Rhodopsin Generation in the Rat Model of Diabetic Retinopathy.* Am J Pathol, 2017. **187**(10): p. 2222-2231.

309. Chen, J., et al., *Interphotoreceptor Retinol-Binding Protein Ameliorates Diabetes-Induced Retinal Dysfunction and Neurodegeneration Through Rhodopsin.* Diabetes, 2021. **70**(3): p. 788-799.

310. Gonzalez-Fernandez, F., *Interphotoreceptor retinoid-binding protein—an old gene for new eyes.* Vision Research, 2003. **43**(28): p. 3021-3036.

311. Yokomizo, H., et al., *Retinol binding protein 3 is increased in the retina of patients with diabetes resistant to diabetic retinopathy.* Sci Transl Med, 2019. **11**(499).

312. Jin, M., et al., *Upregulated circRNA ARHGAP10 Predicts an Unfavorable Prognosis in NSCLC through Regulation of the miR-150-5p/GLUT-1 Axis.* Mol Ther Nucleic Acids, 2019. **18**: p. 219-231.

313. Li, X. and H. Ren, *Long noncoding RNA PVT1 promotes tumor cell proliferation, invasion, migration and inhibits apoptosis in oral squamous cell carcinoma by regulating miR1505p/GLUT1.* Oncol Rep, 2020. **44**(4): p. 1524-1538.

314. Kumagai, A.K., *Glucose transport in brain and retina: implications in the management and complications of diabetes.* (1520-7552 (Print)).

315. Kumagai, A.K., W.M. Glasgow Bj Fau - Pardridge, and W.M. Pardridge, *GLUT1 glucose transporter expression in the diabetic and nondiabetic human eye.* (0146-0404 (Print)).

316. You, Z.P., et al., *Suppression of diabetic retinopathy with GLUT1 siRNA.* Sci Rep, 2017. **7**(1): p. 7437.

317. Holoman, N.C., et al., *Reduction of Glut1 in the Neural Retina But Not the RPE Alleviates Polyol Accumulation and Normalizes Early Characteristics of Diabetic Retinopathy.* J Neurosci, 2021. **41**(14): p. 3275-3299.

318. Zhou, J., et al., *LncRNA XIST inhibits hypoxia-induced cardiomyocyte apoptosis via mediating miR-150-5p/Bax in acute myocardial infarction.* (2284-0729 (Electronic)).

319. Ghiasi, S.M., et al., *Endoplasmic Reticulum Chaperone Glucose-Regulated Protein 94 Is Essential for Proinsulin Handling.* Diabetes, 2019. **68**(4): p. 747-760.

320. Nakamura, O., et al., *Bilberry extract administration prevents retinal ganglion cell death in mice via the regulation of chaperone molecules under conditions of endoplasmic reticulum stress.* Clinical Ophthalmology, 2017. **Volume 11**: p. 1825-1834.

321. Li, P., et al., *MiR-150 attenuates LPS-induced acute lung injury via targeting AKT3.* Int Immunopharmacol, 2019. **75**: p. 105794.

322. Zhang, Y., et al., *Overexpression of miR-150 Inhibits the NF-κB Signal Pathway in Intervertebral Disc Degeneration through Targeting P2X7.* Cells Tissues Organs, 2019. **207**(3-4): p. 165-176.

323. Liu, T., et al., *NF-kappaB signaling in inflammation.* Signal Transduct Target Ther, 2017. **2**.

324. Christian, F., E.L. Smith, and R.J. Carmody, *The Regulation of NF-kappaB Subunits by Phosphorylation.* Cells, 2016. **5**(1).

325. Moreno, R., et al., *Specification of the NF-κB transcriptional response by p65 phosphorylation and TNF-induced nuclear translocation of IKKε.* Nucleic Acids Research, 2010. **38**(18): p. 6029-6044.

326. Dröge, W., *Free Radicals in the Physiological Control of Cell Function.* Physiological Reviews, 2002. **82**(1): p. 47-95.

327. Kawahara, T., et al., *Silodosin inhibits the growth of bladder cancer cells and enhances the cytotoxic activity of cisplatin via ELK1 inactivation.* Am J Cancer Res, 2015. **5**(10): p. 2959-68.

328. Fujioka, S., et al., *NF-kappaB and AP-1 connection: mechanism of NF-kappaB-dependent regulation of AP-1 activity.* Mol Cell Biol, 2004. **24**(17): p. 7806-19.

329. Zeng, K., et al., *Resveratrol Inhibits Diabetic-Induced Müller Cells Apoptosis through MicroRNA-29b/Specificity Protein 1 Pathway.* Molecular Neurobiology, 2017. **54**(6): p. 4000-4014.

330. Zhang, J., C. Cui, and H. Xu, *Downregulation of miR-145-5p elevates retinal ganglion cell survival to delay diabetic retinopathy progress by targeting FGF5.* Biosci Biotechnol Biochem, 2019. **83**(9): p. 1655-1662.

331. Zwanzig, A., et al., *Neuroprotective effects of glial mediators in interactions between retinal neurons and Muller cells.* Exp Eye Res, 2021. **209**: p. 108689.